

Advances in Memristor Circuits and Bioinspired Systems

Advances in Memristor Circuits and Bioinspired Systems

Edited by
Alex Pappachen James



RESEARCH PUBLISHING

Published by

Research Publishing

Blk 12 Lorong Bakar Batu, #03-03, Singapore 348745.

e-mail: editorial@rpsonline.com.sg

ADVANCES IN MEMRISTOR CIRCUITS AND BIOINSPIRED SYSTEMS

Edited by: Alex Pappachen James

Copyright © 2015 SCASA & ICP 2015 Organisers. *All rights reserved.*

ISBN: 978-981-09-4424-7

This book, or parts thereof, may not be reproduced in any form or by any means, electronic or mechanical, including photocopying, recording or any information storage and retrieval system now known or to be invented, without written permission from the SCASA & ICP Organisers or the Publisher.

Disclaimer:

No responsibility is assumed by the SCASA & ICP Organisers/Publisher for any injury and/or damage to persons or property as a matter of products liability, negligence or otherwise, or from any use or operation of any methods, products or ideas contained in the material herein. Contents, used in the papers are how it is submitted and approved by the contributors after minor changes in the formatting. Whilst every attempt made to ensure that all aspects of the papers are uniform in style, the SCASA & ICP Organisers, Publisher or the Editor(s) will not be responsible whatsoever for the accuracy, correctness or representations of any statements or documents presented in the papers.

Design, CRC & Printed by iTEK CMS Web Solutions. e-mail:enquiries@itekcms.com

Printed in Singapore.

Preface

This book, *Advances in Memristor Circuits and Bioinspired Systems*, is a collection of research works presented at Nazarbayev University in pursuit of excellence in two distinct areas of systems applications by observing biological systems and emerging technology of memristors circuits. In particular, the book features the collection of papers presented at *Workshop on Bioinspired Sensors, Circuits, Systems and Applications*, and *Integrated circuits and programming conference (ICP 2015)*, that took place on 23-25 February, 2015, and 16 April, 2015 respectively.

A wide spectrum of interesting research ideas is presented in this book as short papers, full length papers and review papers. All the contributing papers have undergone several rounds of review and the overall acceptance rate of the papers is 25%. It presents a mix of theory and practice that is fundamentally inclined towards realistic applications. This will be useful for researchers and students with interest to technologies related to biosensors, memristors, image processing and computational modelling.

It is also imperative to note that the works presented in this book is largely as a result of undergraduate research work undergone during normal taught coursework hours. This book is a mandate of proof that research ideas can originate from taught courses and can encourage young researchers to practise theory and turn that into realistic application. I hope that the materials presented in the book will be useful to researchers and community at large.

“Great minds think differently. And every mind is differently great.”

Alex Pappachen James

Contents

<i>Preface</i>	v
Application of Nonlinear Acoustics for Detection of Biological Anomalies <i>Grant Ellis</i>	1
Background Subtraction based Application: City Decorative Plantings' Preservation <i>Aidar Zhetessov and Dauren Tlekov</i>	2
CFD Modeling of Blood Seggregation and Cells Damage in Ventricular Assist Devices (VAD's) <i>Luis R. Rojas-Solórzano</i>	6
Control of Automobile Audiosystem by Gestures <i>Abuzhan Aidaraliyev and Dauren Leskhan</i>	13
Drawing Using Web Camera — Object Recognition and Object Tracking <i>Aidana Massalimova and Zarina Amantayeva</i>	15
Electronic Attendance Using Face Recognition <i>Alimzhan Sultangazin and Janyzbek Kusmangaliyev</i>	18
Evaluation of Memristor Emulator for Memristor Circuit Applications in SPICE Simulator <i>Yerzhan Sapenova and Nursultan Ornov</i>	22
Gate-Diffusion Input (GDI) Technique for Low Power CMOS Logic Circuits Design <i>Yerkebulan Saparov and Aktanberdi Zhakupov</i>	28
Intelligent Mirror — Personalized Advertisement <i>Ratbek Zhapparov and Magauiya Zhussip</i>	30
Maze Solving by Memristive Network <i>Yernar Bainazar and Ruslan Tazhkenov</i>	33
Memristor-based Relaxation Oscillators Using Digital Gates <i>Yerkhan Sapiyev and Azamat Utekeyev</i>	37
Memristor Spice Model and Its Applications to Circuit Simulation of Memory Cells <i>BekishevDanyiar and Kapan Arman</i>	40
Simulation and Analysis of Reconfigurable Threshold Logic Gates Using Memristive Devices <i>Alfiya Kulmukhanova and Abduvakhit Junussov</i>	43
Simulation of Full Adder Design using Hybrid Memristor-CMOS based Technology <i>Yerden Kypshakpayev and Kuatbek Mukabak</i>	46
Simulation of Memristive Threshold Logic Cell <i>Rizukov Yerlan and Ryskaliyev Aibek</i>	51

Simulation of the Generic Memristive Circuit Model with Parasitic Components <i>Saltanat Salpenova and Merey Balgabayev</i>	54
Simulation of Pinched Hysteresis Loops of Two Memristor SPICE Models <i>Akzharkyn Izbassarova and Daulet Kengesbek</i>	57
The Development of Object Recognition Application to Automatically Count the Number of Passengers Entering the Bus <i>Serikbolsyn Myrzakhmet and Abzal Adilzhan</i>	61
The Memristor Circuits and Applications <i>Alex Pappachen James</i>	65
The Model of TiO ₂ Metal-Oxide-Metal Memristor based on Device's Physical Parameters <i>Rassul Bairamkulov</i>	67
The Real-Time Heart Rate Monitoring Using Fingertip and Its Application in Health Care <i>Nurbolat Aimakov and Diana Sadykova</i>	73
The Representation of Memristor Model in MATLAB [®] and Simulink [®] Environment <i>Sanzhar Askaruly and Bakhtiyar Rakhmetov</i>	76
Traffic Light Recognition System for People with Color Blindness <i>Timur Ibrayev and Radkhan Sarmukhanov</i>	80
Translational Biomechanics in Glaucoma <i>Match Wai Lun Ko</i>	84
Vehicle Detecting, Tracking and Counting for Traffic Control Systems <i>Kamilla Aliakhmet and Temirlan Zharkynbek</i>	91
WBC Identification and Counting — Detection and Counting of White Blood Cells in Blood Test <i>Dauken Seitkali and Madiyar Bazylkhanov</i>	95
<i>Author Index</i>	103

Electromagnetic Detection Techniques for Bio-Sensing Applications

Grant A. Ellis

Workshop on Bioinspired Sensors, Circuits, Systems and Applications, February 23-25, 2015, Nazarbayev University, Astana Kazakhstan

Abstract: There is increasing interest in placing medical implants or biosensors inside human tissue for monitoring bio-functions. This requires that power and communications be provided wirelessly to interrogate the buried sensors thereby reducing the need for surgery and for the ability to tele-monitor patients. Applications include monitoring glucose for diabetes, pH, temperature, blood pressure, and non-invasive wound healing. Also, electromagnetic waves in tissue experience high attenuation at high frequencies (e.g. > 5 dB / cm at 3 GHz) restricting data rates and resulting in the need for low-power RF bio-sensors.

During this presentation, electromagnetic complex dielectric measurement of human tissue using an open ended coaxial (capacitive) probe and calibration including the tradeoff between probe resolution and sensitivity are discussed. An oscillator control circuit is identified as a potential candidate for use in discriminating between wet and dry skin tissue. An RF transponder circuit topology utilizing an op-amp for the control circuit implemented using commercially available low-power, low-profile CMOS device and SMT-based technology is also described.

Two techniques are described for communicating and providing wireless power to buried bio-sensors. Proximity coupling is shown to provide low loss broadband coupling for sensors that may be shallowly buried. Focused near-field adaptive phased arrays have previously been used to kill deep cancerous tumors wherein the array focus is located at the tumor target and nulls are placed around healthy tissue to reduce side effects such as burning. Adaptive techniques have usually been required since there is variation in tissue parameters between patients such as tissue density and blood flow. Adaptive phased array technology could also be applied to interrogate deeply buried biosensors.

Potential research topics are identified including:

1. Application specific *in vivo* wireless monitoring of bio-medical functions using RF circuits and variable capacitance based sensors e.g. MEMs for glucose monitoring.
2. Design and analysis of near-field phased array antennas in lossy (dispersive) tissue including:
 - (i) non-uniform plane wave propagation (α , β , $\alpha \cdot \beta \neq 1$ not parallel), and
 - (ii) tuning circuits for compensating for active scan impedance variation (mismatch loss) vs. scan angle θ .
3. Silver nanoparticles are now commercially available and seeing many therapeutic applications including use in wound dressings. Analytical models of electromagnetic mixing properties of silver nano particles of various particle size distribution (~20 - 100 nm) also in human tissue.

Background Subtraction based Application: City Decorative Plantings' Preservation

Short Paper

Aidar Zhetessov

Electrical and Electronic Engineering department
Nazarbayev University
Astana, Kazakhstan
aidar.zhetessov@nu.edu.kz

Dauren Tlekov

Electrical and Electronic Engineering department
Nazarbayev University
Astana, Kazakhstan
dauren.tlekov@nu.edu.kz

Abstract— Thousands of people visit public parks every day during summer resulting in trampled grass lawns and flower plantings and it is very important issue because these plantings act as city decorations and air cleaners. Our approach to this problem is to install surveillance cameras above plantings to be protected. Cameras will send real-time video captures to the monitoring center, where program will use background subtraction technique to determine whether someone stepped on planting. Experiment results show that program works properly: it detects violation, records a video and extracts useful information. Some of problems faced during tests are false positives from shadows and lack of illumination during night. The fact that shadows outdoors are darker and bluer than their surroundings is used to eliminate false positives, while low illumination can be dealt with either by street lights or additional IR cameras utilizing same principle in infrared spectrum region. Approach can be used in private property security service.

Keywords— *planting; camera; violation; background subtraction; video capture; extracted information*

I. INTRODUCTION

Nowadays decorative plantings have become integral part of any public park, showplace and city streets in general. Acting as city adornments and air cleaners, decorative plantings are very important. Therefore, it is necessary to protect them from human impact. This becomes even more important in case of densely populated cities as well as cities of international importance like capitals and touristic centers. A good example of such a touristic center is a Taj Mahal palace in Agra, India. Surrounded by walls, the touristic area comprises several palaces including Taj Mahal as well as many decorative plantings and fountains. It is very hard to preserve this large area clean due to its size and vast number of tourists visiting it every day. Another possible implementation place is Astana city's central park, where we can see many unintended footpaths on grass.

Many people either do not consider this problem significant or have other solution approaches; therefore, our

main contribution to this work is a proposal of new application area for surveillance methods. Another rather technical contribution suggests using rougher but faster human detection method.

Overall, the goal of this work is to develop a “decorative planting protector” algorithm using Open CV computer library.

II. METHODOLOGY

In this section we will explain our solution approach to the problem of plantings. First of all, camera is installed on suitable position. Suitable position is the one, from which a boundary between planting and non-planting as well as some region within the planting are clearly seen. Then we apply background subtraction technique to each frame of the ongoing live capture to differentiate between background (stationary) and foreground (moving) objects. Frame threshold as well as other processing techniques is used afterwards to obtain foreground mask. Foreground mask is a processed form of the frame in which foreground and background objects are shown as white and black pixels respectively. Next we draw the region of interest within the foreground mask to incorporate the planting inside it. The number of white pixels inside mentioned interest region is counted and if it is greater than a predefined threshold value, algorithm will consider violation occurred. Indeed, great number of white pixels inside interest region means that there are foreground objects on planting, which is obviously a violation. On the other hand, small white pixel fluctuations, which can occur due to flowers' movement under wind or illumination changes, should not be considered as violation. Finally, the condition above triggers live video recording and extraction of some useful information to be applied later as a proof of violation. The flowchart visualizes our algorithm, while subsections below will describe the procedure in more detail.

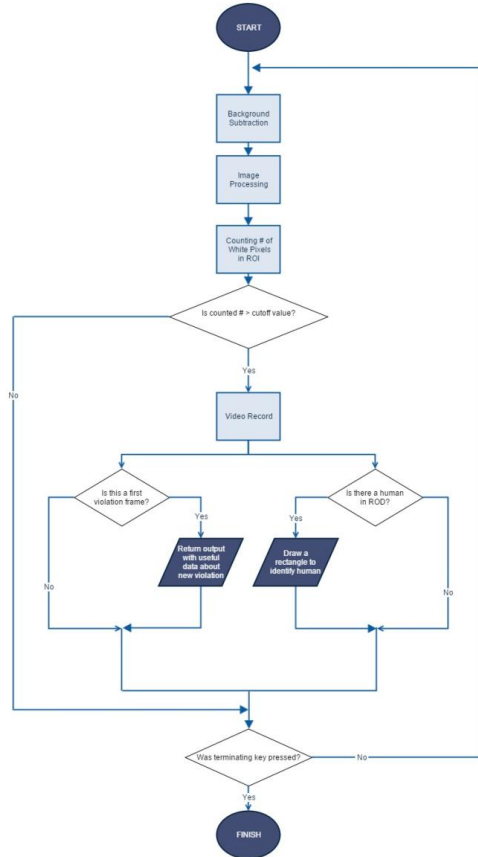


Fig. 1. Single frame process

A. Adaptive background estimation

In this project frame foreground mask was obtained using Mixture of Gaussian 2 (MOG2) background subtraction technique. This choice is justified by several reasons. The first one is that the method estimates several running averages, each one according to the formula:

$$\mu_t = (1 - \alpha)\mu_{t-1} + \alpha p_t \quad (1)$$

Here μ_{t-1} is a current mean pixel value, μ_t is an updated mean pixel value, p_t is current pixel value and α is a learning rate [1]. This allows determining background accurately even if pixel value fluctuates. Second, the method also estimates several variances, which can be used to find the probability of particular pixel value to be part of background. Obtained information is useful for selecting appropriate threshold value for differentiating between foreground and background [1]. Third, the method is trained to accept foreground object as part of background in case of its inactivity and vice versa [1]. Finally, technique deals with shadows and works fast enough to be implemented in real time applications [2].

B. Region of Interest (ROI) definition

To define the ROI we draw a rectangle containing the planting within the foreground mask. Plantings can be various in shapes but for simplicity we observed a rectangular planting, which can be easily incorporated into rectangle. Another assumption was about camera position. We assumed that unclosed boundary divides frame view into two regions – planting and non-planting, meaning that camera does not observe whole planting at once. If it was able to get the whole planting into one frame, boundary would definitely be closed. For better understanding refer to Fig. 2-4.

C. Violation condition

We define two conditions for violation occurrence. The first one states that the number of white (moving) pixels in interest region of the foreground mask should be greater than some cutoff value. It helps to distinguish between significant movements (violations) and insignificant oscillations (flower motion). Second one is initial condition. It states that the first frame does not contain violation. Indeed, when capture is started, first frame's foreground is always white and therefore can be incorrectly treated as violation. This problem does not occur in subsequent frames as algorithm has already learned the first background from the first frame.

D. Useful information extraction

To capture the violation algorithm triggers video recording as soon as conditions above are satisfied. All frames satisfying those conditions are recorded into one video file. If in previous frame no violation took place, while in current frame it happened, meaning that current frame is the first one recording new violation, algorithm returns useful information about violation number, current live capture frame number and recording frame number. These returned data can be used to determine number of violations, occurrence time of each violation and its respective frames in recorded video.

Other useful information to extract is presence of people during violation. Indeed, we do not want to bother ourselves with every bird, dog or wind blow. On the other hand, we do not want to make our application slow because of precise but bulky human detection techniques such as cascade classifier and HOG descriptor [3]. In fact, both these techniques were tested in real time application and did not give satisfactory computation speed. To deal with this problem we define own classifier, which is not as precise but nevertheless good enough to distinguish between human and cat, for example.

Firstly we define new rectangular region within foreground mask called region of detection (ROD). ROD is slightly greater than ROI, so ROD includes ROI. ROD's dimensions are picked up such that exactly one person can fit in the gap between ROD and ROI (Fig. 6). ROD can be thought of as neighborhood of ROI, so when violation occurs, algorithm draws contours of all the foreground objects in the ROD and encloses them into red rectangle in case they satisfy the constraints. Constraints are introduced to distinguish human and include expected area and dimensions' ratio. All the objects with area greater than some value and aspect ratio in

the neighborhood of 3 (that is approximation for human height/width) are treated as humans and therefore warning about human presence is returned. In recorded video they are also enclosed into red rectangle. Although this method is very rough, it is quite sufficient in our case because we need qualitative rather than quantitative analysis. Moreover, it does not slow down program's performance.

III. RESULTS

This section is about obtained results. Since plantings outdoors have not bloomed yet, trials were conducted inside Nazarbayev University atrium. Several videos were recorded on iPad's camera, which sent captured frames to computer through Wi-Fi connection. Overall performance was quite good as the program always correctly responded to violation. Example frames are represented below.



Fig. 2. Background overview



Fig. 3. Region of Interest



Fig. 4. Region of Detection



Fig. 5. No violation and violation frame samples



Fig. 6. ROD foreground in case of non-violation and violation

A significant movement # 1. Frame # in live capture: 535
 Frame # in recorded violation video: 1
 Human participated violation

Fig. 7. Returned useful information

Here Fig. 2 shows background view of one of the scenes. Planting – non-planting boundary here is unclosed and clearly seen. Moreover, it precisely cuts out planting's rectangular region – region of interest, which can be observed in Fig. 3. Region of detection shown in Fig. 4 has its height greater than that of ROI by the value of human height. This can be seen in Fig. 6, which depicts ROD's foreground mask in two cases. Actual frame samples are shown in Fig. 5. People in right picture were enclosed in rectangles because they were in ROD during violation. People on left picture were not enclosed even if they were in ROD because at that time no violation occurred. Note that only right frame will be recorded, since it's the one with captured violation. Fig. 7 depicts returned useful information including violation serial number as well as respective frame in live capture and recorded violation video. These can be used to find out violation occurrence time and total number of violations within given time interval. Also one can check whether people participated to particular violation or not.

IV. DATA ANALYSIS

Here we interpret the results, discuss their meaning and importance, relate them to similar works and provide insight into future improvements. Frames in Fig. 5-6 obtained from one of the trials suggest that algorithm works well in trial conditions in the way that it does not draw contours of people walking nearby when there is no violation even if they are in detection region. Also we see that algorithm does not draw small rectangles associated with planting movements under walking human even if its contours are determined (right picture in Fig. 6). Moreover, proper usage of threshold and advantage of selected background subtraction method resulted in algorithm indifference to shadows. However, sometimes it has problems with permanent enclosing a person into rectangle during violation and splitting large bounding box into right number of rectangles. Barićević D. and Delibaltov

D. have encountered similar problems in their project. Their proposed solution to the first problem was to add tracking algorithm, which is thoroughly explained in their paper. To solve the second problem they suggested counting white pixels column-wise and applying threshold to resulting foreground mask's histogram. By doing that, they got correct number of tracking objects in each frame [4]. We can use these ideas for improvement of our work in future

Returned response in Fig. 7 implies that in general algorithm returns output accurately. All useful data is represented in understandable way, but the problem is that sometimes algorithm considers new frame as part of new violation while in reality it's continuation of old one. To deal with this problem we can introduce another boundary condition stating that new violation can start only after some time interval since end of previous violation; otherwise captured frames are part of that violation.

V. CONCLUSION AND RECOMMENDATIONS

To sum up, this work develops real time surveillance algorithm for decorative planting's preservation. Adaptive background estimation helped adjusting to various lighting conditions. Inner part of introduced interest region comprised whole planting. Then violation condition was imposed on that region. Response, triggered by the condition, includes estimation of violation's serial number, its respective frame number in live capture and recorded video as well as statement on human presence. Algorithm can be used in private property surveillance system or as a foundation for further improvement of similar projects.

Acknowledging weaknesses, algorithm had problems with permanent human detection and distinguishing between

separate violations. These can be solved by adding tracking and column-wise counting separation methods as well as imposing timing condition as it was explained in data analysis section.

Also observable plantings were limited by some assumptions like interest region's form and boundary nature, which are dependent to camera position. Revising application for other plantings would need more elaborated work and our project can act as starting point for those.

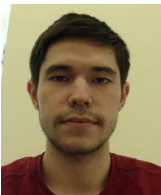
Although algorithm deals with shadows, it is useless in no light conditions. Therefore, for night surveillance one can use IR cameras as it was explained by Ju Han and B. Bhanu [5].

VI. ACKNOWLEDGEMENT

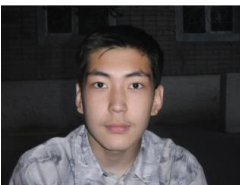
We would like to thank our reviewers for their useful comments. Also special thanks to our fellow students Serikbolsyn Myrzakhmet and Abzal Adilzhan for their useful comments and help in video recording.

VII. REFERENCES

- [1] R. Laganiere, *OpenCV 2 Computer Vision Application Programming Cookbook*. Birmingham: Packt Pub., 2011.
- [2] T. Bouwmans, F. Porikli, B. Höferlin and A. Vacavant, Background modeling and foreground detection for video surveillance.
- [3] Navneet Dalal and Bill Triggs. Histograms of oriented gradients for human detection. *IEEE Computer Society Conference on Computer Vision and Pattern Recognition*, pages 1063–6919, 2005.
- [4] Barićević D., Delibaltov D., *Bike/Pedestrian Tracking and Classification*.
- [5] Ju Han and B. Bhanu. Detecting moving humans using color and infrared video. *IEEE International Conference on Multisensor Fusion and Integration for Intelligent Systems*, 30:228–233, 2003.



Aidar Zhetessov was born in Karagandy, Kazakhstan on November 15, 1995. He has finished Kazakh-Turkish high school in Astana on May 25, 2013. During high school years, he participated to physics Olympiads and reached some achievements, the brightest of which was Silver Medal award in International Physics Olympiad. Because of this achievement, he was admitted directly to undergraduate program at Nazarbayev University, where he is currently seeking for his bachelor degree in Electrical & Electronic Engineering.



Dauren Tlekov was born in Aktobe, Kazakhstan, in 1995. He received the academic degree from the Kazakh-Turkish Lyceum high school, Aktobe, Kazakhstan, in 2013. When he was 17 years old, he started to participate in math competitions, the best one of which was Silver Medal award in International Zhautykov Olympiad, Almaty, Kazakhstan. In 2014, he was admitted to Nazarbayev University as a direct student of School of Engineering. Currently, he is trying to receive his B.E. degree in Electrical and Electronic engineering at Nazarbayev University, Astana, Kazakhstan.

CFD Modeling of Hemolysis in Medical Devices used in the Treatment of Cardiovascular Disease (CVD)

L. Rojas-Solórzano¹, T. M. Mubita², Mansur Zhussupbekov¹ and LyazzatZhanshayeva¹

¹ School of Engineering, Nazarbayev University, Astana, 010000, Rep. of Kazakhstan.

² Dept. of Thermodynamics and Transport Phenomena, Simon Bolivar University, Caracas, 89000, Venezuela.

Corresponding author: luis.rojas@nu.edu.kz

Abstract—Designing blood-wetted devices (i.e., parts of artificial organs or accessories to interface the blood treatment or medication process) requires special attention to avoid the generation of trauma to blood cells, either by lack of biocompatibility or by exposing blood cells to high shear stress during an extended period of time.

This investigation focused on the prediction of mechanical hemolysis through stenotic connectors, when blood is modeled as a non-homogeneous fluid composed by plasma, red blood cells and platelets. Thus, firstly, a multiphase model is tuned up to capture the non-uniform distribution of blood cells and secondly, the damage differential equation, based on Giersiepen's correlation, was applied only to the red blood cells, improving the prediction of hemolysis generation. It is demonstrated that this segregated multiphase model gives a much closer estimate of blood hemolysis than obtained values through typical numerical homogeneous models.

NOMENCLATURE

CCS	Comparative Shear Stress
F	Force terms (e.g. lift force, virtual mass, and drag)
g	Gravity
$\frac{H_L}{H_L}$	Normalized linear index of hemolysis
$\overline{H_L}$	Average hemolysis index
H_b	Plasma hemoglobin
H_{GW}	Damage fraction
H	Cell, mesh, or grid size
I	Unit tensor
MIH	Modified index of hemolysis
p_k	Pressure shared by all phases
RBC	Red Blood Cells
Q	Flow rate
R_{kp}	Interaction force coefficient between phases
\mathbf{u}_k	Velocity vector of phase k
VAD	Ventricular Assist Devices
t	Time
\mathcal{H}	Average value of hemolysis index at domain outlet
α_k	Volume fraction of phase k
Γ	Boundary of computational domain
λ_k	Bulk viscosity
μ_k	Dynamic viscosity
ρ_k	Density fraction
σ_k	Stress tensor of phase k
τ	Shear stress
Φ	Diameter

I. INTRODUCTION

The treatment of cardiovascular disease (CVD) many times require the use of assist devices, interfaces, connectors, etc., that need to operate in direct contact with the blood stream and therefore are usually named blood-wetted components or devices (BWD). However, there are significant challenges to overcome due to the un-physiological conditions generated inside these devices, which lead to complications including alterations of normal blood function taking the form of damage to erythrocytes (hemolysis), activation of platelets and leukocytes, as well as thrombosis [1].

The hemolysis is typically caused by the destruction of membrane integrity of red blood cells (RBC), e.g., pore formation or rupture and the release of hemoglobin from the erythrocyte into the plasma. In BWD, mechanical damage resulting from high shear stress levels and exposure times to these stress levels are the main cause of hemoglobin release [2]. Correlations were established under the assumption of experimentally feasible conditions, which implied hemolysis under steady shear at short time intervals. The most widely used model was developed in [3] as a power law function for the damage fraction, H_{GW} , based on *in vitro* hemolysis data [4] in a Couette system in which human RBC suspension was exposed to defined shear stresses τ , for defined times, t :

$$H_{GW} = 3.62 \times 10^{-7} \tau^{2.416} t^{0.785} \quad (1)$$

Power law correlations as Eq. (1) have been implemented in CFD calculations using post processing techniques in Lagrangian and Eulerian frames of reference, as well as by solving transport equations for damage fraction (H_{GW}). In the Lagrangian particle tracking approach, the damage function is applied theoretically to individual cells within the flow field. The temporal variation however, raises the question of how to map the damage criteria obtained by constant-shear experiments to a cyclical or arbitrary shear history found typically along the trajectory of a blood cell [5]. Reference [6] shows a recent employment of a fluid-structure-interaction (FSI) approach to obtain detailed behavior of the flow inside aortic valve prostheses, resolving all the spatio-temporal scales by means of Direct Numerical Simulation. They considered modifications of the power law correlation to assume: (a) an instantaneous reaction of the RBCs to shear or; (b) an

equivalent stress associated to the deformation of the RBC in the flow, based on phenomenological similarity in shape between droplet and RBC under shear flows. In the first case the model takes into account the load history previously sustained by the blood cell predicting higher blood damage than the second case.

In the spatial non-uniformity addressed by implementation of an Eulerian approach, the damage index is integrated over all the cells in the numerical space. For example, a hyperbolic advection equation to assess a linearized damage function based on the Giersiepen-Wurzinger blood damage correlation is thoroughly derived in [7].

In spite of the intense research on blood damage modeling, there is currently no consensus on suitable models that relate fluid dynamics information, such as stress and shear rate, to clinical properties, such as the modified index of hemolysis (MIH).

II. NUMERICAL MODEL SETUP

An Eulerian multiphase flow model where the plasma is taken as the continuous phase, while red blood cells and platelets are taken as the fluid dispersed phases is proposed. The cells interact strongly with the plasma via interface momentum transfer, but not cell-to-cell or cell-to-wall interaction is considered in this first attempt.

A. Computational domain and boundary conditions

Two benchmark connectors from [8] were chosen for this study taking advantage of the availability of experimental data and the very subtle differences in their design and marked singular hemolysis generation in each one of them.

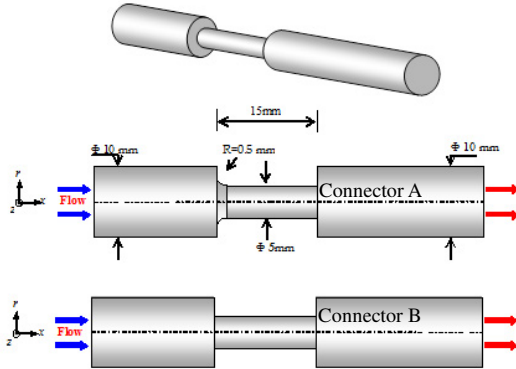


Fig. 1. Computational domain close up, starting with the full 3-D view of the stenotic connector.

Fig. 1 illustrates a schematic of the computational domains showing the connectors with their abrupt inner diameter reduction from 10 mm to 5 mm, stenosis length of 15 mm and further expansion back to 10 mm. Connector type (A) has an

identical design to type (B), but the leading edge of stenosis was radiused ($R=0.5$ mm) as shown in Fig. 1.

The numerical simulations were performed using an Eulerian-Eulerian multiphase model. The blood is considered as a fluid that consists of plasma, RBCs and platelets (PLTs). The plasma is modeled as a continuous fluid with a viscosity of 0.0012 [Pa s] and a density of 1025 [kg m^{-3}]; RBCs and platelets are taken as a spherical particle-like fluid dispersed with a density of 1100 [kg m^{-3}] and 1040 [kg m^{-3}], respectively. Continuous and dispersed phases are modeled as isothermal and Newtonian viscous fluids. A Sauter mean diameter of $6 \mu\text{m}$ for RBCs and $2.0 \mu\text{m}$ for PLTs were taken. In this study the viscosity of the dispersed phases are considered to be constant through the computational domain, with a value of 0.002 [Pa s].

Initially, the whole tube was full of the mixture of plasma, RBCs and platelets with uniform volume fractions of 58%, 40% and 2%, respectively. The inlet velocity profile was assumed to be fully developed and zero-pressure boundary condition at the exit of the domain. A non-slip condition was assumed at the walls.

B. Computational methodology

The numerical simulations of the 3D, steady, laminar, multiphase flow in the computational domain was performed using ANSYS-CFX © v12. The numerical model here proposed is based on the Eulerian-Eulerian approach where no energy equation was considered, therefore the mass conservation and volume fraction (Eqns. 2-3), momentum (Eq. 4), turbulence and damage (Eqns. 6-8) were the governing equations for the model:

$$\frac{\partial \alpha_k \rho_k}{\partial t} + \nabla \cdot (\alpha_k \rho_k \mathbf{u}_k) = 0 \quad (2)$$

Phase volume fractions must accomplish that:

$$\sum_{k=1}^n \alpha_k = 1 \quad (3)$$

Momentum equation:

$$\begin{aligned} \frac{\partial}{\partial t} (\alpha_k \rho_k \mathbf{u}_k) + \nabla \cdot (\alpha_k \rho_k \mathbf{u}_k \mathbf{u}_k) \\ = -\alpha_k \nabla p_k + \nabla \cdot \sigma_k + \alpha_k \rho_k \mathbf{g} \\ + \sum_{p=1}^n R_{kp} (\mathbf{u}_k - \mathbf{u}) + F \end{aligned} \quad (4)$$

Where:

$$\sigma_k = \alpha_k \mu_k (\nabla \mathbf{u}_k + \nabla \mathbf{u}_k^T) + \alpha_k \left(\lambda_k - \frac{2}{3} \mu_k \right) \nabla \cdot \mathbf{u}_k \mathbf{I} \quad (5)$$

As the local Reynolds number in the stenotic nozzle exceeds 3200, turbulence effects were considered by applying the shear stress transport (SST) model with a low turbulence intensity at the entrance. This is a hybrid turbulence model which uses the $k-\epsilon$ model in the fully turbulent region far from the wall and the $k-\omega$ model in the near wall region. The SST turbulence model has previously proven to be appropriate and enough accurate in the prediction of fundamental features of turbulent flows

through small connectors [9] and therefore, will not be scrutinized in this investigation.

Numerical predictions of the mechanical blood hemolysis were obtained by applying the methodology proposed [10]. However, as mentioned before, in this work the hemolysis predictions were computed over the entire domain through damage transport equation (Eqns. 6-8), weighted by the RBCs volume fraction to enforce damage prediction only where RBCs are expected to be located.

$$\left(\frac{\partial}{\partial t} + \bar{u} \cdot \nabla\right) H_L = \vartheta(1 - H_L) \quad (6)$$

where:

$$\vartheta = (3.62 \times 10^{-7})^{1/0.785} \tau^{2.416/0.785} \quad (7)$$

$$H_L = H_{GW}^{1/0.785} \quad (8)$$

To compute the scalar shear stress field, the full stress tensor is reduced to a single comparative scalar value which has the following form in terms of the tensor components:

$$\tau_{CSS} = \sqrt{\frac{1}{2}(\tau_{11}^2 + \tau_{22}^2 + \tau_{33}^2) + (\tau_{12}^2 + \tau_{13}^2 + \tau_{23}^2)} \quad (9)$$

$$\tau_{CSS} = \sqrt{\frac{1}{2}\tau_{ij}\tau_{ji}} \quad (10)$$

Assuming Newtonian fluid, then:

$$\tau_{CSS} = \mu \sqrt{\frac{\partial u_i}{\partial x_j} \left(\frac{\partial u_i}{\partial x_j} + \frac{\partial u_j}{\partial x_i} \right)} = \mu \sqrt{\frac{\partial u_i}{\partial x_j} S_{ij}} = \mu S \quad (11)$$

For turbulent regime an analogy with the case of viscous stresses is done by replacing the elements from Eqn. 9 by the appropriate Reynolds stresses and considering the product of the effective viscosity on shear rate:

$$\tau_{CSS,T} = (\mu + \mu_T)S = \mu_{eff}S \quad (12)$$

Hemolysis results are presented in the form of MIH following the definition developed in [7]:

$$MIH = \mathcal{H}10^6 \quad (13)$$

Where

$$\mathcal{H} = (\bar{H}_L)^{0.785} \quad (14)$$

The average hemolysis index \bar{H}_L is computed by integrating the value of H_L over the outflow boundaries of the computational domain (Γ_+), which would then correspond to in vitro hemolysis experiments[11]:

$$\bar{H}_L = \frac{1}{Q} \int_{\Gamma_+} \mathbf{u} \cdot \mathbf{n} H_L d\Gamma_+ \quad (15)$$

C. Verification of grid independency

A second-order discretizationscheme was used to calculate the advection terms in the discrete finite volume equations. The

standard calculation is case dependent and takes a CPU time from 8 to 36 hours on a processor AMD Turion⁶⁴ with operative systems MS Windows 7, SP2.

In order to corroborate that the solution is independent of the grid resolution, a study of grid convergence was undertaken. With this study, the truncation error is reduced and the best degree of grid resolution is defined. The method consists in starting with an initial grid and then, make consecutive refinements to observe the effect of the grid [12]. The chosen method for discretization error estimation is the Grid Convergence Index (GCI) based on the Richardson Extrapolation (RE) method, that involves comparisons between three different grid sizes [13].

In order to quantify the discretization error, the systematic procedure recommended by Celik was followed.

Three structured and stepped grids (coarse, medium and fine) with hexaedricalelements were prepared by using ICEM (ANSYS, USA); the finite elements mesh carefully modeled the near-wall region. Table I, gives the number of computational cells for each one of the meshes generated. The refinement factors $r_{21}=h_{\text{medium}}/h_{\text{fine}}$ and $r_{32}=h_{\text{coarse}}/h_{\text{medium}}$ were 1.3.

TABLE I
MESHES USED IN GRID INDEPENDENCY STUDY

Mesh	Elements
Coarse	35,856
Medium	86,144
Fine	231,000

The PLTs volume fraction for three meshes and the corresponding discretization error estimation in form of errors bars for the fine grid are shown in Fig. 2. The three grids used with the GCI method show that the apparent order of accuracy ranges from 0.14 to 9.66 %.

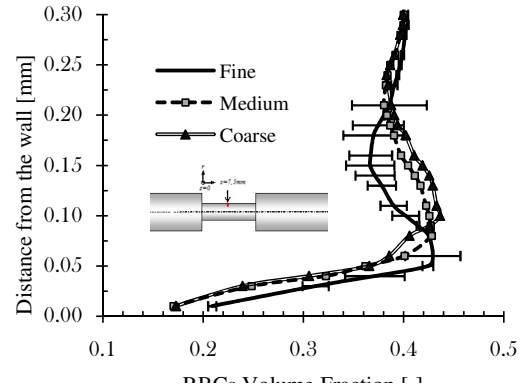


Fig. 2. Platelets concentration in a section of the tube obtained for three different meshes; with discretization error bars at the fine grid for connector A.

D. Validation of multiphase segregation model

The validation of the multiphase segregation model was performed on the goal of reproducing the Fahraeus-Lindqvist (F-L) phenomenon described in [14] as the forced segregation of platelets towards the walls when blood flow is established in small straight conducts. To validate the segregation model, two different geometries, shown in Fig. 3 where the F-L phenomenon has been observed were assessed.

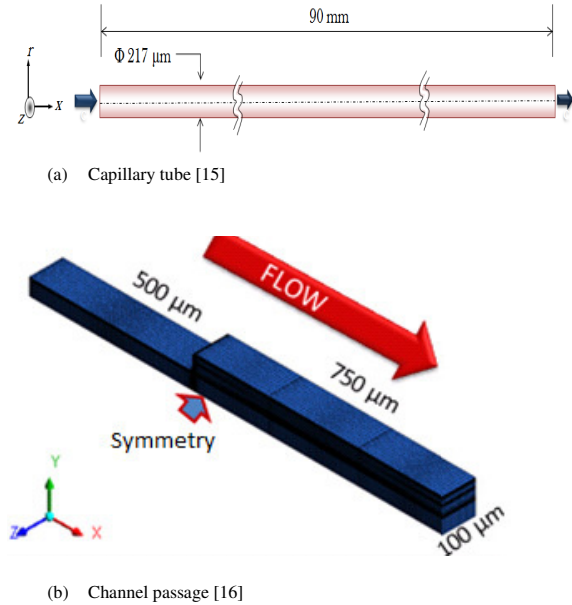


Fig.3. Computational domains to test segregation model for: (a) Capillary tube; (b) Channel passage.

The capillary tube inlet condition was adjusted to obtain a 555 s^{-1} shear rate, as used in the experiments, which resulted in a homogeneous velocity of $1.505\text{E-}02 \text{ m/s}$. The inlet flow condition for the channel passage was set to 15 mL/h to equally match experimental data. Both cases were simulated with the multiphase model using 40% and 2% volume fraction of RBCs and PLTs, respectively. The conditions of the disperse phases (RBC's and PLTs) were varied assuming solid-solid, liquid-liquid and liquid-solid spherical particles along a liquid background (Plasma) to assess also any differences on that regard. Mesh verification was again performed and results are presented with a verified mesh.

Fig. 4 depicts the F-L phenomenon computed using the multiphase model with different configuration of phases for the capillary tube and with the liquid-liquid disperse configuration for the channel passage (after observing in the former, that this was a reasonable best fit model option). In both geometries, the enhancement of the PLTs concentration towards the wall is clearly captured and a peak concentration lies in about the same region where experiments found it. However, none of the two

simulated geometries could depict the same magnitude in the PLTs concentration peak, opening space to discuss future improvements in the model. Nevertheless, capturing the segregation and peak location observed in the F-L phenomenon represents an important achievement of the model.

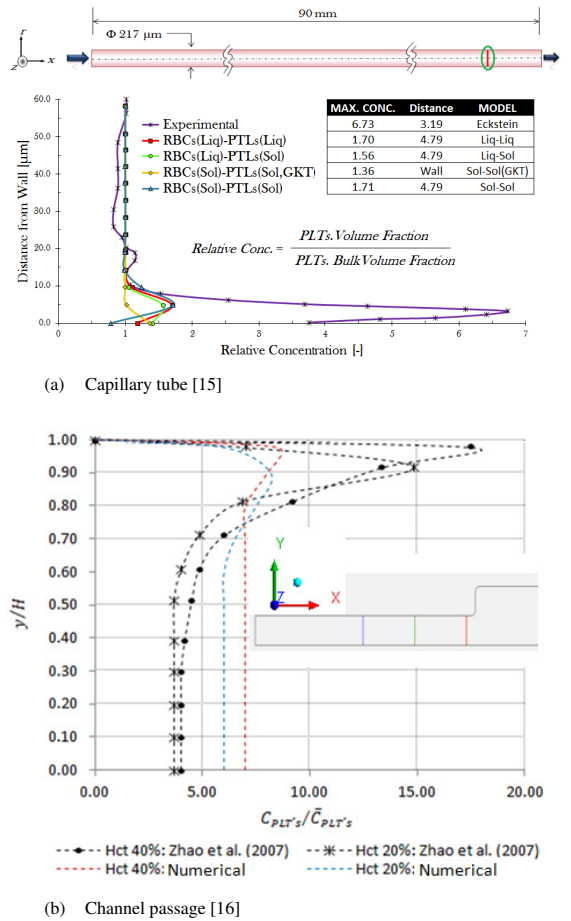


Fig. 4. Computed vs. Experimental F-L effect in: (a) Capillary tube; (b) Channel passage.

Next section presents the assessment of the hemolysis using the proposed model, acknowledging the underprediction of concentration of PLT's near the walls and in turn, the overprediction of RBC's in the same region. This overprediction of RBC's concentration in the region where the larger shear stresses occurs will be considered in the discussion of results.

III. RESULTS AND DISCUSSIONS

As stated previously, the shear stress (τ) can be regarded as the main biomechanical cause of the occurrence of induced hemolysis and according to [17] the blood cell damage is different in laminar and turbulent flow; so, it is important to establish an accurate way to calculate τ and avoid overestimation in the calculation of damage. Usually, such blood damage is predicted as functions of viscous shear stress (for laminar flow) or Reynolds stress (for turbulent flow), on the basis of in vitro experiments on blood.

Although, flow along the connectors is turbulent in this research the dynamic and effective viscosity were both considered in the calculation of the shear stress to compare the influence in the hemolysis estimation and for a quantitative assessment of potentially critical flow regions inside the domain. Figures 5a and 5b show viscous and turbulent wall shear stresses, respectively, in a plot representing a section through the connector on a plane placed in axial position of the connector A.

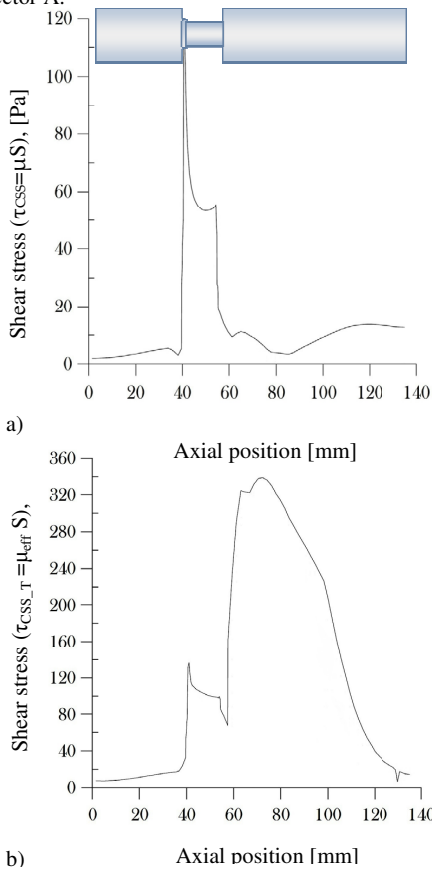


Fig. 5. Distribution of shear stress on an axial plane through connector A: a) Viscous stresses; b) Turbulent stresses

The computed results show that wall shear stresses obtained at the inlet and the stenosis area are quite similar in average for both cases; however, a critical zone inside the nozzle or region where it is expected the highest damage are different considering that there is a threshold shear stress, 150 Pa, above which extensive cell damage is expected [18]. It can be seen that turbulent stresses are higher than viscous stresses in the outlet region of the contraction; this means that hemolysis occurrence is more severe in that area (Fig. 6) and not in the stenosis which differs from what was intuitively expected, since the abrupt reduction in diameter at the stenosis entrance were expected to be the hot spot area of hemolysis generation inside the connector.

When only viscous stresses are taken into account almost no hemolysis occurs, since stresses barely reach up the critical value for which the total rupture of the RBCs is considered.

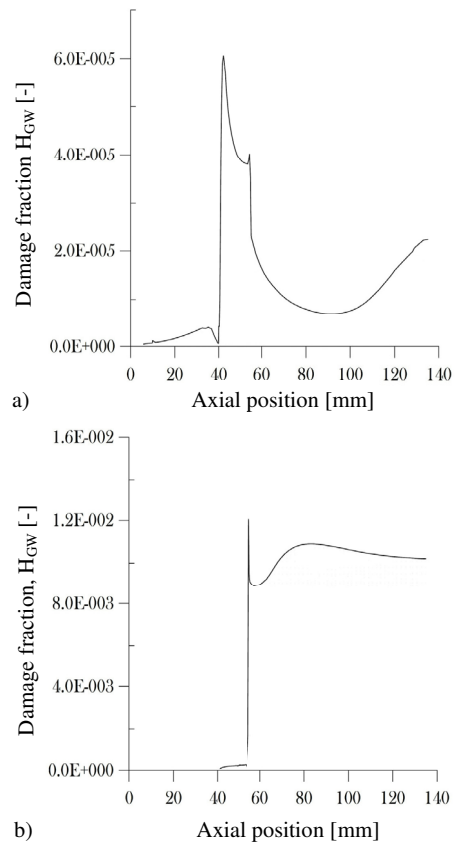


Fig.6. Damage fraction computed for connector A with: a) Viscous stresses; b) Turbulent stresses

The analysis suggests that Reynolds stress is not adequate as a predictor of cell loading in the calculation of the hemolysis in turbulent regime; indeed the time-average stress acting on fluid cells should be computed as defined by the Newtonian constitutive law with the molecular viscosity in Eqn. 11, using the mean velocity field computed with assumption of the eddy viscosity. Using the shear stress as resulting from the mean velocity and the effective viscosity (Eqn. 12) would lead to overestimation of the damage. On this regard, it is fundamental to recall the origin of the eddy viscosity, which is a mathematical term that appears as a fluctuating exchange of momentum when using Reynolds averaging, and that is conveniently associated, via Boussinesq's assumption to the diffusive component of the momentum equation. Therefore, the use of the eddy viscosity is merely to produce a closed form to the Reynolds Averaged Navier-Stokes (RANS) equations and represents a convective term more than a diffusive one. Therefore, in this investigation only the molecular viscosity is used to calculate the CSS.

In order to estimate and classify the connectors in terms of total damage generated and compared with results obtained in [8], the Modified Index hemolysis (MIH) is calculated by using the formulation proposed in [10]. The numerical methodology used to estimate the RBCs damage premised that the variation of the concentration of free hemoglobin into the plasma per unit time is constant, which implies that addresses the problem of hemolysis generation from a macroscopic view. Tables II and III show the experimental value of MIH after six hours of flow through the connector type A and B type and those obtained numerically by modeling blood as a multiphase fluid, and the comparison of the former with the results considering a homogeneous model, respectively.

TABLE II
COMPARISON OF EXPERIMENTS AND HEMOLYSIS PREDICTIONS (MIH) FOR THE TWO CONNECTORS, USING A MULTIPHASE MODEL

Connector Type	Umezū <i>et al.</i> (1992) [8]	Multiphase model
A	1.32	5.52
B	4.45	19.77

When the damage occurrence is analyzed in both connectors, it can be observed that the rate of damage is greater in connector type B, in which the inlet to the stenosis section is not curved. This implies that the shape of the inlet has a dramatic influence on hemolysis generation. When Umezū and colleagues compared the results obtained in both connectors, determined that this slight change in the internal form of stenosis contributed to a 70% reduction in hemolysis. Although, numerically the multiphase model is still overestimating the hemolysis generation, it is capturing approximately the same rate of change between connector A and B that was measured experimentally.

TABLE III
COMPARISON OF MIH PREDICTIONS FOR CONNECTOR A, USING MULTIPHASE AND HOMOGENEOUS MODELS

Homogeneous Model	Multiphase model	Umezū <i>et al.</i> (1992) [8]
37.05	5.52	1.32

It is clearly observed how the segregated multiphase model accounted much better the RBC damage than the homogeneous model. The hypothesis of calculating the damage only where RBC's should be positioned proved to be effective and led to better results than traditional homogeneous model. Nevertheless, it must be accounted that the current multiphase model despite capturing the F-L phenomenon, still has an important underprediction of the peak concentration of PLT's close to walls and therefore an overestimation of RBC's present in that region (see Fig. 4). Reducing the gap to refine the prediction of the F-L effect may reduce even further the estimation of hemolysis in the connectors getting much closer to experiments. This surely should be one of the key validation goals when further improvements will be added to current multiphase model in this ongoing research.

IV. CONCLUSION

A multiphase numerical methodology to estimate blood damage associated to flow through medical devices has been proposed in order to estimate hemolytic damage. The proposed model allows to establish with acceptable accuracy the distribution of cells through flow micro-connectors and applies the damage correlation proportionally to the concentration of RBC in every location. Results showed a marked decrease in the over-estimation typically obtained from homogeneous Eulerian-Eulerian models. Nevertheless, further development is needed in the multiphase model to account for extra phenomena not considered yet, but preliminary envisioned.

ACKNOWLEDGMENT

The authors gratefully acknowledge the Deanship of R&D at Simon Bolívar University for their financial support through a Research Assistantship grant awarded to Tania Mubita to perform this investigation. Also, we want to thank Nazarbayev University for the support of this investigation through the Research Seed Grant № KΦ-14/11.

REFERENCES

- [1] Fraser, K., Taskin, M., Griffith, B., & Wu, Z. (2011). The use of computational fluid dynamics in the development of ventricular assist devices. *Medical Engineering & Physics*, 33, 263-280.
- [2] Arwatz, G., Smits A.J. (2013). A viscoelastic model of shear-induced hemolysis in laminar flow. *Biorheology*, 50, 45-56.

- [3] Giersiepen, M., Wurzinger, L., Opitz, R., & Reul, H. (1990). Estimation of shear stress related blood damage in heart valve prostheses in vitro comparison of 25 aortic valves. *Artificial Organs*, 13 (5), 300-306.
- [4] Wurzinger, L., Opitz, R., & Eckstein, H. (1986). Mechanical blood-trauma. An overview. *Angiologie*, 38, 81-97.
- [5] Wu, J., Antaki, J., Snyder, T., Wagner, W., Borovetz, H., & Paden, B. (2005). Design optimization of blood shearing instrument by computational fluid dynamics. *Artificial Organs*, 29 (6), 482-489.
- [6] De Tullio, M. D., Nam, J., Pascazio, G., Balaras, E., & Verzicco, R. (2012). Computational prediction of mechanical hemolysis in aortic valved prostheses. *European Journal of Mechanics B/Fluids*, doi:10.1016/j.euromechflu.2012.01.009.
- [7] Garon, A., & Farinas, M. (2004). Fast Three-dimensional Numerical Hemolysis Approximation. *Artificial Organs*, 28 (11), 1016-1025.
- [8] Umezu, M., Murayama, Y., Nogawa, A., & Kijima, T. (1992). The Effects of Inner Shapes of Plastic Connectors Blood in a Extracorporeal Circulation. *7th International Conference on Biomedical Engineering* (pp. 197-199). Singapore: JCH GOH & A Nather.
- [9] Salazar, F., Rojas-Solórzano, L., & Blanco, A. (2008). Turbulence modeling in the numerical estimation of hemolysis in hemodialysis cannulae. *Revista de la Facultad de Ingenieria U.C.V*, 23 (4), 93-98.
- [10] Farinas, M., Garon, A., Lacasse, D., & N'dri, D. (2006). Asymptotically Consistent Numerical Approximation of Hemolysis. (ASME, Ed.) *Journal of Biomechanical Engineering*, 128, 688-696.
- [11] Lacasse, D., Garon, A., & Pelletier, D. (2007). Mechanical hemolysis in blood flow: user-independent predictions with the solution of a partial differential equation. *Computer Methods in Biomechanics and Biomedical Engineering*, 10 (1), 1-12.
- [12] Celik, I. (2008). Procedure for estimation and reporting of discretization error in CFD applications. *J. of Fluid Engineering*, 130, 1-4.
- [13] Roache, P. (1994). Perspective: A method for uniform reporting of grid refinement studies. *J. of Fluids Engineering*, 116, 405-413.
- [14] Eckstein, E., & Belgacem, F. (1991). *Biophys. Journal*, 60, 53-69.
- [15] Yeh C., Calvez A., Eckstein E. (1994). *Biophysical Journal*, 67, 1252-1259.
- [16] Zhao, R., Kameneva, M., & Antaki, J. (2007). Investigation of platelet margination phenomena at elevated shear stress. *Biorheology*, 44, 161-177.
- [17] Kameneva, M., Burgreen, G., Kono, K., Repko, B., Antaki, J. & Umezu, M. (2004). Effects of turbulent stresses upon mechanical hemolysis: experimental and computational analysis. *ASAIO Journal*, 50, 418-423.
- [18] Leverett, L., Hellums, J., Alfrey, C., & Lynch, E. (1972). Red Blood Cell damage by Shear Stress. *Biophysical Journal*, 12, 257-273.

Control of automobile audiosystem by gestures

Abuzhan Aidaraliyev

Electrical and Electronic Engineering
Nazarbayev University
Astana, Kazakhstan
abuzhan.aidaraliyev@nu.edu.kz

Dauren Leskhan

Electrical and Electronic Engineering
Nazarbayev University
Astana, Kazakhstan
dauren.leskhan@nu.edu.kz

Abstract. Distraction of the driver by automobile audio system appears to be one of the main causes for accidents. Finding alternative solution of controlling audio systems may decrease the risk of crashes and fatalities. Following project describes gesture control of such systems. The work seems to be effective and cheap solution for the problem. (Abstract)

Keywords—automobile; gesture recognition; audio system; distraction; programming.

I. INTRODUCTION (HEADING 1)

Nowadays automobiles are the most widespread type of transport. The statistics show that there are more than 1.2 billion cars around the globe and this number is increasing gradually [1]. However, automobiles appears to be the most dangerous vehicles too, since the National Center for Statistics and Analysis reported that only in America there were about 7000 fatalities on the road in the first quarter of 2014 [2]. One of the main causes of numerous car crashes is distraction of the driver by different devices in the vehicle. These can be mobile telephone, audio system or eating food during the trip [3]. The following project was aimed to decrease potential distraction sources by focusing on the audiosystems. It can be visible that the possibility of controlling the device without the necessity of looking at it would be significantly helpful in this case. Hence, using hand gestures for making changes in the work of the system seems to be the most efficient solution. Our project seems to play considerable role in decreasing the road accidents and in saving people's lives. The followed research in this area showed that there are similar technologies existing in the current automobiles, however, most of them are implemented in the high class cars with an extremely expensive prices. Therefore, another objective of the work was to make the whole system as cheap as possible in order to provide the opportunity of using it to almost every car driver. This can be achieved by applying light structure, available components and simple coding. We created a C++ program involving OpenCV GUI that uses usual camera of 0.3 megapixels to analyze the real time image on the presence of gestures that were stored earlier.

II. IMPLEMENTING THE IDEA

Our project requires the program to read the hand gestures and apply appropriate function in accordance with them. For instance, moving an open hand to right or left sides will

change the stations or audio tracks, up and down will help to control the volume while raising a fist will play or stop the music. These goals were achieved by programming the system to obtain and analyze the real time video from the camera and send appropriate commands to the audio system. It is understandable that to work with the gesture recognition there is a need to obtain specific binary image of the environment, where hand will be treated with the white color, while background with black. It is one of the simplest algorithms to be implemented in our case.

A. BGR to HSV

In order to do this several possible variants were studied and analyzed where the most appropriate ones - Background Subtraction method and conversion of original image to the one with HSV format (Figure 1) which further is configured to the binary were chosen to further consideration. The initial draft of the project used the first method, however, the review of the work demonstrated that second variant seem to be more stable for our conditions.

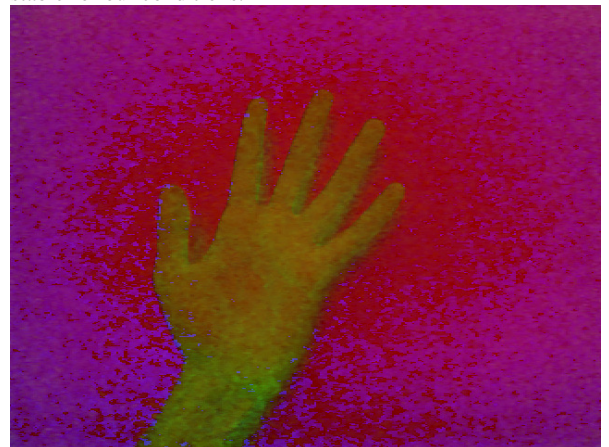


Figure 1. HSV format.

B. HSV to Binary

The conversion of the original BGR format to HSV one, and applying appropriate configurations to stabilize image and subtract unnecessary noises leads to the binary output which is represented in the Figure 2.



Figure 2. Binary representation of the hand.

C. Object Tracking

After that, the program starts analyzing contours of the hand in order to find geometrical centre. By pointing it and tracking the point program evaluates the behavior of the hand motion. We put the borderlines at each edges of the image which are used to examine if the hand crosses them (Figure 2). For example, if geometrical centre crosses right borderline, it means that hand moved to the right side, what in its turn will cause the audio track to change.

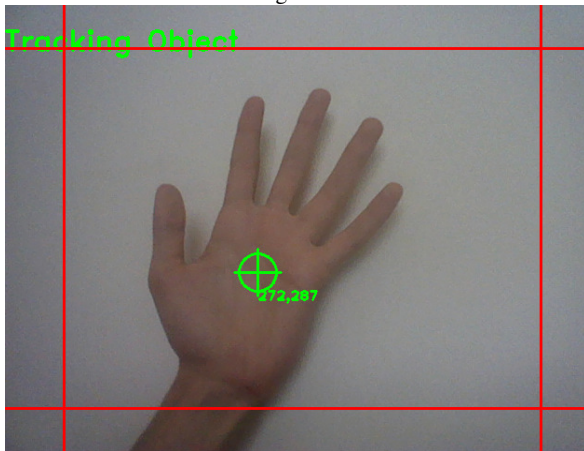


Figure 3. Final representation.

III. RESULTS

The implementation of the project on the personal computer demonstrated acceptable results. The conversions of original images were successful and tracking systems also showed adequate performance. The work required 0.3 megapixel camera and had quite simple programming code and structure what meets the objectives mentioned in the introduction part. Project appears to become cheap and stable tool in the car that decreases the distraction sources for the driver thereby helping safe driving.

IV. LIMITATIONS

There several limitations to be considered in this project, despite the overall successful implementation. First of all, the main problem may be illumination in the car, since the object recognition requires the use of specific colors in the image. The possible solution for this problem is to use light indicator that evaluates lighting in the car. Thereby the program will adapt to the current illumination and use specific configurations for each possible case. Another problem is the possible random movements, which may be considered as gestures by the program. However, this problem also may be solved by giving the stable range of values for the speed of the hand ignoring too fast movements.

V. CONCLUSION

The implementation of this program is believed to increase the safety driving by decreasing the destruction of the driver. Moreover, simplicity of the programming and manufacturing together with cost efficiency (only camera installation is required, the board computers already exists on the most of the modern automobiles) make this project even attractive. The preliminary results showed quite successful behavior of the project despite some problems to solve for the future implementation.

References

- [1] Voelcker, John. 2014. "1.2 Billion Vehicles On World's Roads Now, 2 Billion By 2035: Report." Green Car Reports. Last modified July 29, 2014.
- [2] National Center for Statistics and Analysis. 2014. "Early estimate of motor vehicle traffic fatalities for the first quarter of 2014." Washington, DC: National Highway Traffic Safety Administration.
- [3] QBE. "What are the top causes of road accidents in Australia?" Last modified February 23, 2015.

Drawing Using Web Camera

Object Recognition and Object Tracking

Aidana Massalimova, Zarina Amantayeva
Department of Electrical and Electronic Engineering
Nazarbayev University
Astana, Kazakhstan
aidana.massalimova@nu.edu.kz, zarina.amantayeva@nu.edu.kz

In the modern world, the computer vision became an essential tool in human interaction with digital systems. The major principle of this current study is that object with pre-defined color is tracked through web camera and, thus, resulted trace or trajectory of the object is displayed on the drawing screen. Visual C++ with embedded OpenCV libraries is the platform used to create this project. This project is designed as an interactive application for user through web camera. However, it can be further developed for the usage of artist, so that going paperless will be one of the ways to help the planet and save a few trees.

Keywords—OpenCV, image processing, object recognition, object tracking, drawing, web cam, paint, Visual C++.

I. INTRODUCTION

Recently, OpenCV plays one of the key roles in image processing implemented in C or C++ applications. Embedded design helps to have low level, low size and low price mobile implementation of computer applications. Owing to OpenCV libraries, it became possible for human to provide an interaction with the digital world using computer vision.

The goal of this project was to develop an application that will provide an opportunity of drawing through the web camera. This idea was established on the basis of Fernando's studies related with color based method, which is considered as the easiest way to detect and segment an object from an image. An important condition for successful segmentation of object using color based method is that object and background should have a significant color difference. In related work, which was used as a base for this project, the tracking of an object depended on its color. In particular, the tracking was performed upon red object. Drawing was achieved by tracking the path of this object, and simultaneously displaying it (object) on the separate threshold screen (see Figure 1).

Opportunities that were provided in the related work that we used were quite limited and consisted of simple detection and tracking of colored object. Contribution that was made to this project is connected with addition of several features improving the interface and abilities of this application. It was decided to add color palette, using which user will be able to choose color of the brush and draw different pictures, also brush thickness change option was added to the program. In this project, user can save his result as well as close the program without pushing button on the keyboard.

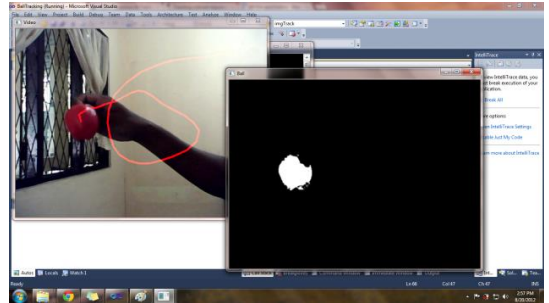


Figure 1. The Output of the Related work.

By adding all these features, it was tried to make the program as an entertaining application containing object recognition and object tracking processes. Yellow colored object was used as a computer mouse in order to draw separate line. "Mouse" has two sides which are be used as "click" of the comp. mouse. A library of real time vision, namely OpenCV, is used with c++ software programming language. Since we are working with video and image processing, the opencv_highgui should be included along with standard cv, cmath and iostream libraries. The program works in two dimensions, namely in x,y positions

This project is similar to a simple Paint program; however, the distinguishing feature of it will be the fact that it will be more entertaining and interactive. Importance of this project can be evaluated basing on the possible areas of its implementation. Possible areas of use might be primary schools (make children's work in Paint more interesting), or it can be used as a base for development of an application which will allow blind to draw using their hands. Also, idea of the program can be taken as a base for development of new direction in art of drawing and painting. Furthermore, the amount of papers used by artists can be reduced and hence this may result in ecological and economic savings.

II. METHODOLOGY

A. Object tracking and object recognition

Object recognition is considered to be the first step in the project implementation. Since the program is focused on detecting yellow-colored object, the color based segmentation is accomplished. Indeed, the high efficiency of object detection is achieved, when the color difference between the object and background is considerable. Apart from the original video obtained through web camera, binary video is also

processed, which assigns yellow area as ones and non-yellow area as zeros by thresholding the yellow color. Consequently, binary video displays yellow object in white and the rest background in black. Due to the fact that the primary video is in 8-bit, unsigned integer, BGR format, this video format is converted into HSV format. The major reason behind this decision is the fact HSV color space is reckoned to be the most favorable color space in image segmentation. In fact, HSV stands for its three matrices know as Hue, Saturation and Value. Hue is considered to be the indicator of the color, whereas Saturation and Value are the qualitative readings of the mixture of the current color with white and black respectively. Therefore, Hue value of the yellow color is specified to range from 20 through 30; and both Saturation and Value are dependent on the lightening condition of the environment. In this study, the boundaries of yellow color in terms of HSV are declared using CvScalar data type [3]. The next step is defining CvCapture device. This structure includes information which is required for reading frames from a camera. The domain of camera is set to zero, which indicates that any camera can be utilized [2]. Due to the fact that video is divided into multiple frames in video processing, while-looping is used to read each frame in sequence. After obtaining a frame, this frame is transferred into the thresholded image as discussed before (Figure 2)

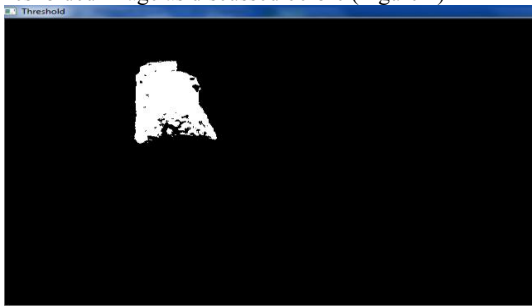


Figure 2. Thresholded Image.

Image processing is prone to a variety of noises, which is affected by an error of acquiring wrong values of pixels from the source image. These noises can be handled using smoothing, which is discovered to be a significant tool in reducing background noise during image processing. In this case, Cv_Median smoothing type is decided to be implemented, which is capable to resist outliers by selecting the middle points [1].

`cvSmooth(frame, frame, CV_MEDIAN,5, 5)`

Additionally, mirroring effect can be reached using a flipping function of `cvFlip(frame,NULL,1)`; however, this was found to be unnecessary, since mirroring effect was already part of the properties of the current web camera.

The final step is defining the centre coordinates of the object and drawing a trajectory of the object. The position of the center of the object is identified by computing the moments, so that we need to determine the first order spatial moments around x and y axis and the zeroth order central moments of the binary image. Therefore, memory was

allocated to the moment structure and thus computations of contour moments are performed in order to estimate the object position [2]. On the basis of this structure, two first order moments and an area of the zeroth order moment are estimated, so that dividing two first order moments by area constituted x and y coordinates of the yellow-colored object:

$X = 1\text{st order spatial moment around x-axis} / 0\text{th order central moment}$;

$Y = 1\text{st order spatial moment around y-axis} / 0\text{th order central moment}$.

After determining the magnitude of line connecting previous point with current point, line is automatically presented in drawing window. For the ease of understanding the algorithm of object detection and tracking, the flow chart was established and represented in Figure 3.

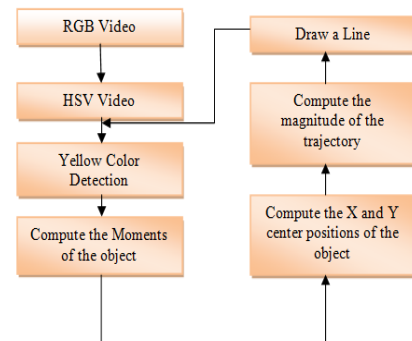


Figure 3. The flow chart of object detection and object tracking algorithm.

B. Graphical User Interface

There are three screens: threshold, drawing and video. Threshold is used for object clarity detection; video screen is the main interactive screen from which input is read and which represent user key features of the program, and, finally, drawing screen is the display allowing user's drawing to be illustrated on white background.

The Graphical User Interface of this program includes color panels, thickness of the brush, saver and eraser of the image. The function is recognized immediately after holding the object in front of the desired panel and studying the pixels of the holding object. The interface of the display was developed using Paint embedded to Windows operating system. This image interface was afterwards added to the display as a panel (Figure 4):

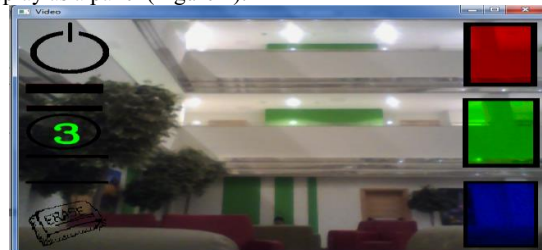


Figure 4. Graphical User Interface.

Each box has special coordinates, and by detecting the position of object and comparing it with each box's coordinates, the desired function can be chosen, and the text saying function chosen appears using `cvPutText` function [4]. Comparison of the coordinates is done by using `if/else` statements. The program decides whether the user has chosen some function, for example he wants to change brush thickness, by not only comparing coordinates, but also counting for how long object coordinates are coincide with the function boxes' coordinates with the use of embedded counter.

1. Brush color

The program uses 5 colors. 3 colors: blue, green, red are used for painting while white and black are used for threshold image and for clearing the screen. Firstly, we need to declare these colors in RGB color code using `CV_RGB` drawing function.

Color palette shown in the video screen contains, as it was mentioned before, 3 colors (blue, green, red). Comparison of the coordinates with the objects' one can be done in the following way:

```
if(posX > 530 && posY > 370) // for blue color
{ lineColor = blue;
  cvPutText( frame, "Blue color has been selected.",
  cvpoint, &font, blue );}
```

2. Brush Thickness

Default line thickness is set to be 3 and default color is green. Brush thickness box is located in particular part of the video screen as it was mentioned before, so that by changing the y-position of the object, line thickness can be chosen again by applying `if/else` statement. For example:

```
If (posX < 100 && posY > 140 && posY < 400)
{ThicknessOfLine = 6 - ( posY/60-1 ); // changing thickness
of the line from 1 to 5 basing on Y position of the object}
```

3. Erase/clear screen

White color will work as an eraser in this program, in case user selects eraser, each frame is checked for painting existence and the colorful line is erased by white color in drawing screen, the new image is saved automatically using `cvSaveImage` function [2].

4. Exit

Exit from the program can be done it two ways: by keeping our object on exit box in video screen for certain amount of time so that the program confirms user's decision to leave the program or by simply pushing the Esc button on the keyboard.

III. RESULTS AND FURTHER CONCERNS

At this moment the program is basically finished. Object recognition system and object tracking are working on

satisfactory level as can be seen from Figure 5. Moreover, in this phase user can select all desired special options from provided interface. Image and video processing speed are working with negligible lagging, which is not very noticeable. Several conditions should be taken into account in order to launch the program successfully:

- Maximum distance between web camera and object cannot extend 2.5m;
- Yellow colored object and background should have a significant color difference;
- Object with pre-specified color can be used.

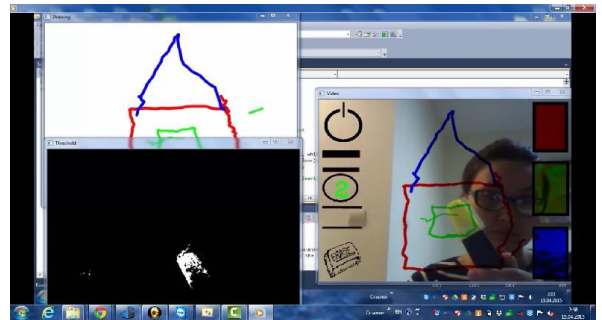


Figure 5. The Output Display of the program.

IV. CONCLUSION AND RECOMMENDATIONS

In this study, efficient object detection and object tracking moving target systems were proposed, so that the combination of these systems allowed designing a simple drawing application. This project is argued to be the new path of human-machine interaction. The examination of distinct algorithms of image processing led to the comparatively successful results. The further and better developments will be on the basis of the current research studies. This program can be enhanced by applying gesture control and providing more color pellets and variety of figures such as rectangle, triangle, circle and etc, so that existing program can be advanced as paint and notepads controlled by the gesture.

REFERENCES

- [1] D. Baggio, S. Emami and D.M.Escriva, *Mastering OpenCV with Practical Computer Vision Projects*. Birmingham,UK: Packt Publishing Ltd,2012.
- [2] G. Bradsky and A.Kaehler, *Learning OpenCv*.Sebastopol,CA: O'Reilly Media,2008.
- [3] OpenCV 2.4.11.0 documentation.Last Accessed:31.04.2015.URL: <http://docs.opencv.org>.
- [4] R.Laganieri, *OpenCV 2 Computer Vision Application Programming Cookbook*. Birmingham,UK: Packt Publishing Ltd,2011.
- [5] S. Fernando.Color Detection & Object Tracking.Accessed date: March 15,2015. URL: <http://opencv-srf.blogspot.ro/2010/09/object-detection-using-color-seperation.html>.

Electronic Attendance Using Face Recognition

Alimzhan Sultangazin
Department of Electrical and Electronic Engineering
School of Engineering
Nazarbayev University
Astana, Kazakhstan
Email: alimzhan.sultangazin@nu.edu.kz

Janysbek Kusmangaliyev
Department of Electrical and Electronic Engineering
School of Engineering
Nazarbayev University
Astana, Kazakhstan
Email: janysbek.kusmangaliyev@nu.edu.kz

Abstract—This project will use Open CV face recognition API module to register attendance of students in class. For this purpose, a camera stream will be analyzed frame by frame. During analysis, the faces will be detected and compared with photos in a face database stored on a computer. If the match is found, a certain student will be checked as present. This approach to taking attendance is considerably harder to circumvent than conventional or electronic attendance based on student IDs because it requires the presence of a student.

Index Terms—face recognition, education, attendance

I. INTRODUCTION

The topic of this paper stemmed from the problem of attendance in our university. Often, instead of going to the lecture, students would ask someone to sweep their ID card over the card reader for them to create an impression that they have attended the lecture. This made us think about possible solutions to this problem. The first idea that came to mind was to use face recognition as a means of taking attendance.

Although fairly easy for humans, implementation of face recognition using computers have been a topic of rigorous research for a long time. The main difficulty was to identify what features should the computer look for and compare. One of the first face recognition algorithms was based on geometric features of the face. It used certain marker points (ex. position of nose, eyes, ears) to create feature vectors. The algorithm would measure a distance between feature vectors of the sample and reference image [1].

Newest face recognition algorithms take a more holistic approach. The algorithms present in OpenCV are Eigenfaces method, Fisherfaces method and Local Binary Patterns Histograms (LBPH) method [2]. Eigenfaces method treats a facial image as a point in a high-dimensional image space. To reduce the number of dimensions, Principal Component Analysis (PCA) is used. Its aim is to identify axes with maximum variance, find new orthogonal basis and create a new lower-dimensional "face space". The algorithm is not robust to external disturbances, such as light, and therefore must be used with caution.

Fisherfaces method utilizes Linear Discriminant Analysis (LDA), which unlike PCA takes into account classes. Since PCA does not consider classes, it may reject components, which carry discriminative information, by maximizing the variance. In its turn, LDA maximizes the variance within the class only and, thus, preserves the discriminative information.

The two methods above require a large amount of images per person. For example, to achieve a recognition rate of 96%, these algorithms need 10 different images of the same person [2]. A LBPH algorithm can perform fairly accurately with a small number of images per person because, instead of looking at an image as a high-dimensional vector, it describes only local features of an object.

The problem that stood before us was to:

- 1) Find a student photo database for experiment
- 2) Process the images in the database to feed them to the face recognition algorithm
- 3) Determine the face recognition algorithm suitable for our purposes
- 4) Implement the program in a user-friendly way
- 5) Analyse and measure the accuracy of the algorithm in different exterior conditions (such as lighting)

The novelty of this paper is that face recognition is being discussed as a means of control of classroom activities. Moreover, the effects of lighting and distance from camera during face recognition are going to be analysed and discussed. Note that the assumption is made that the students will come to the camera one by one and the distance between the camera and face of the student will be sufficient. The teacher is going to monitor the correctness of recognition and press button to register attendance of a student when recognition is successful.

Due to time limitations, the mathematical nature of face recognition algorithms was not studied rigorously, and the algorithms were merely used with their performances analyzed.

II. METHODOLOGY

First, it was necessary to obtain a database of frontal face photos. The photos were taken from portal my.nu.edu.kz site

using wget program looping through all 2nd year students.

Then, the photos were cropped to include only the facial features, scaled to size 200x200 and rotated to be aligned at the eyes. To achieve this, first, Open CV was used to automatically determine the positions of eyes on all of the photos. Second, these positions were used to rotate an image by a certain angle, so that the line between the eyes would be parallel to the lower edge of the image. Finally, the images were cropped to include only the facial features. The rotation and cropping was performed using Python Imaging Library (PIL). An example of an image used for facial recognition is shown on Figure 1.



Fig. 1. Example of the cropped image used in face database

Now that the database was ready, it was time to determine an algorithm that was to be used for face recognition. Our database had only one image per person and, therefore, if used with this database, algorithms like Eigenfaces and Fisherfaces would not produce a high recognition rate. However, by trial and error, it was determined that the best algorithm to use was Fisherface algorithm.

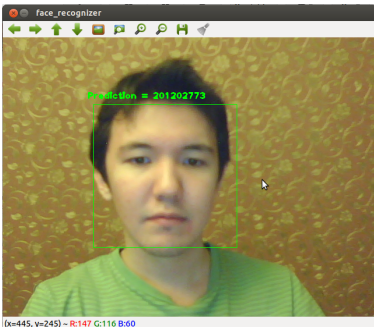


Fig. 2. Face recognition with ID indicated

The routine of a face recognition software is usually as follows:

- 1) Detect the faces on the image
- 2) Feed faces to the face recognition algorithm
- 3) Compare the faces with faces in the database

In our software, an additional step is required: to document the attendance of a student in the class.

To break the problem into pieces, it was decided to start by implementing a program that would recognize a person sitting in front of the web camera, place his face into a rectangle and write his ID number on the top. First, a mechanism to load photo database into the program was needed to be developed. For this purpose, we used a CSV file with paths to each image followed by its identifier (ID number). These images were then passed to LBPH FaceRecognizer to train it. Again, the main

difficulty was that in database there was only one photo per person. Then, an algorithm was written that would determine the position of the face on the web camera feed and crop it from the background. This algorithm was implemented using Haar Cascades with CascadeClassifier. In particular, the Haar Cascade of the frontal face was used. After that, the face from the web camera was compared with faces from the database and, if the match was found, the ID number of the student from the database would be shown. The operation of this preliminary program is shown on Figure 2. For development of this program, the tutorial from OpenCV documentation [3] was extensively used.

Finally, the means of storing attendance of a student was developed. To store a face in the list, a teacher would need to press space when the face is recognized.

To summarize, the program performs the following actions throughout execution:

- 1) Reads CSV file to get paths of database images and loads these images and their labels into two vectors. Return error if this action could not be performed
- 2) Initializes Face Recognizer algorithm and feed all images and labels to it. Also, set a threshold number for recognition, so that the faces that are not present in the database would be rejected.
- 3) Initializes Cascade Classifier and load frontal face Haar Cascade.
- 4) Connects to the web camera feed.
- 5) Repeatedly loops through images from web camera feed and detects all the faces.
- 6) Crops the faces and resizes them to the size of images from the face database.
- 7) Feeds the faces from web camera feed to the Face Recognizer.
- 8) Draws a rectangle around the face and projects a response of face recognizer over it.
- 9) Waits for 'space' key to be pressed to add a student to the attendance list. When 'escape' is pressed, exits the program.

One of the problems, which has appeared during the implementation of our electronic attendance program, is to create a database of existing students for a test. Since the purpose of our project was to develop a face recognition for the purposes of attendance for our class, it has been decided to get photos and IDs of all 2nd year Electrical Engineering students. The procedure for download of all 2nd year students has been described above. However, it does not demonstrate how only Electrical Engineering students were sorted out. In order to sort only Electrical Engineering students, the list with names taking the same Electrical Engineering class has been downloaded from the Moodle. After having the list of names of all 2nd year Electrical Engineering students, the problem was to assign IDs to these names so that we could search our database of all 2nd year students and sort Electrical Engineers out. In order to solve this problem, the list of all people somehow affiliated with Nazarbayev University Mail has been downloaded from Gmail. This list included about 4500 people with names, IDs and positions. Additional script has been

written to find the names from the list of Electrical Engineering students with the whole contact list of Nazarbayev University Mail and to take the corresponding ID. After this, we had a complete list of 2nd year Electrical Engineering students with names and IDs and, thus, we now could proceed to formation of our database. In overall, 66 Electrical Engineering 2nd year students were sorted out, constituted our database. For this experiment, several variations of the database have been used to demonstrate the programs success rate. In other words, we used different number of items inside the database to test what is the impact of the size of the database on the success rate. Initially, five photos have been used with an increment of five for each test until a complete database of 66 photos for a test was reached. In addition to the criterion of the size of the database, another two criteria have been used. One of them is the luminosity of the face of the subject, and another is the distance from the face to the capturing camera. In this experiment, the luminosity is an uncertain factor, which has been defined by three states:

- 1) Well-lighted
- 2) Half-lighted
- 3) Poorly-lighted

The examples of well-lit, half-lit and poor-lit environments are shown on Figures 3-5. These states were determined by relying on human factor only.

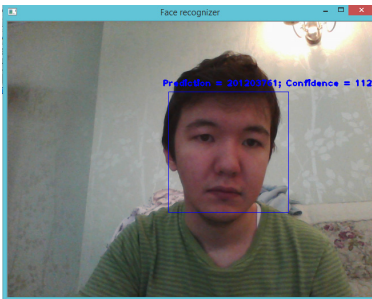


Fig. 3. Well-lit environment

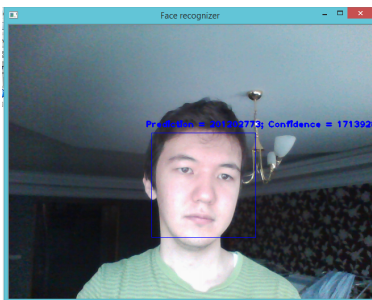


Fig. 4. Half-lit environment

For the distances, three states have been determined:

- 1) 20 cm
- 2) 40 cm
- 3) 60 cm

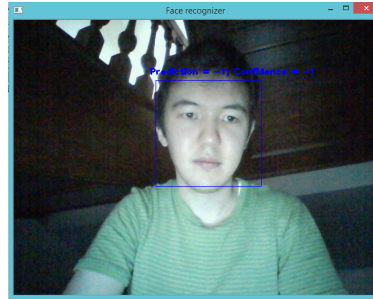


Fig. 5. Poorly-lit environment

For each state of criteria, several tests have been performed with the database size ranging from 5 photos to 66 photos. The results can be observed in the Results and analysis of data section.

III. RESULTS AND ANALYSIS OF DATA

TABLE I
RECOGNITION RATE OF THE PROGRAM UNDER DIFFERENT LIGHTING

Database size	Recognition rate (%)		
	Well-lit	Half-lit	Poorly-lit
5	10	10	6
10	10	10	6
15	10	9	5
20	9	8	5
25	10	9	4
30	9	8	5
35	9	8	5
40	8	6	4
45	7	7	3
50	7	6	2
55	7	5	3
60	6	3	3
65	6	4	

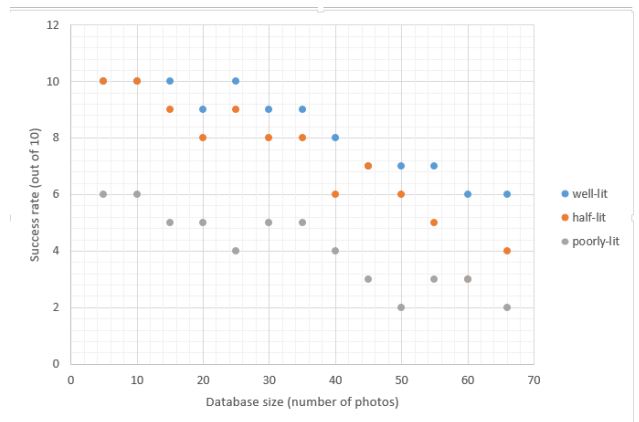


Fig. 6. The relationship between the database size and success rate for different degrees of luminosity

From Table 1 and Figure 6, it can be seen that with the decrease of the luminosity, the success rate drops. This

TABLE II
RECOGNITION RATE OF THE PROGRAM DEPENDING ON DISTANCE OF THE FACE FROM CAMERA

Database size	Recognition rate (%)		
	20 cm	40 cm	60 cm
5	9	10	7
10	9	10	8
15	7	8	7
20	7	9	8
25	8	9	8
30	6	10	7
35	7	10	5
40	6	9	6
45	6	8	4
50	7	8	5
55	6	8	3
60	5	8	5
65	5	7	2

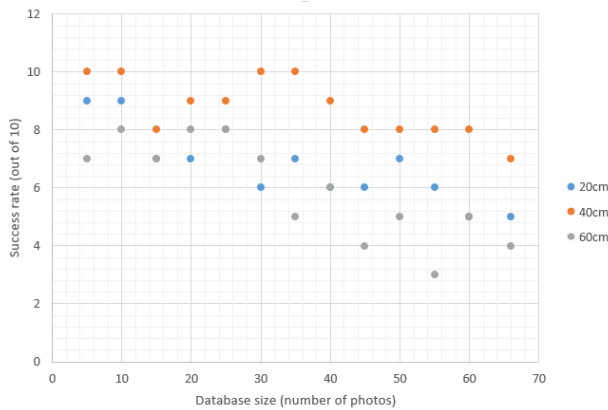


Fig. 7. The relationship between the database size and success rate for different distances

means that in order to ensure the maximum capability of this program, the user has to provide the well-lit environment.

Regarding distances (Table 2 and Figure 7), it can be said that the optimal distance from face to the capturing camera is about 40 cm. However, additional tests can be performed to find more accurate results for distance. Due to time restrictions, we were not able to conduct tests many distances.

From both Tables 1 and 2, it can be seen that increasing database size leads to a rapid reduction in recognition rate. This implies that the program should be used with caution for large classes.

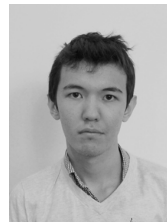
IV. SUMMARY, CONCLUSIONS, AND RECOMMENDATIONS

Overall, the face recognition algorithm provided by OpenCV is suitable for purposes of electronic attendance for small classes. However, there is still work to be done to increase the recognition rate for larger classes. A suggestion can be made to make an algorithm that would learn from its mistakes: for example if it recognizes a person wrongly, an operator can write a correct identification number manually to the computer, and the program would store this web camera feed as a new face in the face database.

Considering cases when the program would fail, it can be said that a student can deceive the program simply by putting the photograph of another student in front of the web cam to take Fig. 2. Face recognition with ID indicated the attendance. Surely, the algorithm would not detect whether a student or his photo is appearing on the web cam. In favor of our program, it can be said that still it is much easier for a faculty to spot cheating during web cam attendance rather than a paper signed or electronic attendance taken using ID card. This is because it is much harder to take an attendance furtively with a photo. In addition, several programming techniques can be applied to the algorithm in order to avoid cheating on attendance. For example, the function predict of the FaceRecognizer can be used to assess the quality and, thus, credibility of a taken video image frame. In this regard, a threshold can be applied to raise the quality of the images to be accepted and, thereby, to filter unnecessary frames.

REFERENCES

[1] T. Kanade, "Picture processing system by computer complex and recognition of human faces," Ph.D. dissertation, Kyoto University, 1973.
 [2] P. Wagner, "Face recognition with opencv," http://docs.opencv.org/modules/contrib/doc/facerec/facerec_tutorial.html, 2015, [Online; accessed 23-March-2015].
 [3] —, "Face recognition in videos with opencv," http://docs.opencv.org/modules/contrib/doc/facerec/tutorial/facerec_video_recognition.html, 2015, [Online; accessed 22-March-2015].



Alimzhan Sultangazin was born in Karagandy. He received his high school diploma from Nazarbayev Intellectual School Astana in 2012. He is currently an undergraduate student in the BEng in Electrical and Electronic Engineering program at Nazarbayev University. His research interests include face recognition software and analog electronics. His recreational interests include singing, playing piano, and fishing.



Janysbek Kusmangaliyev was born in Almaty, Kazakhstan in 1994. He received his High School Diploma from the Nazarbayev Intellectual School, Astana, Kazakhstan. He is currently a student at Nazarbayev University, Kazakhstan and is pursuing his Bachelor degree in Electrical and Electronic Engineering. His main research interests include gesture control, face recognition and power electronics. His other interests include tennis, airplanes, auto racing and fine arts.

Evaluation of Memristor Emulator for Memristor Circuit Applications in SPICE Simulator

Yerzhan Sapenov
School of Engineering,
Nazarbayev University
Astana, Kazakhstan
ysapenov@nu.edu.kz

Nursultan Ornov
School of Engineering,
Nazarbayev University,
Astana Kazakhstan
nornov@nu.edu.kz

Abstract— this work presents findings on verification of memristor emulator model. Memristors are devices, which resistance value depends on the current, which has previously flown through it. Memristor hardware model needs to maintain such features of memristors as programmable memristance, nonvolatile performance and ability of being connected with other devices in memristive circuits. Analyzed model is composed from widely available solid state components and can be used in the systems of several memristors. It makes this emulator convenient for educational and demonstration purposes as well as for initial analysis of memristive circuits. Examination of the emulator using SPICE has shown expected results, including pinched hysteresis loop on voltage-current plane and linear dependence of charge on flux. In addition, operation of system at different temperatures and frequencies was studied.

Keywords—memristor; emulator; SPICE model

I. INTRODUCTION

Memristors are two-port electrical devices changing their resistance depending on the current that has flown through the device previously [3]. It became a fundamental electrical element in one row with inductor, capacitor and resistor, because the memristor provides a functional relation between flux and charge [1]. Memristors' common feature is a pinched hysteresis loop on the current-voltage characteristics graph. Another important feature of such devices is non-volatile resistance meaning that value of device resistance does not change if no power is supplied to it.

These unique characteristics of memristor make it suitable for memory and neuromorphic applications such as Cellular

neural networks for image processing [8],[9]. Another possible application fields of memristors are microwave electronics [10] and PID control [8]. Moreover, resistive switching devices for memory and logic application could also be realized with memristors [13],[14],[16]. Typically, memristors are nano-scale horizontal devices, build using TiO₂ technology [18], but they also could be produced using SrTiO₃ [16]. In addition, memristors could be realized as a 3-D vertical device [15].

The cost of fabrication of nano-scale devices along with a huge potential of memristor applications require device emulator for initial analysis of memristive circuits. There are proposed SPICE emulator models, which could be used for simulation applications [10]. However, hardware model is required for physical implementation of memristive circuits.

In order to be useful, the hardware model needs to have programmable and nonvolatile memristance. Another requirement is that memristor model could be directly connected to other electrical devices in memristive circuits. Moreover, this emulator should consist of widely available solid-state components to ensure that it could be easily constructed. Most of the proposed emulators are based on transformation of non-linear inductors, resistors, and capacitors into memristors [1],[17]. And while the model proposed in [17] utilizes both analog and digital circuits, only analog devices are

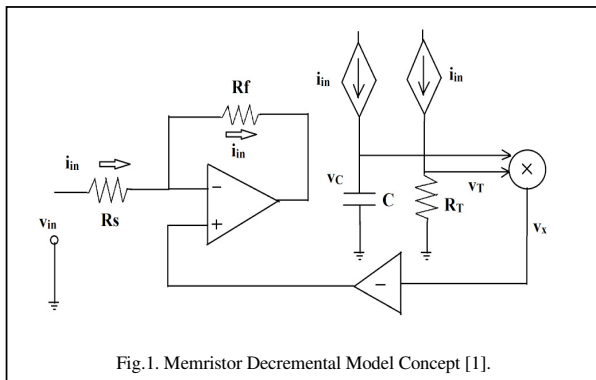


Fig.1. Memristor Decremental Model Concept [1].

TABLE I. SPICE SIMULATION PARAMETERS

Parameter	Value
Input voltage	$2V_{pk-pk}$
R_s	16kOhm
R_T	4kOhm
R1, R3-R6	10kOhm
R2	90kOhm
C	0.1uF
NMOS W/L	35
PMOS W/L	90
Supply voltage for current mirrors	$\pm 5V$
Supply voltage for op-amps and AD633	$\pm 15V$

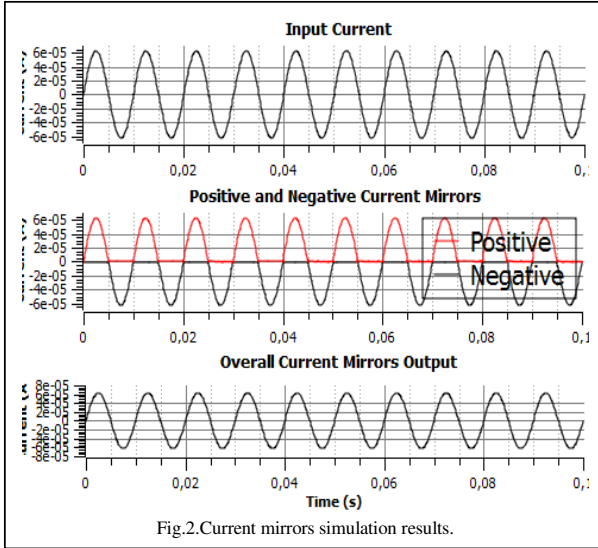


Fig.2.Current mirrors simulation results.

used in emulators proposed in [1] and [19]. Advantage of using only analog circuits is improved connectivity of the model with other circuit elements[21-24]. Even though, model proposed in [19] is not expandable. Therefore, the model proposed in [1] is selected for analysis in this work. The objective of this paper is to evaluate the performance of this memristor emulator model, including examination of transient characteristics along with frequency and temperature dependencies of these characteristics.

II. METHODOLOGY

Examined model could be operated in either incremental or decremental mode. The main difference between them is that the pinched hysteresis loop lays in the first and third quadrants of I-V plane for the former, and in the second and fourth for the latter. Since operation of both models is analogical, only decremental mode is studied in this work.

A. Concept Description

Concept of decremental memristor emulator is presented on the Fig. 1. The main idea of this emulator is using capacitor characteristics of charging and discharging to obtain variations in overall resistance. Input voltage for this configuration is given by the equation (1)

$$v_{in} = R_s i_{in} - v_x \quad (1)$$

In this equation, v_x is the output of analog multiplier and is given by the equation (2). The first term in (2) corresponds to capacitor voltage, while the second represents voltage across the resistor R_T .

$$v_x = \frac{q_C(t)}{C} \times R_T i_{in} \quad (2)$$

Therefore, by combining equations (1) and (2)

$$v_{in} = \left(R_s - \frac{R_T}{C} q_C(t) \right) i_{in} \quad (3)$$

And, finally, equation (4) describing input resistance is obtained from equation (3).

$$R_{in} = \frac{v_{in}}{i_{in}} = R_s \left(1 - \frac{R_T}{C R_s} q_C(t) \right) \quad (4)$$

In equation (4), the first term in brackets represents a fixed part of memristance. The second term varies due to the changing capacitor charge. This term corresponds to a variable part of memristance.

B. Design Description

Both resistor R_T and capacitor C in (3) need to be supplied by the same current which is produced by the input voltage source. Therefore, in SPICE implementation six current mirrors are constructed using BSIM3 long-channel MOSFET models [20]. The MN0-MN2 current mirror regenerates the positive part of the input current, while MP0-MP2 current mirror copies the negative part. The MP1-MP3 and MP1-MP4 reproduce the current from the MN0-MN2 current mirror on the resistor's and capacitor's outputs respectively. Analogically, The MN1-MN3 and MN1-MN4 reproduce the current from the MP0-MP2 current mirror. Consequently, the full copies of input current on resistor and capacitor are obtained. The layout of the current mirrors in the circuit is shown in the Appendix A. Their operation could be observed on the Fig. 2. It shows that the output currents supplied to resistor and capacitor perfectly copy the input current as expected.

Analog multiplier AD633 [4] is used for combination of output voltages from R_T and C . It operates at frequency range up to around 300 kHz which is suitable for the examined emulator model.

Transfer function of this multiplier is given by (5).

$$W = \frac{(X1-X2)(Y1-Y2)}{10} + Z \quad (5)$$

During the implementation of the project, error in abbreviation was found in [1]. Authors exchanged W and Z ports of AD633 multiplier, which caused simulation issues.

Fig. 3 illustrates the performance of the AD633 analog multiplier. In order to study multiplier's operation, to SIN signals with different frequencies were supplied as inputs. On

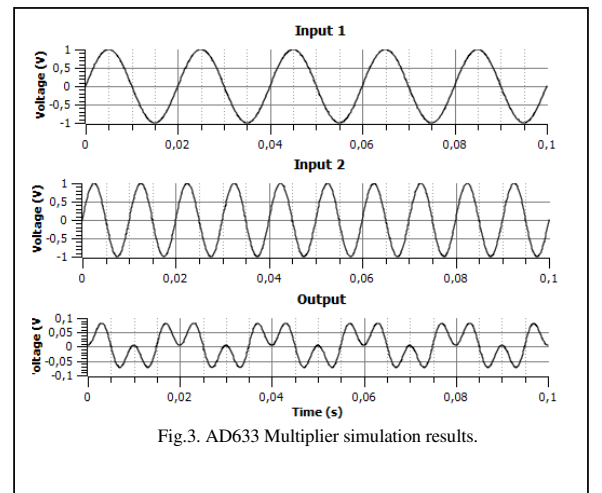
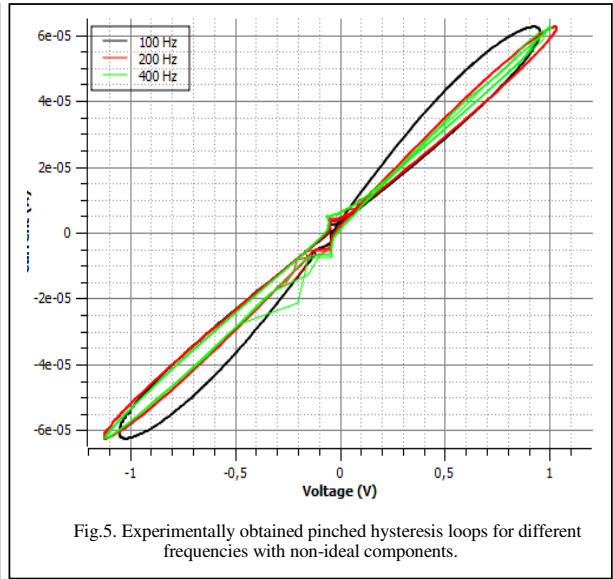
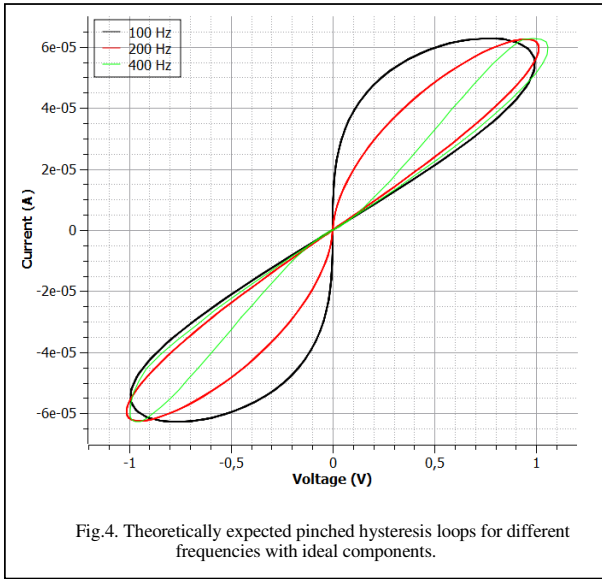


Fig.3. AD633 Multiplier simulation results.



the Fig. 3, first two graphs are input signals, and third graph is representative of the output signal. Analog multiplier takes points of input graphs at each time instance, mathematically multiply them and divide by 10, as mentioned in(5). Since multiplier works as expected, it was selected to be used in the simulation of memristor emulator.

As shown in (5), output of AD633 needs to be scaled 10 times. Scaling is performed using operational amplifier $U2$ with gain of 10. $U1$ amplifier is used as a buffer in order to prevent capacitor from undesired discharge when there is no input signal. This buffer provides nonvolatile properties to the examined model. Combination of R_5 and $U0$ is used to convert input voltage into input current. Examined model is made expandable by insertion of analog adder which is constructed using $U3$ and $U4$ amplifiers. All amplifiers in the models are TL082 [5]. The final layout of the circuit could be found in the Appendix A and simulation parameters are specified in the Table 1.

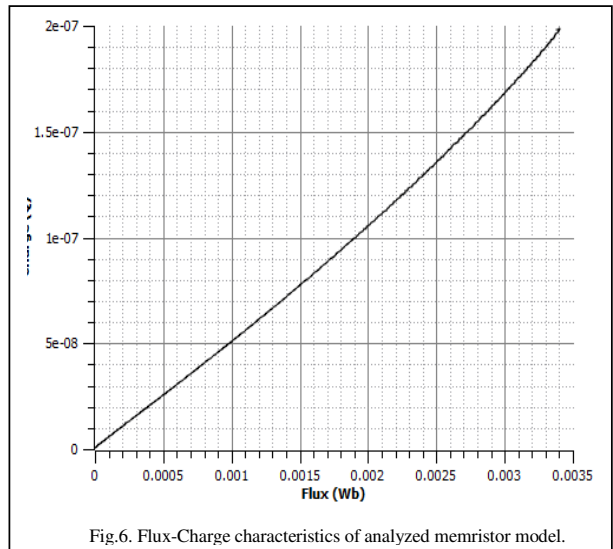
III. RESULTS AND DISCUSSIONS

By implementing the SPICE simulation of the system the data for the input current and voltage are obtained. The theoretically expected pinched hysteresis loops for different frequencies of input signal are illustrated on the Fig.4. They were obtained from mathematical analysis of emulator performance by assuming ideal operation conditions. It could be observed that current changes approximately from $-65\mu\text{A}$ to $65\mu\text{A}$. The waveform of the current is periodic. There are two corresponding values of current for each voltage point. Therefore, value of current and memristance at present state is selected among two possible values depending on its value at the previous state. Also, it is possible to conclude that with increasing the frequency the width of hysteresis loop decreases and memristor behaves more like a resistor. It means that the memristor emulator would eventually perform as a resistor if frequency of operation is further increased.

Theoretical expectations could be compared with simulation results provided on the Fig. 5. It could be seen that the emulator model with real-life components also has hysteresis loops on voltage-current plane. However, the width of the loop for the same frequency is much smaller compared to ideal scenario. Additionally, the hysteresis loops do not have such perfect shape as on the previous figure, which could be due to parasitic effects of the sub circuits.

The charge-flux characteristics of memristor model are presented on the Fig. 6. They are very close to the ideal, where the line should be straight, because the basic idea of the memristance is that the change in the flux causes linear change in charge. Fig. 6 shows that while flux changes from 0 to 3.5 mWb , charge increases up to $0.2 \mu\text{C}$.

The variation of the emulator memristance with time is



presented on the Fig. 7. Memristor changes its value between 2kOhm and 16kOhm. As it could be observed, memristance decreases with increase of voltage and increases when input voltage decreases. Moreover, maximum memristance is limited by the value of R_S while minimum value is limited by R_T and C . This observation totally agrees with theoretical expectations.

The simulation timings is represented on the Fig.8. It shows that the delay time of the system is equal to 117.5922us. It could be concluded that this time delay is acceptable.

The Fig. 9 displays the influence of the operation temperature on the memristor emulator performance. The shapes of the pinched hysteresis loop under different temperature conditions remain the same. When temperature increases, the loop moves in the direction of negative voltage.

IV. CONCLUSIONS

Memristor emulator is required for modeling behavior of real device performance using widely available components. In this study, the performance of memristor emulator model presented in [1] is verified using SPICE simulator. Such important features of real memristors as programmable memristance, nonvolatile operation and connectivity with other devices in memristive circuits were found to be preserved in the hardware model. Expected forms of pinched hysteresis loops were obtained. Moreover, decrease of the width of these loops with increase of input signal frequency was observed.

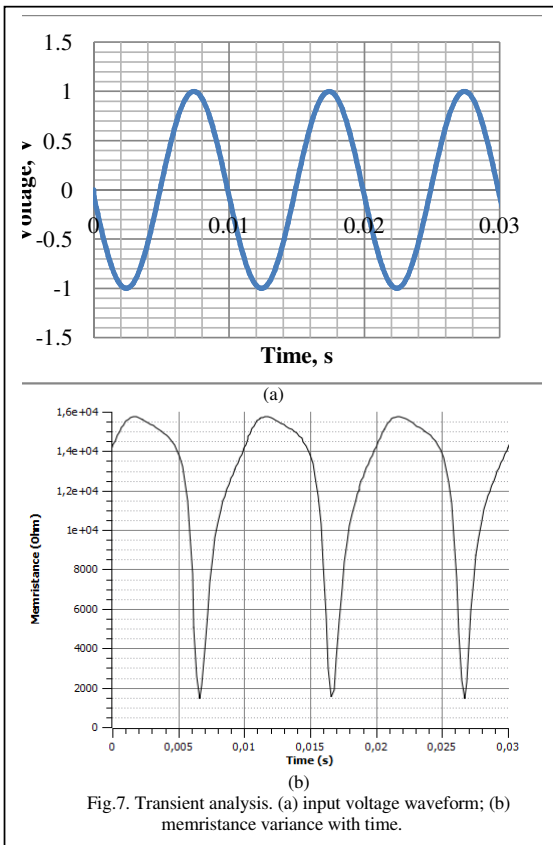


Fig.7. Transient analysis. (a) input voltage waveform; (b) memristance variance with time.

Measurement result summary	
Me1	= 117.5922u
Parsing	0.05 seconds
Setup	0.04 seconds
DC operating point	0.20 seconds
Transient Analysis	6.68 seconds
Overhead	0.94 seconds

Total	7.91 seconds

Fig.8. Delay calculation in SPICE.

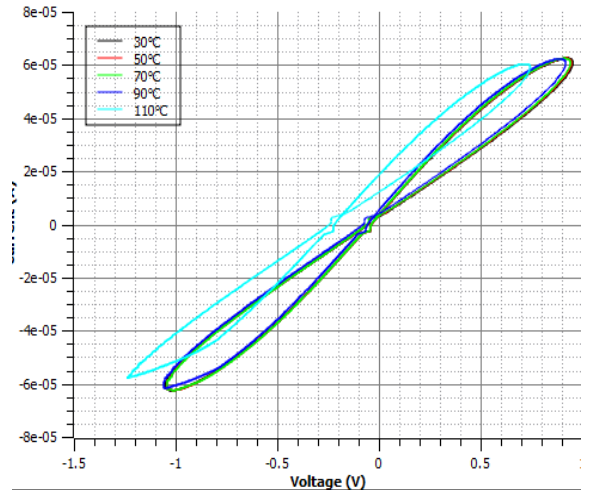


Fig.9. Obtained pinched hysteresis loops under different temperature conditions.

The obtained results from simulations of examined model coincide with predicted theoretical behavior. Consequently, this emulator works in desired manner and is applicable for construction of memristor application circuits as well as for educational purposes.

REFERENCES

- [1] Hyongsuk Kim; Sah, M.P.; Changju Yang; Seongik Cho; Chua, L.O., "Memristor Emulator for Memristor Circuit Applications," Circuits and Systems I: Regular Papers, IEEE Transactions on , vol.59, no.10, pp.2422,2431, Oct. 2012
- [2] Nandini A.S.; Madhavan S.; Sharma C., "Design and Implementation of Analog Multiplier with Improved Linearity," International Journal of VLSI design & Communication Systems (VLSICS) Vol.3, No.5, pp.93,109, Oct. 2012
- [3] L. O. Chua, "Memristor-the missing circuit element," IEEE Trans. Circuit Theory, vol. CT-18, no. 5, pp. 507-519, Sep. 1971
- [4] Analog Devices, "AD633 Data Sheet" [Online]. Available: <http://www.analog.com/media/en/technical-documentation/data-sheets/AD633.pdf>
- [5] Texas Instruments, "TL082 Data Sheet" [Online]. Available: <http://www.ti.com/lit/ds/snosbw5c/snosbw5c.pdf>

[6] C. Yang, H. Choi, S. Park, M. Pd Sah, H. Kim and L. Chua, 'A memristor emulator as a replacement of a real memristor', *Semicond. Sci. Technol.*, vol. 30, no. 1, p. 015007, 2014.

[7] A. Adamatzky and L. Chua, *Memristor Networks*. Cham: Springer International Publishing, 2014.

[8] Z. Dong, S. Duan, X. Hu, L. Wang and H. Li, 'A Novel Memristive Multilayer Feedforward Small-World Neural Network with Its Applications in PID Control', *The Scientific World Journal*, vol. 2014, pp. 1-12, 2014.

[9] S. Duan, X. Hu, Z. Dong, L. Wang and P. Mazumder, 'Memristor-Based Cellular Nonlinear/Neural Network: Design, Analysis, and Applications', *IEEE Trans. Neural Netw. Learning Syst.*, pp. 1-1, 2014.

[10] K. Xu, Y. Zhang, L. Wang, M. Yuan, Y. Fan, W. Joines and Q. Liu, 'Two Memristor SPICE Models and Their Applications in Microwave Devices', *IEEE Trans. Nanotechnology*, vol. 13, no. 3, pp. 607-616, 2014.

[11] D. Strukov, G. Snider, D. Stewart and R. Williams, 'The missing memristor found', *Nature*, vol. 453, no. 7191, pp. 80-83, 2008.

[12] M. Aono and T. Hasegawa, 'The Atomic Switch', *Proc. IEEE*, vol. 98, no. 12, pp. 2228-2236, 2010.

[13] B. Gao, B. Chen, F. Zhang, P. Huang, L. Liu, X. Liu and J. Kang, 'Multi-bit nonvolatile logic implemented with metal-oxide based resistive switching device', *Solid State Communications*, vol. 205, pp. 51-54, 2015.

[14] M. Kozicki, C. Gopalan, M. Balakrishnan and M. Mitkova, 'A Low-Power Nonvolatile Switching Element Based on Copper-Tungsten Oxide Solid Electrolyte', *IEEE Trans. Nanotechnology*, vol. 5, no. 5, pp. 535-544, 2006.

[15] '3-D Vertical Dual-Layer Oxide Memristive Devices', *IEEE Trans. Electron Devices*, vol. 61, no. 7, pp. 2581-2583, 2014.

[16] H. Nili, S. Walia, S. Balendhran, D. Strukov, M. Bhaskaran and S. Sriram, 'Nanoscale Resistive Switching in Amorphous Perovskite Oxide (α -SrTiO₃) Memristors', *Advanced Functional Materials*, vol. 24, no. 43, pp. 6741-6750, 2014.

[17] Q. Li, A. Serb, T. Prodromakis and H. Xu, 'A Memristor SPICE Model Accounting for Synaptic Activity Dependence', *PLoS ONE*, vol. 10, no. 3, p. e0120506, 2015.

[18] Y. V. Pershin and M. Di Ventra, "Practical approach to programmable analog circuits with memristors," *IEEE Trans. Circuits Syst. I*, vol. 57, no. 8, pp. 1857–1864, Aug. 2010.

[19] R. Multu and E. Karakulak, "Emulator circuit of memristor with linear dopant drift made using analog multiplier," in *Proc. 2010 National Conf. Elect., Electron. Comput. Eng. (ELECO)*, 2010, pp. 380–384.

[20] Mosis. T67P SPICE BSIM3 VERSION 3.1 PARAMETERS. [Online]. Available: https://www.mosis.com/cgi-bin/cgiwrap/umosis/swp/params/ibm-05/t67p_5hp-params.txt

[21] Maan, A.K.; Kumar, D.S.; Sugathan, S.; James, A.P., "Memristive Threshold Logic Circuit Design of Fast Moving Object Detection," *Very Large Scale Integration (VLSI) Systems*, *IEEE Transactions on*, vol. PP, no.99, pp.1,1 doi: 10.1109/TVLSI.2014.2359801

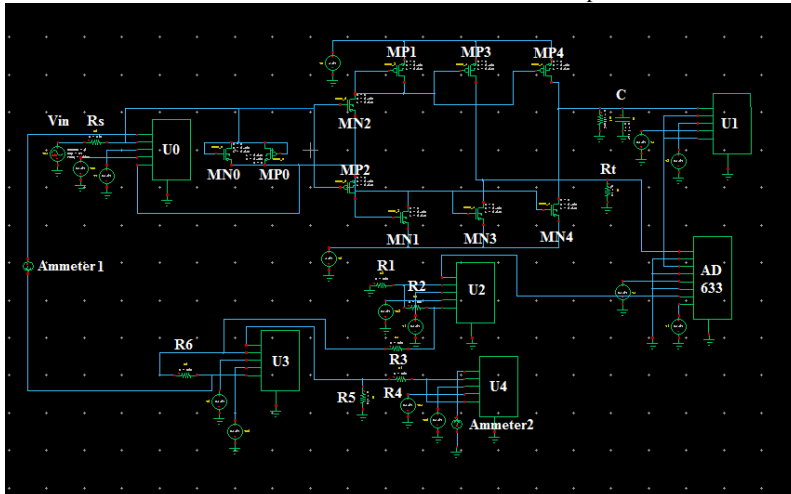
[22] James, A.P.; Kumar, D.S.; Ajayan, A., "Threshold Logic Computing: Memristive-CMOS Circuits for Fast Fourier Transform and Vedic Multiplication," *Very Large Scale Integration (VLSI) Systems*, *IEEE Transactions on*, vol. PP, no.99, pp.1,1 doi: 10.1109/TVLSI.2014.2371857

[23] Ibrayev, T., Fedorova, I., Maan, A. and James, A. On Design of Memristive Amplifier Circuits. *Circuits and Systems*, 5, 2014, 265-273. doi: 10.4236/cs.2014.511028.

[24] James, A.P.; Francis, L.R.V.J.; Kumar, D.S., "Resistive Threshold Logic," *Very Large Scale Integration (VLSI) Systems*, *IEEE Transactions on*, vol.22, no.1, pp.190,195, Jan. 2014 doi: 10.1109/TVLSI.2012.2232946

APPENDIX A

A full schematic of the decremental memristor emulator with expandable architecture [1]





Nursultan Ornov has completed secondary education in the school-gymnasium #1 in Schuchinsk, Akmola region, Kazakhstan with distinction. He is currently working on his B.S degree in electrical and electronics engineering at Nazarbayev University, Astana, Kazakhstan.

His main research interests include multilevel power converters, smart grids and memristors.



Yerzhan Sapenov has completed secondary education in the Republic Physics and Mathematics School after O.Zhautikov, Almaty, Kazakhstan. He is going to receive B.S degree in electrical and electronics engineering at Nazarbayev University, Astana, Kazakhstan.

His main research interests include wireless sensor network, MIMO, multi-hop communication systems and memristors.

Gate-Diffusion Input (GDI) Technique for Low Power CMOS Logic Circuits Design

Yerkebulan Saparov, Aktanberdi Zhakupov

ABSTRACT

Today's main challenges for most of the VLSI circuit designers are to decrease the area of the circuit and reduce power dissipation. The leading world companies are working on continuous improvement of the existing technologies. Quest for ideas in optimization of productive speed, reducing the propagation delays and power consumption along with compactness and minimization of production costs of triggers are the main objectives of producers of electronics and digital equipment. The question of improvement of logical gate design is particularly acute. Particularly, the power consumption is one of the key factors in any integrated circuit. Considering the complexity of modern integrated circuits, processors now consume large amount of power as they make maximum number of internal transitions. Therefore, the most actual question is to find the techniques to effectively implement low power systems in integrated circuits design.

INTRODUCTION

CMOS logic and Pass-transistor logic (PTL) is widely used in the present days in low power systems of integrated circuits. CMOS logic requires large amount of transistors even for a simple AND gate. 6 transistors are necessary to build a CMOS AND/OR gate. It is quite obvious that each transistor will increase power losses. PTL implementation contains a major problem, which is that after each stage, difference between high and low logic levels decreases.

The gate diffusion input is a brand new method for constructing low power digital circuits. It is supposed that Gate Diffusion Input (GDI) Technique is one of emerging options on reduction of production delays of the processor, decrease in power consumption and dissipation along with the simplification of production of integrated micro-schemes. Implementing this method may diminish power losses in the circuit, decreases propagation delay and total area of digital circuits.

In this paper, efficiencies of AND gate and OR gate design using CMOS logic, PTL logic and the GDI technology will be compared. The purpose of this work is to analyze the Gate Diffusion Input (GDI) Technique on the example of the AND gate and OR gate through their key characteristics of their work, power consumption and applicability. The main tools of the carried-out analysis are the simulation of an integrated

circuit constructed using GDI technique and pass transistor logic (PTL) (calculations of timing), conducted calculations of power consumption and dissipation, and also the analysis of compactness on the example of the AND gate and OR gate layouts by different techniques of construction.

TWIN-WELL PROCESS

The main differences of GDI technique lies in the fabrication process of transistors. Regular CMOS cells are fabricated using the method shown in Figure 1, while GDI cells need Twin Tub CMOS Fabrication shown in Figure 2.

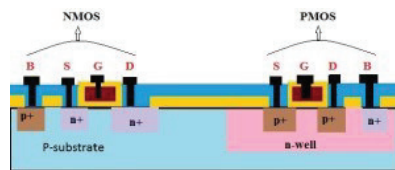


Figure 1. Regular CMOS fabrication [1]

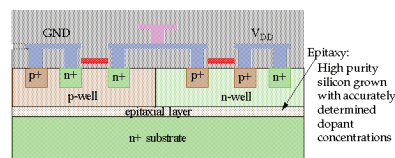


Figure 2. Twin tub-CMOS Fabrication Process [2]

In this process, it is possible to optimize transistors' body effect, gain and threshold voltage, and prevent from possible latch up. Basic GDI cell consist of NMOS and PMOS cells connected in a certain way. Figure 3 shows that there are 4 terminals in a cell: G – common gate input for both, NMOS and PMOS, P – outer diffusion node of PMOS, N – outer diffusion node of NMOS, and D – common diffusion mode.

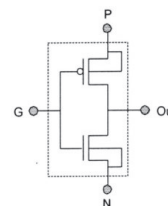


Figure 3. Basic GDI cell [5]

Bulk terminals of both NMOS and PMOS transistors are linked to N and P terminals accordingly, to allow arbitrary bias. GDI structure have three inputs (G, N, P) instead of two, which allows implementation of more complex logic gates using less transistors. Usually, in CMOS cell VDD is connected to PMOS and GND to NMOS, while in GDI technique both P and N terminals can be assigned with independent signal inputs, decreasing the transistor count and consequently the power dissipation across transistors [4].

BASIC LOGIC FUNCTION

In this paper, two logic function, AND gate and OR gate, were taken as a subject of investigation. As it can be seen in the Figure 4, numbers of transistors used are incredibly decreased in the case of Gate Diffusion Input Technique in comparison with CMOS logic.

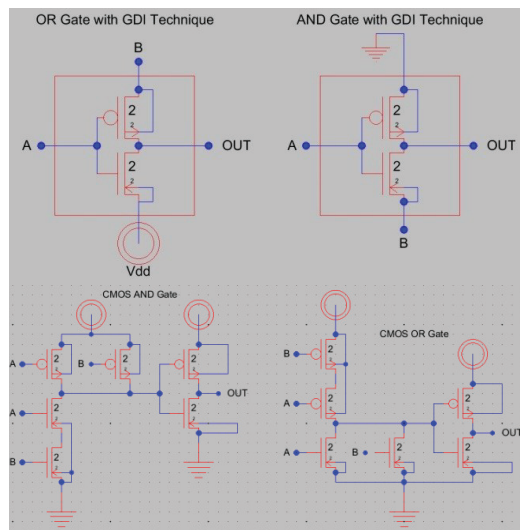
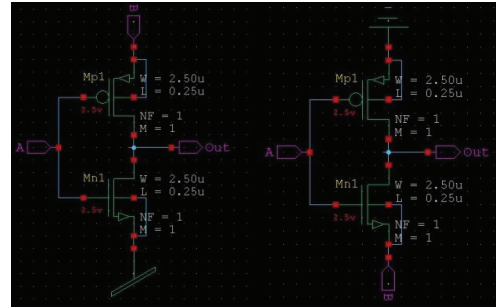


Figure 4. AND gate and OR gate using GDI and CMOS logic

SPICE parameters for simulating GDI cells differ a lot from that of the regular CMOS cells. Therefore, data for power efficiency were obtained from the referred papers. The Table 1 below shows how efficient is GDI technique in comparison with CMOS logic. W/L parameters are: W=2.50u, L=0.50u, M=1, NF=1 [3].

Table1. Power consumption values for AND gate and OR gate in GDI and CMOS logic [5]

Gate Type	Logic Expression	Power (μ W)			
		GDI	CMOS	Transmission Gate	nMOS Pass Gate
AND	AB	25.7	34.1	30.8	30.1
OR	A+B	26.3	32.9	36.2	32.6



Figures 5-6. OR gate and AND gate with GDI technique (Tanner EDA software)

Tests made by fabricating test vehicles demonstrated that the GDI technique reduces power consumption up to 45% with some significant improvements in performance arisen and decrease in the number of transistor compared to CMOS and PTL logic [6].

CONCLUSION

Overall, GDI Technique can enrich VLSI designers' toolbox in the near future. This technique, which is specifically designed for low-power applications, justifies its purpose by showing lowest power dissipation level among CMOS gates. Test chips showed huge improvements in performance, decreased number of transistors and area size over other logic gates.

REFERENCES

- [1] Agarwal, T. 'Step by Step CMOS Fabrication Processing Technology', Buy Electronics & Electrical Projects in India, 2014. [Online]. Available: <http://www.edgefx.in/understanding-cmos-fabrication-technology/>. [Accessed: 07-Apr- 2015].
- [2] Ece.unm.edu, 'CMOS Processing Technology', 2015. [Online]. Available: http://www.ece.unm.edu/~jimp/vlsi/slides/chap3_2.html. [Accessed: 10- Apr- 2015].
- [3] Kenia, K. and Kenia, N. 'GDI Technique: A Power-Efficient Method for Digital Circuits', International Journal of Advanced Electrical and Electronics Engineering, vol. 1, no. 3, pp. 87-93, 2012.
- [4] Kumar, M. A., Selvarani, R. and Kumar, T. Proceedings of International Conference on Advances in Computing. India: Springer, 2013.
- [5] Morgenshtein, A., Fish, A. and Wagner, I. 'Gate-diffusion input (GDI): a power-efficient method for digital combinatorial circuits', IEEE Trans. VLSI Syst., vol. 10, no. 5, pp. 566-581, 2002.
- [6] Morgenshtein, A., Fish A. and Wagner, I. 'Gate-diffusion Input (GDI) – a Technique for Low Power Design of Digital Circuits: Analysis and Characterization', Circuits and Systems, vol. 1, no. 1, pp. 477-480, 2002.

Intelligent Mirror – Personalized Advertisement

Ratbek Zhapparov

Student, Department of Electrical and Electronics
Engineering, Nazarbayev University.
Astana, Kazakhstan.
Email: ratbek.zhapparov@nu.edu.kz

Magaiyya Zhussip

Student, Department of Electrical and Electronics
Engineering, Nazarbayev University
Astana, Kazakhstan.
Email: magaiyya.zhussip@nu.edu.kz

Abstract

Image processing has a wide range of applications. In this paper, we are proposing to apply extracted information from image in advertisement industry. Advertisements on banners and LCD display have critical purpose for producers/service providers to sell their product and for consumers to make a decision. However, due to the absence of personalized advertisement there is a gap between consumers and advertisement. To fill this gap and solve this problem we are proposing a software called “Intelligent Mirror”. It will be able to detect gender, age, accessories, and cloth brand of the person in front of the mirror and depending on that provide personalized advertisement on the LCD display. However, due to the time limitations, at this stage our software is able to classify gender and provide gender specific advertisement on LCD mirror display.

Keywords: face detection; Fisherface method; gender classification; personalized advertisement;

I. INTRODUCTION

Researchers have done qualitative work and developed various methods and algorithms for image processing. Currently they are being used in surveillance cameras, human/object identification and tracking, and smart human-computer interaction, etc. In our paper, we are proposing to apply image processing in LCD advertisement. LCD advertisements installed at many public places such as shopping centers, airports, and public environments. By advertising products and services, they play crucial role in business promotion. Currently, LCD displays can detect human or moving object with motion sensor and display adverts in predefined sequence.

However, traditional LCD displays are not able to categorize adverts for each person [1]. The efficiency of LCD displays can be increased, if LCD displays are aware about the person in front of it and his/her possible interests. In this way, they can classify and personalize advertisements for each individual. This can be achieved by our software called “Intelligent Mirror”. To be precise, classifying gender, age, recognizing accessories and cloth brands on the human and taking into account weather conditions and season, “Intelligent Mirror” will provide appropriate personalized advertisement for the person. As a result, customers will be able to see

appropriate products of predicted interest while producers/service

providers will find right person as a potential consumer. Consequently, “Intelligent Mirror” may increase to the efficiency of the advertisement for both consumer and producer. For instance, during summer in the elevator of the shopping center, our gadget may display advertisement of women’s sunglasses, hats, new summer collection for the detected lady. However, due to the time limitations as a first version of the “Intelligent Mirror” software, we would focus only on gender specific advertising. Fully completed “Intelligent Mirror” software will be the bridge between producers and consumers and change the way how any product or service is advertised.

II. METHODOLOGY

To implement this software, following milestones have to be completed.

- 1) Face Detection of the person using web camera
- 2) Eye Detection and Face image cropping
- 3) Gender Classification
- 4) Displaying Advertisement

Face Detection

Firstly, “Intelligent Mirror” detects the face of a person from the camera. Algorithm of detecting face of the person is based on Haar feature-based cascade classifier [2]. This cascade classifier is trained by plenty of Haar-like features and then based on them, detects face of the person in a frame. Accuracy of this method achieves 95% and it can faster detect the face of a person than other existing algorithms [3]. Thus, we applied this method in our software to detect the face.

Eye Detection and Face Image Cropping

After face detection, our software takes image of detected face and starts to search for position of eyes. This process is done by Haar Eye Cascade Classifier. Algorithm of the classifier is based on Haar feature-based cascade classifier, which takes small computation time and has an accuracy of almost 93% [3]. After eye detection, the face image is rotated relative to the left eye in order to set both eyes on the same level. Consequently, this might reduce computation time and error rate of gender classification algorithm [4]. Then, rotated image is cropped to resolution of 168x192 pixels in order to obtain

the same pixel resolution as database that we use. Finally, cropped image will be stored and inputted to the gender classification.

Gender Classification:

Several methods can be used to perform gender classification from face images. Widely used four methods are Eigenfaces, Fisherface, Correlation, and Linear Subspace. Fisherface method is highly accurate and comparatively faster than other methods [5]. In addition, it is robust to changes in light intensity, which makes it possible to use in different environments. Therefore, we used Fisherface method for our software to classify gender.

Fisherface method applies feature extraction and classifier module in order to identify gender. Firstly, Fisherface method is “trained” for a certain set of frontal face images with known gender. This is done by extracting geometric “properties and features” from these images. The extracted data will be stored as a database. When the cropped image of detected person inputted to the gender classification, geometric features from image is extracted. Ultimately, classifier module will identify the gender of the person on the cropped image by comparing extracted features with the database. Flow chart of this method is demonstrated in Figure 1.

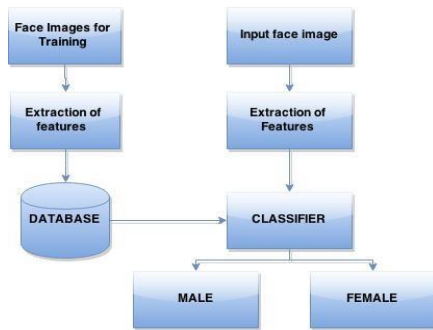


Figure 1. Flow chart of Gender Classification

We used the Extended Yale Database to train our software. The Extended Yale database contains face images of 28 people under 64 different light intensities. In this way, we use 1792 images from Extended Yale. In addition to this, we also created our own database consisting 210 images of 30 Kazakh people.

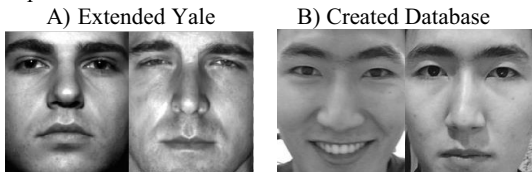


Figure 2. Examples of the Extended Yale Database and Created Database

Displaying Advertisement

Finally, based on identified gender, our software displays gender specific advertisement on LCD displays. “Intelligent Mirror” is capable of displaying several advertisements

simultaneously for only one person at a time. In order to catch attention of potential customer, we are proposing to use traditional mirror at the center. Once person approaches the mirror, “Intelligent Mirror” identifies gender and starts displaying advertisement on LCD displays. Initial design of the “Intelligent Mirror” as a product is shown in Figure 3.

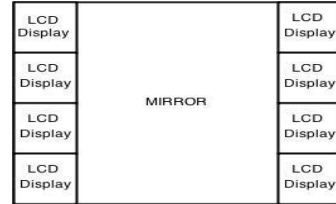


Figure 3. Initial design of “Intelligent Mirror” as a product

Ultimately, working principle of the “Intelligent Mirror” can be summarized in the flow chart demonstrated in Figure 4.

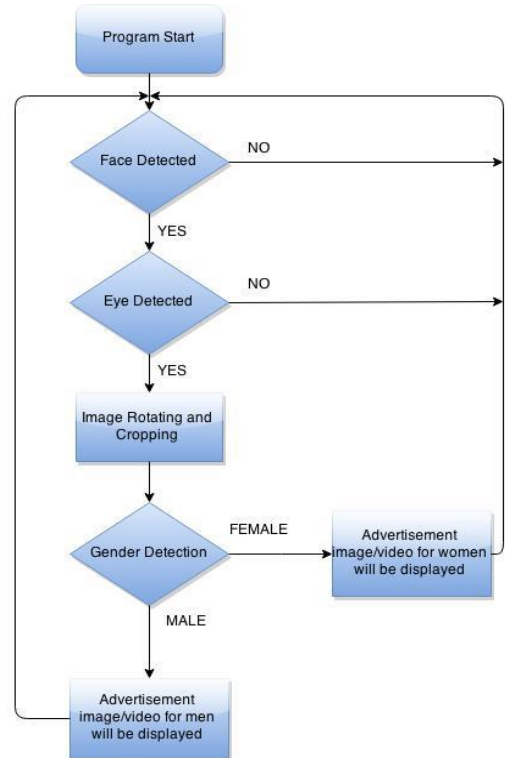


Figure 4. Flow Chart of the “Intelligent Mirror” software.

III. RESULTS

To demonstrate the performance of our software, we have tested it for group of people with different ethnicities. In addition, we also tested it under different lightning conditions, facial expressions, and different databases. Results of these tests are shown in Table 1.

Table 1. Results of the tests under various database and input image

Used database	Number of people	Accuracy
Extended Yale	50 (25 male, 25 female)	78.0%
Our database	30 (15 male, 15 female)	70.0%
Extended Yale + Our database	30(15 male, 15 female)	83.3%

For the first test, we used images of ethnicities that can be found in the Extended Yale database: Indian, Chinese, and European people. As a result, "Intelligent Mirror" correctly identified 39 out of 50 people, where 3 male and 8 female images were identified wrongly. Only 25% of the Extended Yale database contains female images, therefore, this might be the cause of higher error rate for female identification.

At the second test, "Intelligent Mirror" was trained only by our database and we used only images of Kazakh people to test it. Although it contained 210 images, the results of the test revealed medium accuracy. It was observed that "Intelligent Mirror" was not able to correctly classify 5 males and 4 females. The reason behind the error might be lack of images in created database, wearing glasses, and high light intensity variation.

By combining two databases, we achieved the accuracy of 83.3% for classifying gender of Kazakh people. At this time, "Intelligent Mirror" was not able to classify 1 male and 4 females correctly. Considering all obtained results, we notice that "Intelligent Mirror" is capable of providing good results. It was observed that the performance of software can be increased by using database with images of more distinct people rather than many images of one person from different angles. Therefore, database such as FERET and our database with more images, will be used in the completed version of the software.

IV. CONCLUSION

To sum up, this paper proposes software called "Intelligent Mirror" to fill the gap between customers and LCD advertisement. It will solve this issue by personalizing advertisement for each person by classifying gender. The software has been tested for several times using different databases and has achieved maximum gender classification accuracy of 83.3%. To improve the accuracy of our software, database is partially constructed by us. Considering its accuracy rate and non-existence of such novel approaches that would provide personalized advertisement in LCD displays, "Intelligent Mirror" is a unique software that will change the concept of how advertisement should be presented in LCD displays. As a future work, we already started working on identification of age, detection of accessories and cloth brand. Moreover, we will also analyze complex cases, where "Intelligent Mirror" will be able to provide advertisements for several people simultaneously. Complete version of "Intelligent Mirror" will be able to classify gender, detect age, recognize cloth brands, and then using these data provide personalized advertisement for multiple people simultaneously.

REFERENCE

- [1] Brewka, Gerhard, S. Coradeschi, and A. Perini, eds. ECAI 2006: 17th European Conference on Artificial Intelligence. Vol. 141. IOS Press, 2006.
- [2] Viola, Paul, and Michael Jones. "Rapid object detection using a boosted cascade of simple features." In Computer Vision and Pattern Recognition, 2001. CVPR 2001. Proceedings of the 2001 IEEE Computer Society Conference on, vol. 1, pp. I-511. IEEE, 2001.
- [3] Wilson, Phillip Ian, and John Fernandez. 2006. "Facial feature detection using Haar classifiers." Journal of Computing Sciences in Colleges 21(4): 127-133.
- [4] Singh, Omveer, Gautam Bommagani, Sravan Reddy Ravula, and Vinit Kumar Gunjan. "Pattern Based Gender Classification." International Journal 3, no. 10 (2013).
- [5] Belhumeur, Peter N., João P. Hespanha, and David Kriegman. "Eigenfaces vs. fisherfaces: Recognition using class specific linear projection." Pattern Analysis and Machine Intelligence, IEEE Transactions on 19.7 (1997): 711-720.



Ratbek Zhapparov is sophomore majoring Electrical and Electronics Engineering at Nazarbayev University. He graduated with distinctive degree from UCL Foundation Program. He is an active member of Institution of Engineering and Technology Student Chapter. He has previous research experience in signal propagation. His current research interest include millimeter wave and MIMO Communications for cellular systems and transportation vehicles, and antenna design. In fact, this summer (2015) he will be doing millimeter communication for cellular system at Wireless Networking and Communication Group at University of Texas at Austin. He is currently working on development of "Intelligent Mirror" startup project.



Magaiya Zhussip is a second year student majoring in Electrical and Electronic Engineering at Nazarbayev University. He is an active member of Institution of Engineering and Technology Student Chapter. He is interested in different high level languages such as java and android, digital image processing for age detection and gender classification. He is also interested in game development on java platform and participated in a Game Development competition at Suleyman Demirel University. He is currently working on "Intelligent Mirror" project to make it commercially available.

Maze solving by memristive network

Yernar Bainazar

Department of Electrical and Electronic Engineering
Nazarbayev University
Astana, Kazakhstan
e-mail: ybainazar@nu.edu.kz

Ruslan Tazhkenov

Department of Electrical and Electronic Engineeringline
Nazarbayev University
Astana, Kazakhstan
e-mail: rtazhkenov@nu.edu.kz

Abstract — the network consisting of memristors and switches is proposed in this project as a maze solving approach. Two kinds of maze problems: with only one exit path and with several ones are solved by two different methods using the same memristive network.

Keywords — maze solving, memristors, memristive fuse, memristance change with respect to time, shortest path, longest path

I. INTRODUCTION

Optimization problems in networks often require shortest path length calculations to determine the most efficient route. One of the optimization problems is labyrinth or simple maze that has one entrance and exit. The mazes are prototype models in graph theory, topology, robotics, traffic optimization, psychology, and in many other areas of science and technology. Therefore, there are many traditional methods in order to solve maze-escaping issues. These techniques vary from simple algorithms to huge arrays regarding to maze size and numbers of paths. Our paper is going to extend the idea of maze solving problems by using memristive network. Our memristive network will sort paths according to their lengths. We will show simulations by using memristive circuits that will demonstrate the shortest path of 2D maze.

II. PROBLEM STATEMENT

The main problem of maze solving is to find the exit from the labyrinth. There could only one exit path however there could be several ones at the same time and in this case the shortest path should be chosen in order to exit from the maze. So in this project these two maze problems with one exit path and several paths are solved using the same memristive network.

III. PROCEDURES

The main components of the circuit are the memristors which are defined:

$$V(t) = M(x) \times i(t); \quad (1)$$

$$dx/dt = f(x,t); \quad (2)$$

where v is the voltage across memristor, i – current, $M(x)$ – memristance of the device which is dependent on the x – internal state variable.

The simplest abstraction of the memristor is that of a time-dependent resistor:

$$M(t) = W(t)/D \times R_{ON} + (1 - W(t)/D) \times R_{OFF} \quad (3)$$

where $W(t)$ – width of the device, D – active core thickness, R_{ON} – ON resistance, R_{OFF} – OFF resistance.

For the simulation in LTSpice the following characteristics of memristor were used:

$R_{ON} = 100$ Ohms, $R_{OFF} = 5$ kOhms, $R_{INIT} = 1$ kOhm, $D = 10$ nm, $\mu = 1 \times 10^{-14}$ m/sV [1].

For maze problem solution the circuit with switches and memristors shown on Fig. 1 could be used. In this circuit switches represent the walls of the maze which shouldn't be crossed. So if the switch is opened then it means that there is now way in that direction. Voltage source is connected to the entrance of the labyrinth while the ground to the exit.

As the memristors have two opposite polarities while the current in the circuit could flow in both directions the memristive fuse is used which is shown on the Fig 2. Because the same minus polarities of two memristors are connected together the current could also flow into positive side which means that in output characteristics this current will be positive [2].

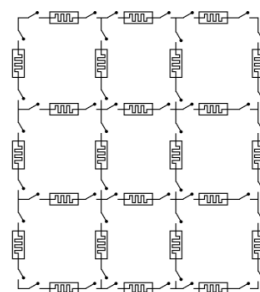


Fig. 1. Memristive network.

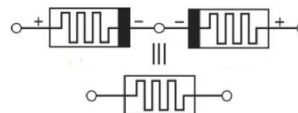


Fig. 2. Memristive fuse.

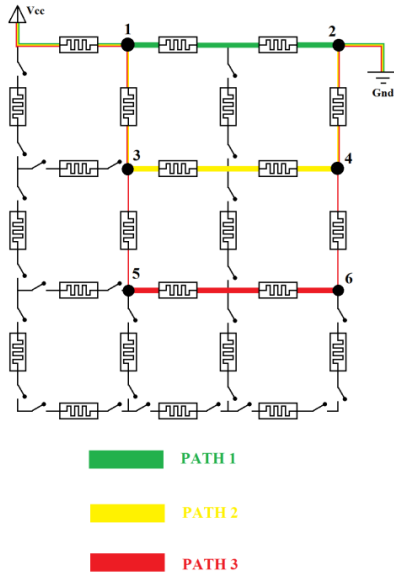


Fig. 8. Memristive network circuit for several paths maze.

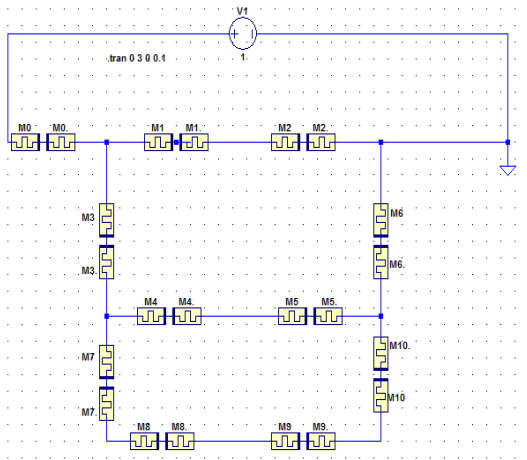


Fig. 9. Equivalent circuit built in LTSpice.

For this maze solution the memristance change with respect to time for different paths (first path – from the node 1 to 2, second path – from the node 3 to 4; third path – from the node 5 to 6) was observed which is calculated by the formula:

$$\Delta M = (V_X - V_Y) / I_{XY} R_{eq} \quad (4)$$

R_{eq} in our case is equal to $4 R_{INIT}$ as there are two memristive fuses between the nodes while the fuses consist of two memristors by their own.

Again the memristive circuit was built in LTSpice program (Fig. 8) and then the circuit was simulated in order to obtain the current flow and voltage drop across each branch of the maze (Fig.9).

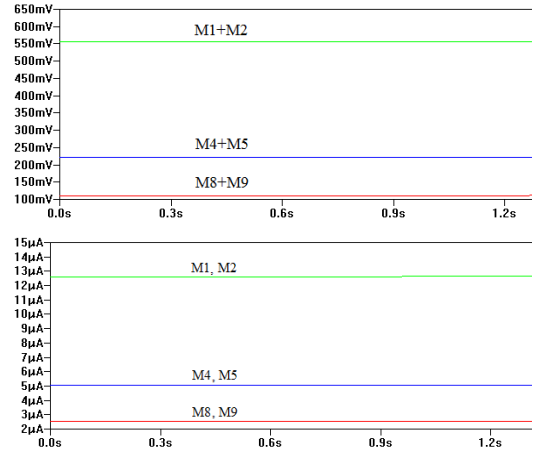


Fig. 10. Memristive network circuit for several paths maze.

Using the simulation values the table of the change of current and voltage drop across each branch with respect to different time was built. Moreover with the help of values obtained using the simulation memristance change was calculated using the formula 4 and these values were also included to the table.

TABLE I. I, V, M CHARACTERISTICS FOR EACH BRANCH

	Time [sec]	0	0,3	0,6	0,9	1,2	2,7	3,0
$V_X - V_Y$ [mV]	M1+M2	0	457,556	558,414	578,156	587,112	607,824	619,778
	M4+M5	0	212,026	222,766	230,462	232,850	239,180	243,170
	M8+M9	0	112,310	113,684	115,232	117,426	119,574	121,584
I_{xy} [μ A]	M1+M2	0	12,626	12,692	13,111	13,375	13,841	14,040
	M4+M5	0	5,030	5,076	5,238	5,317	5,435	5,527
	M8+M9	0	2,525	2,538	2,619	2,669	2,717	2,763
ΔM [k Ω]	M1+M2	0	40,479	40,793	39,998	39,996	40,010	40,004
	M4+M5	0	38,152	39,886	39,998	39,793	40,007	39,997
	M8+M9	0	32,239	39,997	40,097	39,896	39,915	40,144

Using the values from the table the graph of memristance vs time for three branches was built using MSExcel (Fig 11).

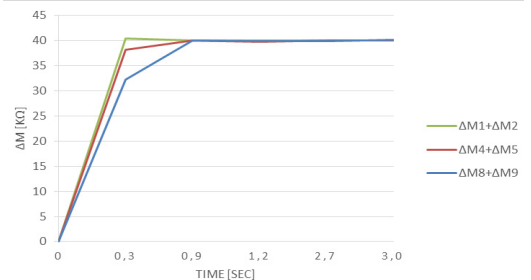


Fig. 11. Memristance change with respect to time for three paths.

From the graph it is observed that the first path (from node 1 to 2) exhibit the greater memristance change than for other paths until it reaches about 1s where all path's memristance changes aproximately equal to each other because all memristors reach the R_{OFF} value. In this case the maximum value is about 40k Ω because R_{OFF} of each memristor used in simulation is 5k Ω while each branch consist of two memristive fuses. It could be conclude that the greatest memristance change is for the shortest path.

For better visualisation the color code of the memristance change was used where the color closer to the red one means greater (Fig.12).

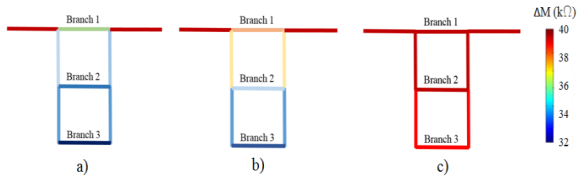


Fig. 12. Color code of three branches for a) 0.3 sec b) 0.6 sec c) 0.9 sec.

From the Fig.12 it is seen that at any time until the memristors reach the R_{OFF} value the memristance of the shorter path is closer to the red color than other branches' colors. When all memristors reach the R_{OFF} the color code of all branches become closer to red color that's why the memristance change with respect to time when all memristors reach this value. The shorter path is closer to red color which means has greater memristance change only when memristances' values are $R_{INIT} < M(x) < R_{OFF}$.

Then a random maze was built in order to observe memristance change and to visualize color code of these values through the whole circuit.

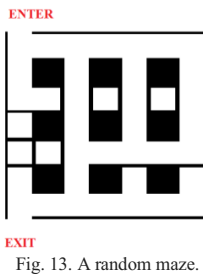


Fig. 13. A random maze.

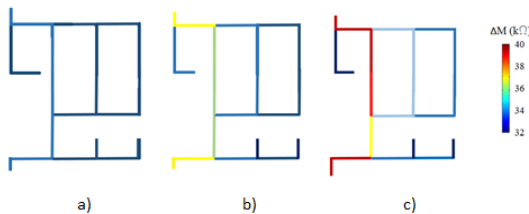


Fig. 14. Color code of random maze for a) 0.3 sec b) 0.6 sec c) 0.9 sec.

From the Fig. 14 it could be summarized that if the solver starts from enter and each time he follows the route with greater memristance change when the routes are intersected then this path will be the shortest one. For example the routes with deadlock have lower memristance values comparing with other routes.

V. CONCLUSION

In conclusion, we have observed that memristors can help to solve mazes in a massively parallel way. In other words, memristive networks are capable of computing shortest path in different variations difficulty mazes. This was experimentally proved by using systems of memristors, resistors and LTSpice software. Furthermore, implementation the maze solving logical algorithm with memristive networks will find huge usage in different area such as subway roads mapping.

VI. REFERENCES

- [1] Biolek Zdeněk, Biolek Dalibor and Viera Biolkova (2009). Radioengineering 18, 210
- [2] Zhanyou Ye, Shi Hong Marcus Wu and Themistoklis Prodrumakis (2013). Computing shortest paths in 2D and 3D memristive networks. Retrieved 31.03.2015 from <http://arxiv.org/abs/1303.3927>
- [3] Pershin Yuriy and Di Ventra Massimiliano (2013). Solving mazes with memristors: a massively-parallel approach. Retrieved 31.03.2015 from <http://arxiv.org/abs/1103.00>

VII. BIOGRAPHIES



Yernar Bainazar was born in Almaty, Kazakhstan on March 27, 1993. From 2004 to 2008, he studied at Russian Embassy School in Beijing, China. From 2009 to 2010, he continued his education at Republican Specialized Physics and Mathematics Secondary School named A.O. Zhaitykova for gifted children in Almaty, Kazakhstan. In 2011, he was graduated from school (with honor) in Astana, Kazakhstan. In 2011, he won admission to UCL's Centre for Preparatory Studies (CPS) and was successfully graduated in 2012.

He is currently a student in the Department of Electrical and Electronic Engineering at Nazarbayev University, Astana, Kazakhstan. His research interests include integrated circuits, wireless networks and power systems.



Ruslan Tazhkenov was born in Astana, Kazakhstan, in 1993. He graduated from Linguistic School №5 in Astana in 2011. In the same 2011 he received scholarship from Nazarbayev University and was enrolled in University College London Undergraduate Preparatory Certificates (UPC) foundation program at Nazarbayev University. In 2012 he was accepted in School of Engineering at his University majoring in Electrical and Electronic Engineering.

Memristor-based relaxation oscillators using digital gates

Yerkhan Sapiyev

Electrical and Electronic Engineering
Nazarbayev University
Astana, Kazakhstan
ysapiyev@nu.edu.kz

Azamat Utekeyev

Electrical and Electronic Engineering
Nazarbayev University
Astana, Kazakhstan
autekeyev@nu.edu.kz

Abstract—This project shows the design of memristor based oscillator, where memristor takes place of reactive element, in this case, it is capacitor. The usage of memristor gives certain advantages, comparing to traditional one. First of all, memristor based oscillator can be fully integrated on-chip giving an area-efficient solution. Secondly, usage of memristor will increase operating range of frequencies and provide wider range of resistance. Analytical solution using mathematical calculations and SPICE simulation results will be demonstrated.

Keywords—memristor; 3-gate oscillator;

I. INTRODUCTION

Oscillator is an electronic circuit, which produces periodic, oscillating signals. Oscillators are widely used in television and radio transmitters, buzzers, quartz clocks and clock signals that regulate computing devices. If behavior of signals is nonlinear that oscillator called relaxation oscillator. Output signals have triangle or square waveform. Conventional relaxation oscillators use reactive elements such as capacitor or inductor. Period of that signals depend on time constant of capacitor or inductor. As known, reactive elements have geometrical and capable limitations, i.e. frequency and size of oscillators are limited. However, there are more attractive replacements for reactive elements.

To overcome faced difficulties we propose to use memristor based oscillators. Memristor has a unique properties, it is a non-linear resistor which changes its state according to total charge passing through. It preserves its resistance after the removal of voltage. So, this property makes memristor an interesting field of study [6-9]. Application of memristor in relaxation oscillators is promising. There are two major advantages of using memristor based oscillator. Firstly, the memristor in oscillator allows providing higher frequency and wider range of resistance. Standard 3-gate oscillator has no physical possibility to provide higher frequency. Secondly, the scale of memristor gives an opportunity to insert such oscillator on chip. These properties makes memristor primary research target for many companies which see potential of such device. For example, HP is planning to start experiments in July, 2015, and to present first computer based on memristor in 2016 [1].

II. METHODOLOGY

The main feature of this oscillator comparing to standard 3-gate oscillator is wider range of frequency. To prove this theoretically, mathematical analysis will be provided below.

The frequency of standard oscillator is:

$$f \approx \frac{0.722}{R * C}$$

where R is the resistance and C capacitance. By replacing capacitor by memristor, the frequency formula will depend on the value of the memristor resistance. As the memristor resistance is:

$$R_m = R_1 * \frac{V_1 - V_2}{V_{OUT} - V_1}$$

the upper and lower values of resistance will be:

$$R_{mp} = R_1 * \frac{1 - \alpha}{\alpha} \quad R_{mn} = R_1 * \frac{\beta}{1 - \beta}$$

From this formula:

$$R_m dR_m = k' V_m(t) dt$$

we can get following integral relation

$$\int_0^{TH} dt = \frac{1}{k' * (V_{OUT} - V_2)} \int_{R_{mn}}^{R_{mp}} (R_1 + R_m) dR_m$$

$$T_H = T_L = \frac{R_{mp}^2 - R_{mn}^2 + 2R_1(R_{mp} - R_{mn})}{2k' V_{oh}}$$

$$f_0 = \frac{k' V_{oh}}{R_1^2} \frac{\alpha^2 (1 - \beta)^2}{[(1 - \beta)^2 - \alpha^2]}$$

So, maximum and minimum oscillation frequency will be

$$f_{min} = \frac{k' V_{oh}}{R_{off}^2} \frac{(1 - \alpha)^2 (1 - \beta)^2}{[(1 - \beta)^2 - \alpha^2]}$$

$$f_{max} = \frac{k' V_{oh}}{R_{on}^2} \frac{\alpha^2 \beta^2}{[(1 - \beta)^2 - \alpha^2]}$$

To prove these work by experimental data Tanner EDA program was used. To get experimental data, the circuit of Figure 1 was built in S-Edit part of this program.

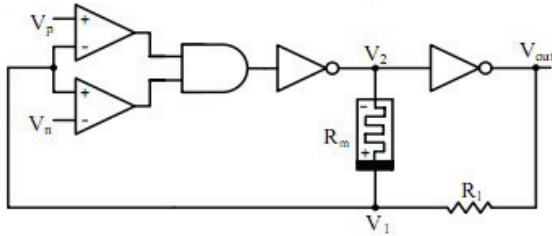


Figure 1. Schematic diagram of memristor-based oscillator.

To simulate this circuit, T-Spice code was written. However, our group faced several fatal errors, which we could not resolve. The screenshot of the error is provided below.

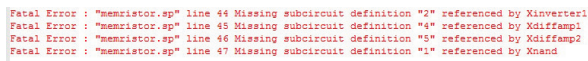


Figure 2. Error analysis

The source of this error could be several parts of the project: part of code working with differential amplifier, code of NAND gate and subcircuit description. Literature review in this area did not give a result. Therefore, we present our code with expected simulation results.

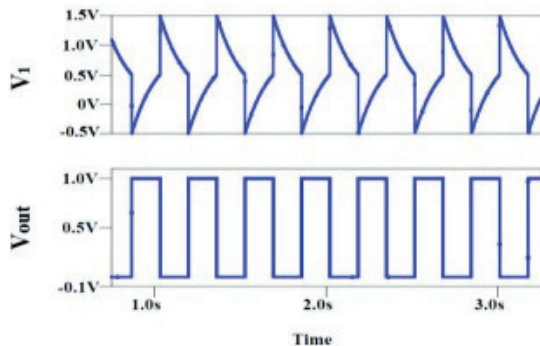


Figure 3. Simulation results for 3-gate oscillator.

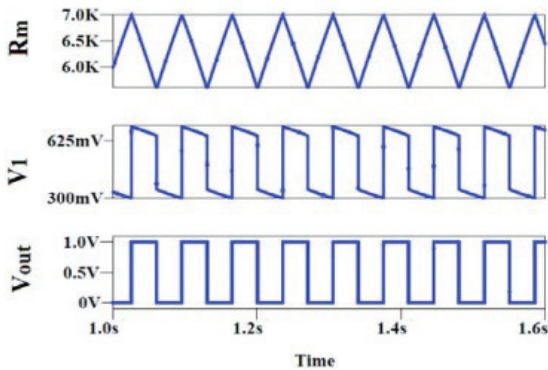


Figure 4. Simulation results for memristor-based oscillator.

As it can be seen from graphs on Figures 3 and 4 prove theoretical expectations.

III. CONCLUSION

In this work, two different type of oscillator were compared. The standard 3-gate oscillator and memristor based oscillator. It was theoretically proven, that memristor based oscillator has wider range of frequency comparing to standard 3-gate oscillator. However, Spice simulation was not achieved, and expected results were presented.

IV. SPICE CODE

```
.hdl memristor.va
XMemristor 1 0 memristor d=10n rin=80k roff=100k ron=1k uv=10f
.SUBCKT inverter
.hdl bsim3v34pMOS.va
.hdl bsim3v34nMOS.va
vd x1 x0 3
vg x2 x0 0
xekv1 x1 x2 3 1 bsim3v34pMOS
xekv2 x3 x2 0 0 bsim3v34nMOS
.ENDS inverter
.SUBCKT diffamp
VS x1 x2 AC 1 SIN(0 10MVPEAK 10KHZ)
VCM x2 x0 SIN(0 0MVPEAK 5KHZ)
VCC x11 x0 DC +15V
VDD x12 x0 DC -15V
Q1 x3 x1 5 Q2N2222
Q2 x4 x2 5 Q2N2222
RC1 x11 x3 1000
RC2 x11 x4 1000
RE x5 x12 7.2K
.model Q2N2222 NPN(Is=3.108f Xti=3 Eg=1.11 Vaf=131.5 Bf=217.5
Ne=1.541
+ Ise=190.7f Ikf=1.296 Xtb=1.5 Br=6.18 Nc=2 Isc=0 Ikr=0 Rc=1
+ Cjc=14.57p Vjc=.75 Mjc=.3333 Fc=.5 Cje=26.08p Vje=.75
+ Mje=.3333 Tr=51.35n Tf=451p Itf=.1 Vtf=10 Xtf=2 Rb=10)
.ENDS diffamp
.SUBCKT NAND
RL x3 x4 500
S1 x3 x5 1 0 SW
S2 x5 x0 2 0 SW
.ENDS
VV1 1 0 SIN(0 5 0.1)
Xinverter1 1 2
Xdifffamp1 +5V 0 4
Xdifffamp2 -5V 0 5
Xnand 4 5 1
R1 2 0 3K
.MODEL SW VSWITCH(VON=2.6 VOFF=2.4 RON=10
ROFF=1MEG)
.tran 0.05 10
.probe
.print v(1,0)
.end
```

[3], [4], [5]

REFERENCES

- [1] M.A. Khatib, M.E. Fouda, A.G. Mosad, K.N. Salama and A.G. Radwan, "Memristor-based relaxation oscillators using digital gates"
- [2] Z. Biolek, D. Biolek, V. Biolkova. "SPICE model of memristor with nonlinear dopant drift"
- [3] No author, Digital electronics. "Design of NAND gate in SPICE and simulation"
- [4] V.Sudheer. "SPICE experiments"
- [5] No author, Circuit center. "Basic digital gates"
- [6] Maan, A.K.; Kumar, D.S.; Sugathan, S.; James, A.P., "Memristive Threshold Logic Circuit Design of Fast Moving Object Detection," Very

- Large Scale Integration (VLSI) Systems, IEEE Transactions on , vol.PP, no.99, pp.1,1 doi: 10.1109/TVLSI.2014.2359801
- [7] James, A.P.; Kumar, D.S.; Ajayan, A., "Threshold Logic Computing: Memristive-CMOS Circuits for Fast Fourier Transform and Vedic Multiplication," Very Large Scale Integration (VLSI) Systems, IEEE Transactions on , vol.PP, no.99, pp.1,1 doi: 10.1109/TVLSI.2014.2371857
- [8] Ibrayev, T. , Fedorova, I. , Maan, A. and James, A. On Design of Memristive Amplifier Circuits. Circuits and Systems, 5, 2014, 265-273. doi: 10.4236/cs.2014.511028.
- [9] James, A.P.; Francis, L.R.V.J.; Kumar, D.S., "Resistive Threshold Logic," Very Large Scale Integration (VLSI) Systems, IEEE Transactions on , vol.22, no.1, pp.190,195, Jan. 2014 doi: 10.1109/TVLSI.2012.2232946



Azamat Utekeyev was born in Kazakhstan in 1993. Graduated Nazarbayev Intellectual School in 2011. Currently, he is 3rd year student of Nazarbayev University majoring in Electrical and Electronic Engineering. His main areas of research interest are communication systems and electrical machines. His hobbies are playing guitar and judo (Japanese wrestling)



Yerzhan Sapiyev was born in Kazakhstan in 1994. Graduated Kokshetau Kazakh-Turkish high school for gifted boys in 2011. Currently, he is 3rd year student of Nazarbayev University majoring in Electrical and Electronic Engineering. His main areas of research interest are communication systems and power generation. He is member of NU Football League team. His hobbies are writing short stories, playing guitar and writing articles about football.

MEMRISTOR SPICE MODEL AND ITS APPLICATIONS TO CIRCUIT SIMULATION OF MEMORY CELLS

BekishevDanyiar, Kapan Arman

Abstract: Memristor is a two-terminal electrical component that depends on charge and flux linkage, simply it is a resistor that has a memory. The working principle of memristor is: it has the resistance that always changes depending on the current that has passed previously. But in past years Hewlett-Packard declared that they produced memristor by the help of TiO_2/TiO_{2-x} structure. In our paper structures, physical characteristics of the memristors will be explained and one of the most important applications of memristor, which is memory cell, will be further examined and simulations of the memory structure will be done, finally results will be demonstrated.

Keywords: Memristor, SPICE, nonvolatile memory, resistance, flux, charge.

1. INTRODUCTION

Before 1971, passive elements of the circuit were only capacitor, inductor and resistor, until Chua derived the fourth passive element called memristor. He found the dependency of the memristor on the electric charge and magnetic flux [1]. Moreover, he proved that the components of memristor cannot be duplicated by using any combinations of resistors, capacitors and inductors. Due to its unique properties, memristors were exploited in many areas such as nonvolatile RAM, neuromorphic circuits [4-7] and programmable IC's [2].

Physical structure of TiO_2 memristor:

Figure 1 shows the construction of the TiO_2 memristor. In the TiO_2 memristor, a thin undoped titanium dioxide (TiO_2) layer with a thin oxygen – deficient doped titanium dioxide (TiO_{2-x}) layer are clamped between two platinum electrodes. TiO_2 is semiconducting material that has high Resistance (R_{off}) but if the O_2 atoms are removed from the material, then empty spaces will act as donor dopants, thus Resistance will be dropped to low values (R_{on}). When a voltage or current is applied to the device, the width of the TiO_2 and TiO_{2-x} layer varies as a function of the employed voltage or current [3]. As a consequence, the resistance between the two electrodes is adapted. Moreover, it is said to be that the main part of the device is the drifting of

the O_2 atoms for the applied Electric Field (E) and current (I).

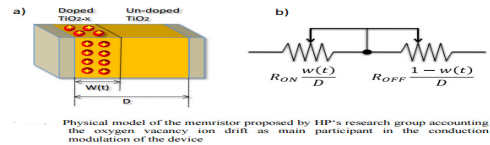


Figure 1. Physical model of memristor

2. METHODS AND DESIGN

The following equation demonstrates accurate model for Memristor Spice Simulation. Memristance is given as a function of the state variable q, and because of that the state equation does not sensitive to truncation errors.

$$R(q(t)) = R_{off} + \frac{R_{on} - R_{off}}{ae^{-4kq(t)} + 1}, \quad a = \frac{R_{ini} - R_{on}}{R_{off} - R_{ini}}$$

In Spice Model, q can be found by integrating port current I with capacitor C_{int} as it is seen from Figure 2. After that q becomes equal to voltage at the node Q. Series connection of R_{off} and controlled voltage source are used as a model for memristive port.

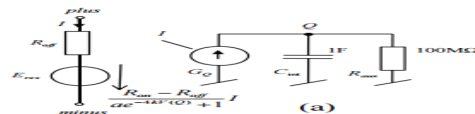


Figure 2. Memristor Circuit

Memristor Simulation:

Figure below is the code that explains the characteristics of Memristor:


```

* Memristor SPICE Model
* Ron, Roff - Resistance in ON / OFF States
* Rinit - Resistance at t=0
* D - Width of the thin film
* uv - Migration coefficient
* p - Parameter of the WINDOW-function
* For modeling nonlinear boundary conditions
* x = W/D Ratio, W is the actual width
* of the doped area (from 0 to D)
*
.SUBCKT memristor Plus Minus PARAMS:
+ Ron=100 Roff=10k Rinit=11k D=10n uv=10f p=10
* DIFFERENTIAL EQUATION MODELING *
*****
Cx 0 x value=( IC(Emem)*uv*(Ron/D)**2*(U(x),p))
Cx x 0 1 IC=(Roff-Rinit)/(Roff-Ron)
* RESISTIVE PART OF THE MEMRISTOR *
*****
Emem Plus aux value=-I(Emem)*U(x)*(Roff-Ron)
Roff aux minus {Roff}
*****
* NONLINEAR DRIFT MODELING *
*****
*window function, according to Joglekar
.func F(x,p)=(1-(2*x-1)**(2*p))
*proposed window function
;.func F(x,i,p)=(1-(x-sttp(-i))**(2*p))
.ENDS memristor

Xmemrist aa 0 memristor
Utest aa 0 SIN(0 1.25 1 0 0)
.tran 0 3s 0 3m
-probe
.end
    
```

3.SIMULATION RESULTS

Figure 3 is the Result of the simulation for the I-V pinched hysteresis loop. Here, we have sinusoidal input voltage at 100Hz and 100kHz. Hysteresis in the circuit is occurred at the time when frequency reached 100KHz.

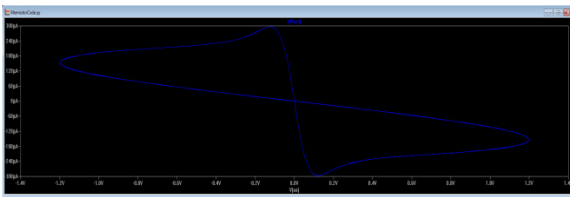


Figure 3: I-V Hysteresis Loop

The figure 4 shows VI characteristics of the Memristor. Here sinusoidal input voltage is drawn with green, and current I with blue color. Vingets maximum value of 1.2V, whereas I takes maximu 300uA. Here, I-V characteristic was matched to 100Hz data.

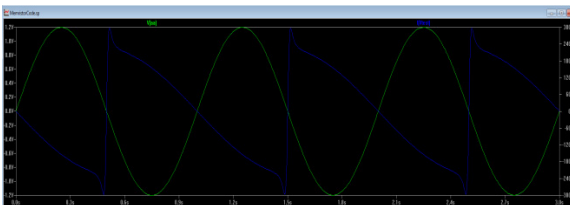


Figure 4: VI characteristics of Memristor

Memory Cell Code and Simulation Results:

```

*Memory cell memristor
*****
.subckt memristor plus minus params: d=100n del=66.6n Su=100u er=5 Uev=0.33
.paran e0=8.854p m=9.109e-31 e=1.602e-19 h=6.626e-34
.paran C0=(e0*er*Su/d) C1=(C0/(1-del/d)) C2=(C0*d/del)
.paran a=(Su*er**2/(4*pi*h*Uev*del**2)) b=(4*pi*del*sqrt(n*e)*pur(Uev,1.5)/h) loga=(log(a))
.func I12(U1)=(U1*abs(U1)*exp(LIMIT(loga-b/MAX(abs(U1),ln),-20,20)))
*****
C1 plus c {C1}
C2 c minus {C2}
Q0 c minus value=(I12(Uc,minus))
Rshunt c 0 100meg
*****
.ends memristor
Vin 1 0 sin 0 7.5 100
Rin 1 2 1
XMC 2 0 memristor
EQ Q 0 value={-sd1(I(Vin))}
.tran 0 50n 20n 50u
-probe
.end
    
```

Memristor can be used in construction of nonvolatile memory. The memristor give a possibility of using quasi capacitor type of data storage like DRAWs but with long life time. The I-V characteristics of memristor, contain both the current and the integral of current. It means that without any extra circuit, only by cutting the charging current, the voltage of the device decreases to zeros directly. Moreover the stored information do not change which means that the control circuit of memory become much simpler. Additionally, the power dissipation of memristor is low in comparison with flash memory and their access time in reading process is fast, also the writing pulse have more amplitude and longer time. In future it is expected that by using fast ions the writing pulse in memristor will become less than flash memories.

The current controlled type memristor was used in design of memory cell. This design propose the excitation (input data) in terms of current type while the measurement (output date) in terms of voltage type. The resistance switching mechanism in memristor is based on Bipolar Resistance Switching. Writing the “0” and “1” logics (corresponding to low and high resistance state) are done by controlling amplitude, frequency and polarity of writing pulse.

The Figure 5 is the hysteresis loop of I-V characteristic for Memristor

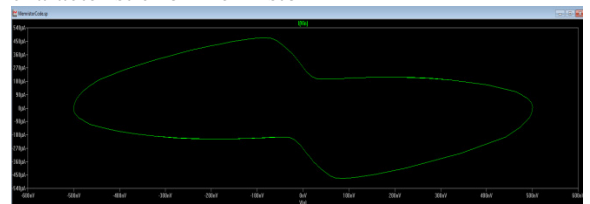


Figure 5: Hysteresis Loop of Memristor memory cell

In Figure 6 “1” writing pulse is applied which has changes the state of system from 0 to 1. After a pulse for reading operation is applied, its graph is represented in figure 3. Then in response to this pulse the output voltage that is read is interpreted as “1”. This pulse causes the system state to be distorted. The operations repeat, next “0” writing pulse, and after a read pulse is applied again. In this memory the circuit control always performs a read operation before any write operation in order to prevent

Simulation and Analysis of Reconfigurable Threshold Logic Gates Using Memristive Devices

Alfiya Kulmukhanova

Electrical and Electronic Engineering Department
 Nazarbayev University
 Astana 010000, Kazakhstan
 akulmukhanova@nu.edu.kz

Abduvakhit Junussov

Electrical and Electronic Engineering Department
 Nazarbayev University
 Astana 010000, Kazakhstan
 ajunussov@nu.edu.kz

Abstract — we present our research on Reconfigurable Threshold Logic (RTL) gates which are combined with memristive devices and CMOS circuits. The OR gate was used to define if the increase of the power or voltage supply time will affect the value of the memristive devices. The result was presented as a SPICE code and simulation graphics.

Keywords—threshold logic gates; memristors; CMOS

I. INTRODUCTION

The following research was conducted basing on paper “Reconfigurable Threshold Logic Gates (TLG) Using Memristive Devices” submitted to Subthreshold Microelectronics Conference. The idea of that paper was to use threshold logic gates and memristors to analyze how TLG with combination of memristors can lead to changes in reconfigurable architectures. The feasibility of threshold logic has been noted in several leading works [5-8], that further ascertain the interest in this topic.

The authors of the paper designed a circuit which was able to operate as four different logic gates by changing the resistance of the memristors. The circuit is shown on the Figure 1 was designed on Cadence software, and then simulated. Simulation was done by changing the input voltage pulses to reach required resistances.

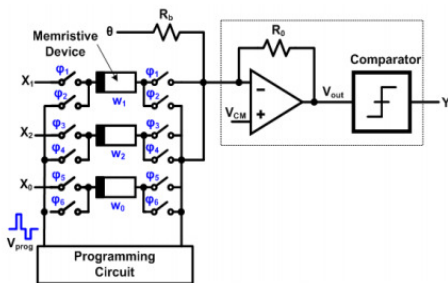


Figure 1. Circuit for memristive devices[1].

They used four basic logic operations: OR, AND, NOR, NAND. In order to get required logic operation, the resistance of the memristors should be set to values described in Table 1.

Table 1. The resistances of memristive devices

Logic operation	R ₁ (kΩ)	R ₂ (kΩ)	R ₃ (kΩ)
NAND	1.33	1.17	3.88
NOR	1.33	1.17	1.33
AND	2.81	4.81	1.33
OR	2.81	4.81	3.88

These resistors are inside the memristive devices, and they are labelled on the Figure 1 as R₁ is w₁, R₂ is w₂, R₃ is w₃.

So, after implementing the circuit above, and gaining expected results, the circuit (Figure 1) was physically realized on a printed circuit board, and memristors were reprogrammed by using FPGA based voltage pulses.

II. OBJECTIVE

For our project the same devices and principle were used. However, instead of simulating all four logic operations, only one is taken into a count: OR. The idea is to remove programming circuit, which is responsible for applying required voltage value to memristive devices, and change their logic operation. Instead of it, the required voltage directly applied to memristors through the X₁, X₂, and X₃ inputs to produce OR logic operation. Then, input voltage is increased manually and output of the summing amplifier will be analyzed. Additionally, it is being planned to increase the time of constant voltage supply, and observe how memristive device will behave.

III. METHODOLOGY

In the paper which is analyzed four logic gates can be performed by a single programming circuit by changing memristor values. It is predicted that some problems may occur with the circuit, if the same gate is used for a long period of time. The reason is that memristive device stores resistance and can change considerably its resistance value over the time, and in that case logic operation will also be changed automatically. Specifically, OR gate is predicted to suffer memristor resistance changes as it constitutes of high resistance weights for all three synapses. In this research OR

gate configuration of proposed reconfigurable logic gates will be analyzed by simplifying the circuit and performing continuous timing analysis.

Trahn et al. performed their research using Silver-Chalcogenide (Ag-Ch) memristive devices [1], and our work is based on KAUST HP memristor model which is available online [2,3]. Original circuit contained 2 parts: programming circuit and logic gate circuit based on summing amplifier with weighted inputs. As we are considering only OR gate, programming circuit was omitted in this work and memristors were preconfigured to the needed values. Off and on resistance values for used memristive devices were changed to those suggested for TLG in Table 1 and initial resistance was set to the R_{off} (high resistance) to obtain the configuration of OR gate directly. Summing amplifier was performed using operational amplifier with active load [4]. Feedback resistance value was taken from the studied paper and is $R_{FS}=2.02k\Omega$. The code was generated using MATLAB and SPICE and circuit was simulated in T-Spice. Figure 2 shows the circuit constructed for the project:

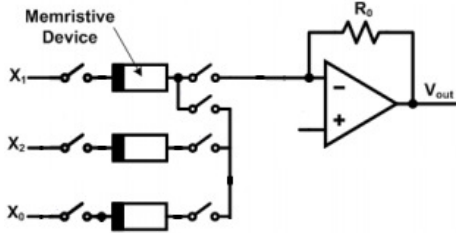


Figure 2. Circuit for OR operation

IV. RESULTS AND DISCUSSION

When Spice code for the circuit (Figure 2) was obtained, it was simulated by using T-spice. Several experiments were done to observe the behavior of the circuit. Obtained results are provided on Figure 3, 4 and 5.

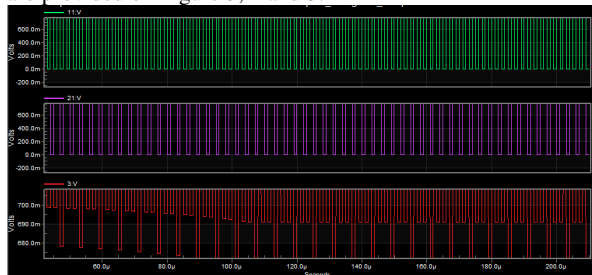


Figure 3. Input voltage = 5V

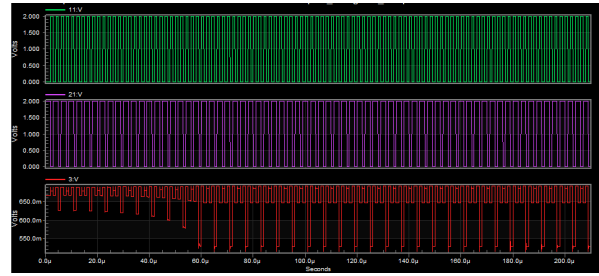


Figure 4. Input voltage = 2V

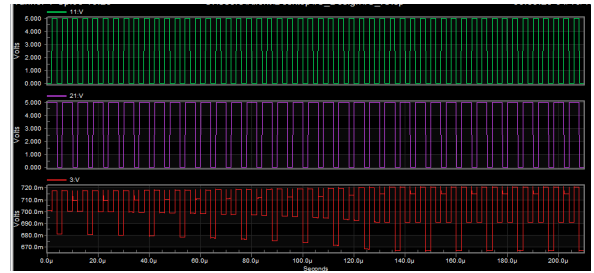


Figure 5. Input voltage = 5V (pulse duration increased)

As it can be seen from the Figure 3, which has an output voltage change at point $t \approx 100\mu s$ with input voltage equal to 5V. When the input voltage was changed to 2V with the same pulse duration (Figure 4), it can be observed that the output voltage starts to change at point $t \approx 60\mu s$. Finally, the Figure 5 provides the simulation result on input voltage equal to 5V and doubled pulse duration and period. In that case, output started to change at approximately $t \approx 120\mu s$. Based on the gained results it can be stated that the memristive device cannot be kept in one configuration for a long period of time, and should be reprogrammed as often as possible. Also, it should be mentioned that with the same duration of the pulse and with decrease of the input voltage output voltage starts to change earlier. When with the constant input voltage and bigger pulse duration, output voltage starts to change later.

CONCLUSION

Reconfigurable threshold logic gates device based on memristors is a promising breakthrough in digital logic design. Memristive devices claimed to be more efficient, consume small area and dissipate less power, and thus are desirable in electronics design. However, memristor's ability to store the resistance depending on flux/charge can be negative aspect for the applications where fast switching or constant resistance value, such as in this project, are required. OR gate was performed during this research, and constraints on constant usage of this configuration were determined. High frequencies should be avoided while using memristive devices in logic gates due to resistance switch of the memristor. Also voltage amplitude has significant effect on the output and operating at higher voltage seems to be more stable. Further research should be conducted to determine exact operating constraints of this reconfigurable threshold logic gates.

REFERENCE

- [1] A. Rothenbuhler, T. Tran, El. H. Barney Smith, and etc, "Reconfigurable Threshold Logic Gates Using Memristive Devices", *Journal of Low Power Electronics and Applications*, vol. 3, pp. 174-193, 2013
- [2] A. G. Radwan, M. Affan Zidan, and K. N. Salama, "On the mathematical modeling of Memristors", 22nd International Conference on Microelectronics (ICM 2010), pp. 284-287, Egypt, December 2010
- [3] A. G. Radwan, M. Affan Zidan, and K. N. Salama, "HP memristor mathematical model for periodic signals and DC", IEEE International Midwest Symposium on Circuits and Systems (MWSCAS), pp. 861-864, USA, August 2010
- [4] T. C. Carusone, D. A. Johns, and K. Martin, "Folded-cascode opamp", *Analog Integrated Circuit 2nd Edition*, 2015
- [5] Maan, A.K.; Kumar, D.S.; Sugathan, S.; James, A.P., "Memristive Threshold Logic Circuit Design of Fast Moving Object Detection," *Very Large Scale Integration (VLSI) Systems*, IEEE Transactions on , vol.PP, no.99, pp.1,1 doi: 10.1109/TVLSI.2014.2359801
- [6] James, A.P.; Kumar, D.S.; Ajayan, A., "Threshold Logic Computing: Memristive-CMOS Circuits for Fast Fourier Transform and Vedic Multiplication," *Very Large Scale Integration (VLSI) Systems*, IEEE Transactions on , vol.PP, no.99, pp.1,1 doi: 10.1109/TVLSI.2014.2371857
- [7] Ibrayev, T. , Fedorova, I. , Maan, A. and James, A. On Design of Memristive Amplifier Circuits. *Circuits and Systems*, 5, 2014, 265-273. doi: 10.4236/cs.2014.511028.
- [8] James, A.P.; Francis, L.R.V.J.; Kumar, D.S., "Resistive Threshold Logic," *Very Large Scale Integration (VLSI) Systems*, IEEE Transactions on , vol.22, no.1, pp.190,195, Jan. 2014 doi: 10.1109/TVLSI.2012.2232946

AUTHOR'S BIOGRAPHY



Alex James.

Alfiya Kulmukhanova is currently an undergraduate student at Department of Electrical and Electronic Engineering, Nazarbayev University. Her interests include image processing, face recognition, memristor based threshold logic. She is currently conducting research on CMOS/memristor based memories under supervision of Professor



Abduvakhit Junussov.

Abduvakhit Junussov is currently an undergraduate student at Department of Electrical and Electronic Engineering, Nazarbayev University. His interests are microcontrollers, sensors and actuators, communication system, and power engineering. For the last year he has been working on research paper named "Analysis of a Reconfigurable Fibonacci Switched Capacitor Converter with a Multiphase Balanced Switching" with Professor Alexander Ruderman.

Simulation of Full Adder design using hybrid memristor-CMOS based technology

YerdenKypshakpayev, KuatbekMukabak
Nazarbayev University
Astana, Kazakhstan

Email: ykypshakpayev@nu.edu.kz, kmukabak@nu.edu.kz

Abstract—Thememristor is a newly developed electrical device which is intended to be used in memory-based technologies. It has better scalability, higher utilization and lower power consumption than CMOS based technologies. In this paper, the full adder is designed using hybrid memristor and CMOS technologies. In simulation process, a new state called “middle state” and new input values called “modified input values” are introduced. This new method solves most of the simulation errors in memristor based circuits.

Keywords—Memristor, memristor modeling, full adder.

I. INTRODUCTION

For the first time, the memristor was introduced by Leon Chua [2] as a nonlinear fourth fundamental circuit element in 1971. Basically, memristor relates the magnetic flux with electric charge. The first physical design of memristor was implemented by the HP labs. As a result the findings proved the hysteresis behavior of the memristor postulated by Chua [2] and ability to use it as a memory device attracted the attention of researchers into this field [6-9].

A memristor is a bipolar device, where the coupling between electron and ion mobility gives the memristive ability to it. According to HP’s realization, a memristor is defined as a thin film of TiO₂ between two Pt metallic contacts and consists of two regions such as R_{ON} and R_{OFF}(Fig. 1). One of the two regions is high doped region (R_{ON}) with width “w”, which is also called as state variable of the memristor. Because, by changing the value of “w”, it is possible to change the resistance of the memristor, hence the state of the memristor. The other one is called as undoped region with high resistance (R_{OFF}). When the doped region is forward biased, the applied voltage increases the width (“w”) of the doped region, consequently, the resistance of the memristor is decreased and the memristor goes to ON state. In contrast, if the doped region is negative biased, it decreases the width (“w”) of the doped region and the memristor goes to OFF state.

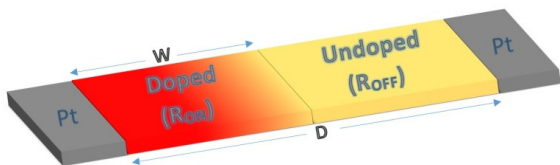


Fig. 1. Memristor device presented by HP labs

This paper aims to design the full adder using hybrid memristor and CMOS technologies. The Section II will describe the memristor linear model with mathematical expressions. Section III concerned with design issues such as SPICE model of memristor, logic gates and full adder design.

II. LINEAR MODEL OF MEMRISTOR

In general, two equations such as ohms law and a state equation are enough to describe memristive system [4]:

$$V = R(w, i) I \quad (1)$$

$$\dot{w} = f(w, i) \quad (2)$$

Based on these two equations, the linear model is defined by the following expressions.

$$V = M(x)i \quad (3)$$

$$M(x) = R_{ON}x + R_{OFF}(1 - x) \quad (4)$$

$$\dot{x}(i) = \frac{\mu_{Ron}}{D^2} i(t) = ki(t) \quad (5)$$

M(x) is the resistance of the memristor. x corresponds to the state variable x=w/D relationship of doped region width to the total width. Value of the state variable x lies between 0 and 1 and defines the state as R_{off} and R_{on} respectively. $\frac{\mu_{Ron}}{D^2}$ is a constant that defines state variable, where μ is the drift mobility of oxide. The linear model is the simplest model that describes the behavior of the memristor.

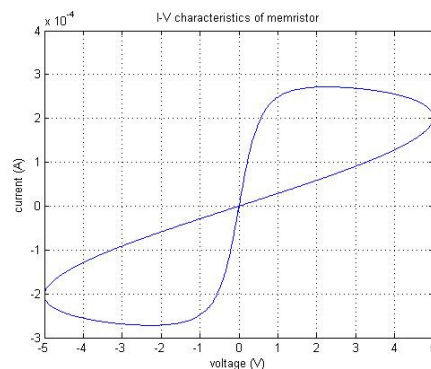


Fig. 2. I-V characteristics of the memristor

The Figure 2 represents the I-V characteristics the memristor which shows the hysteresis behavior of the device. The fact that this loop passes through the origin shows that the memristor does not store energy.

III. METHODOLOGY

A. Memristor model

In order to use the memristor on the logic gate design, it is important to consider its physical model. One of the most common ways of modeling a memristor is using an analog electronic circuit simulator SPICE. There are different types of SPICE software, but due to its simplicity the SPICE simulator developed by "Linear technologies" was preferred. Additionally, the LTspice model for the memristor was found from user Martin Falatic [3]. This model was based on the paper on SPICE model of memristor with nonlinear dopant drift by Czech scientists Bioleks and Biolkova [1]. The memristor model as a new device is thus put into a library with other devices. Physical design of the device can be implemented by putting the spice model on LTspice simulator. In order to test its correspondence with actual memristive behavior it is important to see whether the model given represents the true characteristics of the memristor. Thus the following simple circuit in Figure 3 was constructed.

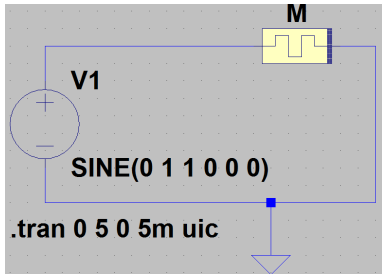


Fig.3.Memristor in electrical circuit

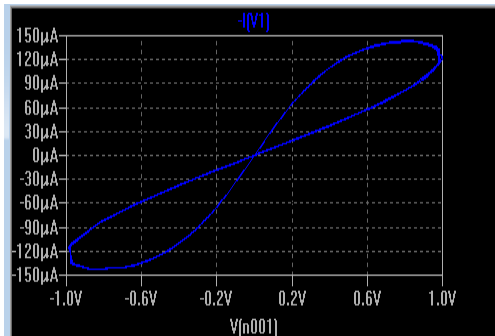


Fig. 4. I-V characteristics of memristor spice simulation

The Figure 4 shows the simulation result obtained from simulating the memristor model proposed by Martin Falatic using LTspice. The graph represents the hysteresis loop for simulations, thus it can be stated that the device shows the actual memristive behaviors.

B. Full Adder

Adder is an electronic device that converts analog or digital binary signals into their equivalent sum. The typical design of full adder requires XOR, AND, OR gates that are designed by CMOS technology. Another way of representing these gates is using memristor, as it is further explained that memristors can be used for performing logical operation. Thus this paper proposes a simplified design for the full adder using a hybrid CMOS and memristor technology. The application of memristors as gates is said to reduce the area, power consumption and increase the performance of the operation. Thus the full adder circuit will be constructed and the simulation will show the input and output signals that will be compared to the expected outcomes.

C. Logic OR

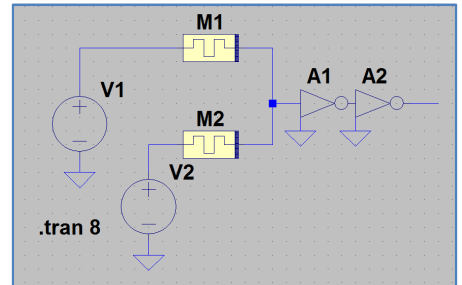


Fig. 5. Hybrid circuit configuration of OR gate

The hybrid CMOS and memristor based OR gate is designed by Nasrudin [5]. As mentioned before, when the doped region is forward biased, the resistance of the memristor is decreased to small value (R_{ON}). In contrast, if the doped region is negative biased, the resistance increases to R_{OFF} . This behavior is used for logic gate construction. The output point is considered as the node between two memristors. It gives the opportunity to use the voltage divider law. For example, when $V1=0$, $V2=1$, the resistance of M1 increases to large value while resistance of M2 is decreased to small value, R_{ON} . The voltage between two memristor is:

$$V_{OUT,OR} = \frac{R_{OFF}}{R_{OFF} + R_{ON}} V_{high} \approx V_{high} = 1$$

With similar method, the other possible outcomes are given below in Table 1.

TABLE I. The properties of hybrid OR gate

V1 (V)	V2 (V)	Resistance of M1 (Ω)	Resistance of M2 (Ω)	Output Voltage(V)
0	0	unknown	unknown	0
1	0	R_{ON}	R_{OFF}	1
0	1	R_{OFF}	R_{ON}	1
1	1	unknown	unknown	1



Fig. 6. Output of hybrid logic OR gate

In Figure 6, the 2 bottom graphs are the input values, red graph is the final output after the 2 inverters, and the top graph shows the node voltage between two memristor. The result showed a wrong result for logic OR gate, that is the input value $V1=0$ and $V2=1$ gave an output “0”, which should be “1”. And this error is happened also for other AND and XOR gates. It can be seen on top graph (cyan), where the voltage between two memristor is increased from 0, and did not reach to 1V, it stayed at 0.5V. It means, now the two memristor have the same resistance, although they are differently biased. Let’s analyze it deeply. Initially, two memristor had the same resistance, assume R_m . When $V1=0$ and $V2=0$, no current is produced and the node between two memristor is certainly “0”. Then, $V1=1$ and $V2=0$, the node voltage between two memristor is increased from 0.5V to 1V since resistance of M2 is increased from R_m to R_{OFF} and resistance of M1 decreased from R_m to R_{ON} . When $V1=1$ and $V2=0$, by theory, the resistance of M1 should increase from R_{ON} (it was R_{ON} last time) to R_{OFF} while resistance of M2 should decrease from R_{OFF} (it was R_{OFF} last time) to R_{ON} . However, the simulation result showed that the one time input pulses were only able to increase the resistance of M1 from R_{ON} to R_m , and decrease the resistance of M2 from R_{OFF} to R_m . It means, that the memristor may not go directly from OFF state to ON state with one pulse. Thus, a recommendation is made to describe the memristor with three states: ON, OFF and Middle state.

TABLE II. Recommended states for memristor

States	ON state	Middle state	OFF state
Resistance	R_{ON}	R_m	R_{OFF}

At each time, after entering the input values and obtaining the corresponding output, the memristor should be returned to Middle state, so it can further go either ON state or OFF state with one pulse. Returning the memristor to Middle state is possible by applying the inverse values of inputs after every pulses. For example, if the input value is 1, then 0 should be applied after some time. Thus, after every calculation, the 2 memristors go back to its Middle state, where they have the same resistance. It is recommended to convert the inputs to “improved input” values. It looks like to the Manchester code, but it does not go below 0. For the output value, only the first half cycle is considered. The second half cycle is designed to return the memristor to

Middle state. Now, let’s simulate the OR gate again with improved input values.

TABLE III. Improved input values

Input	Improved Input
0	01
1	10

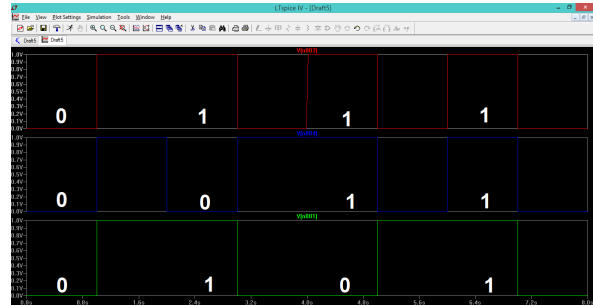


Fig. 7. Output of hybrid logic OR gate with improved input

The simulation results in Figure 7 corresponds the Logic OR gate behavior. Thus, it is concluded that the recommended “Middle state” and “Improved input” methods worked out. With similar method, let’s develop logic AND and Full adder.

D. Logic AND

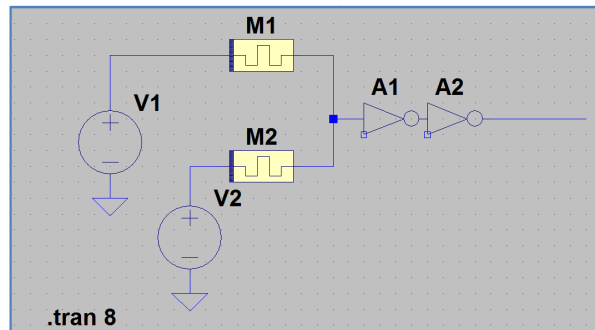


Fig. 8. Hybrid circuit configuration of AND gate

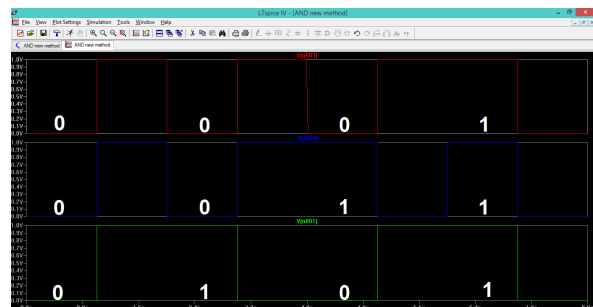


Fig. 9. Output of hybrid logic AND gate with improved input values

E. Logic XOR

The XOR is designed using already simulated OR and AND logic gates.

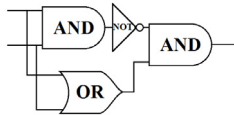


Fig. 10. The logic diagram of XOR

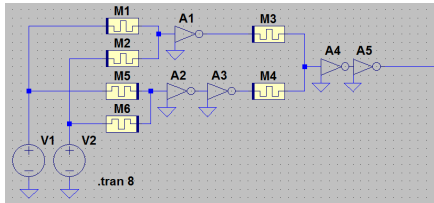


Fig. 11. Hybrid circuit configuration of XOR gate



Fig. 12. Simulation of XOR gate with improved input values

F. Full Adder design

After successfully simulating all the above logic gates, the Full adder can be designed easily according to logic scheme below.

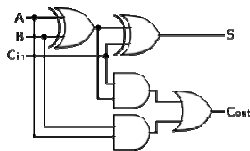


Fig. 13. The logic diagram of full adder

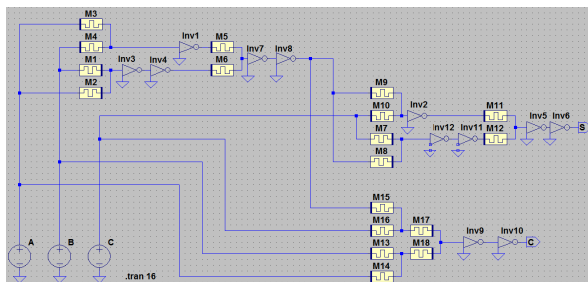


Fig. 14. Hybrid circuit configuration of Full Adder

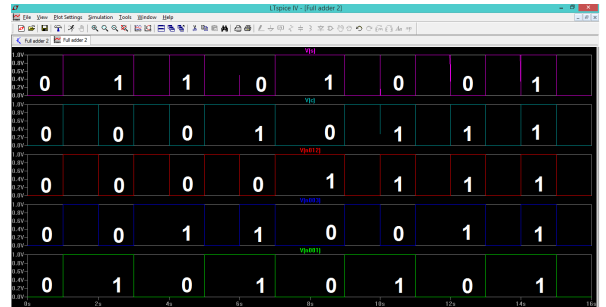


Fig. 15. Simulation results of Hybrid Full Adder

As seen in Figure 15, the full adder simulation results correspond the full adder behavior. The Nasrudin is also designed the hybrid full adder circuit, but the simulation process was failed [5]. However, in this paper, the full adder circuit is designed again and the simulation process is conducted successfully with an improved method. The hybrid full adder circuit uses 18 memristors and 12 inverters.

IV. CONCLUSION

In this paper, the full adder circuit is designed using hybrid memristor and CMOS technologies. The memristor model is based on Bioleks and Biolkova’s design. In the simulation process, a new method is introduced which uses “Middle state” and “improved input values”. By applying proposed method, the simulation results of full adder is determined successfully.

REFERENCES

- [1] Biolek D, Biolek Z. and Biolkova V. “SPICE modeling of memristive, memcapacitive and meminductive systems,” 2009
- [2] Chua L. and Kang S. M. “Memristive Devices and systems”, *proceedings of the IEEE*, vol. 64, pp.
- [3] Faticic M. Memristor simulation with LTspice – a practical example! Available at <http://www.faticic.com/index.php/69/memristor-simulation-with-ltspice-a-practical-example> [accessed at April 30, 2015]
- [4] Mohammad, B.; Homouz, D.; Elgabra, H., "Robust Hybrid Memristor-CMOS Memory: Modeling and Design," *Very Large Scale Integration (VLSI) Systems, IEEE Transactions on*, vol.21, no.11, pp.2069-2079, Nov. 2013
- [5] Nasrudin A. and Adzmi A.F. Nanoelectronics implementation of full adder with memristors, *IEEE2012*
- [6] Maan, A.K.; Kumar, D.S.; Sugathan, S.; James, A.P., "Memristive Threshold Logic Circuit Design of Fast Moving Object Detection," *Very Large Scale Integration (VLSI) Systems, IEEE Transactions on*, vol. PP, no.99, pp.1,1 doi: 10.1109/TVLSI.2014.2359801
- [7] James, A.P.; Kumar, D.S.; Ajayan, A., "Threshold Logic Computing: Memristive-CMOS Circuits for Fast Fourier Transform and Vedic Multiplication," *Very Large Scale Integration (VLSI) Systems, IEEE Transactions on*, vol. PP, no.99, pp.1,1 doi: 10.1109/TVLSI.2014.2371857
- [8] Ibrayev, T., Fedorova, I., Maan, A. and James, A. On Design of Memristive Amplifier Circuits. *Circuits and Systems*, 5, 2014, 265-273. doi: 10.4236/cs.2014.511028.
- [9] James, A.P.; Francis, L.R.V.J.; Kumar, D.S., "Resistive Threshold Logic," *Very Large Scale Integration (VLSI) Systems, IEEE Transactions on*, vol.22, no.1, pp.190,195, Jan. 2014 doi: 10.1109/TVLSI.2012.2232946

Yerden Kypshakpayev is a 3rd year student of Electrical and Electronics Engineering, Nazarbayev University. His interests are analog electronics, switched capacitor converters, digital communication. Currently, He is involved in project on memristor modeling

Kuatbek Mukabak is currently pursuing the B.S. degree in electrical and electronic engineering at Nazarbayev University, Astana, Kazakhstan. His interested area is integrated circuit design, memristor based circuit design and embedded system

Simulation of Memristive Threshold Logic Cell

Rizukov Yerlan
Nazarbayev University
Astana, Kazakhstan
yrizukov@nu.edu.kz

Ryskaliyev Aibek
Nazarbayev University
Astana, Kazakhstan
aryskaliyev@nu.edu.kz

Abstract—This paper is aimed on demonstrating the new method of fast moving object detection conducted with memristors. Commonly, moving object detection is done by comparing the features of sample image with the tested one, which is vastly ineffective at higher rates of image processing due to its algorithmic complexity and time delays. The memristive threshold logic circuit design provides the opportunity to speed up this process.

Keywords—memristor; object detection; spice simulation; BPRT;

I. INTRODUCTION

In this paper, we advance toward to moving object-detection problem. This work will present the new way of frame matching method with the help of bilevel threshold logic cell. Also we are going to introduce schematic representation to object tracking problem that will be able to operate with high frame rate and high resolution video images.

II. METHOD

In order to find out the difference of the reference and the test frames, the several parameters need to be applied. There is a so called BPRT cell, which has voltage value for every pixel as an input $x_i (i=1,2,\dots,n)$ to the memristor, for the reference frame. Each memristor has a weight (conductance) $w_i (i=1,2,\dots,n)$, which has to be configured dynamically. Dynamic allocation of conductance is configured by comparison of each weight value with the average voltage of each pixel. It can either be w_H , if $w_i > x_a$, or w_L , if $w_i < x_a$. Furthermore, there is another parameter called constant weight, w_o . To find the output, x_{out} of the reference frame, the weighted summation model, x_o of all inputs must be calculated. Additionally, the normalized pixel values must be estimated and represented as an average, x_a , which also serves as the logistic threshold t_a . There is a condition that must be satisfied, to find the x_{out} .

$$x_{out} = 1V, \text{if } x_i < t_a \text{ OR}$$

$$x_{out} = 0V, \text{otherwise}$$

It is important to mention that the all the weight configurations for the reference frame are remembered, for the

purpose of comparison of it with the test frame. There are two operations that need to be performed. First one is the comparison of reference frame conductance values with test frame, to get the similarities or dissimilarities from the black to white color change. The same operation is performed for the second case; however, the normalized pixel values are inverted, and new reference frame weights are configured. This is done to find the change in the light to dark color shift, if any. Consequently, if two frames are different, cell output can either be 1 V or 0 V, it can be seen by the bilevel voltage values, if they are the same, that means there is no object in the test frame, or if voltage values are different, which means there is a significant difference, and object is detected.

The average of the input values

$$x_a = 1/n \left(\sum_{i=1}^n x_i \right)$$

The Richard's curve has to be considered, in order to deduce the expression for w_i

$$w_i = w_H / (1 + b e^{cx_i}) + w_L$$

Taking $b e^{cx_i} = 1$ and $x_i = x_a$, the equation for c can be found

$$c = -1 / (x_a \log b)$$

$$w_i = w_H / \left(1 + b e^{-x_i / x_a \log b} \right) + w_L$$

The weighted sum model of

$$x_o = \left(\sum_{i=1}^n x_i w_i \right) / \left(w_o + \sum_{i=1}^n w_i \right)$$

Finally, output expression is given below

$$x_{out} = \frac{b e^{-\beta} \sum_{i=1}^{nx_i} w_i}{1 + b e^{-\beta} \sum_{i=1}^n x_i w_i}$$

$$\text{where } \beta = \frac{\log b}{t_a \left[w_o + \sum_{i=1}^N w_i \right]}$$

III. RESULTS

To perform the object detection process, firstly the template image frame is taken from the video where all the background objects are stationary, and then the subsequent test image frame is compared to it. This process requires two parallel BPRT networks modules, where they separately detect the white-to-dark and dark-to-white pixel intensity changes. The whole network is pyramid shaped, thus if we have 4x4 pixel image every 2x2 pixel pack of it combines into a single cell resulting in four-cell output module. Then outputs of two modules will be combined using AND gate. Since completely similar images will give output of 1V we will be able to see the changes of two different ones with label 0V. The result of applying different frames can be seen below, where the change in the output of pixel can be seen as transaction from 1V to 0V.

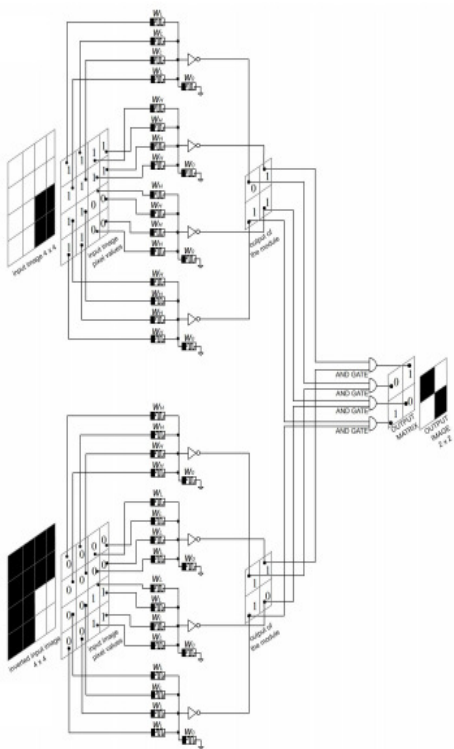


Figure 1. Training of a BRT network for object detection with an input image of size 4x4 pixels. (Maan, A.K, Memristive Threshold Logic Circuit Design of Fast Moving Object Detection)

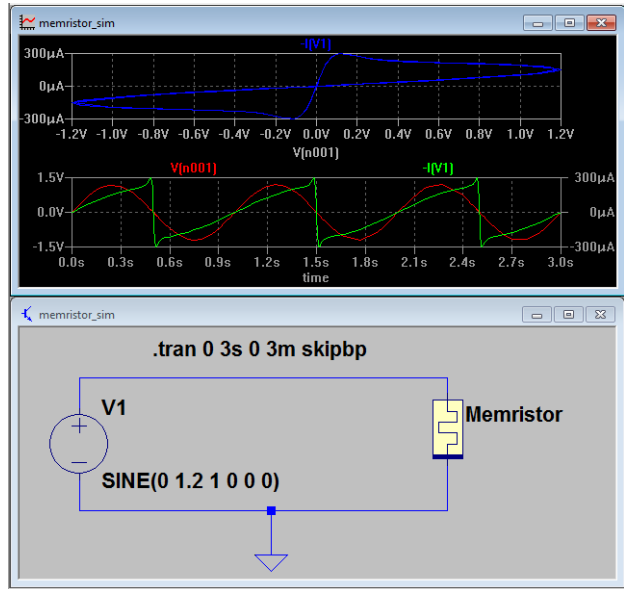


Figure 2. One memristor simple circuit simulation

The simulation was done in LTSpice software were first memristors were simulated in a simple circuit illustrated in figure 2.

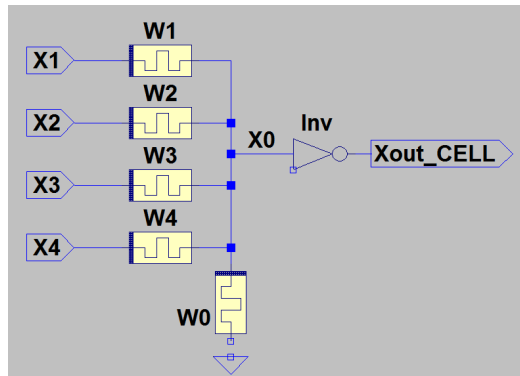


Figure 3. Example of a BPRT cell that uses a four-input pixel values.

After that, we moved on to simulate BPRT cell using the graph in figure 3 and formulas explained in method section for X_o , X_{out} , X_a . Next, our team tried to simulate the 4x4 pixel image presented in Maan, A.K’s paper partially illustrated in figure 1. The schematic was sketched in LTSpice which can be seen in figure 4, and the code for derivation of X_o , X_{out} , X_a was written on matlab. However, unfortunately we could not combine those schematic and code to gain a solid simulation.

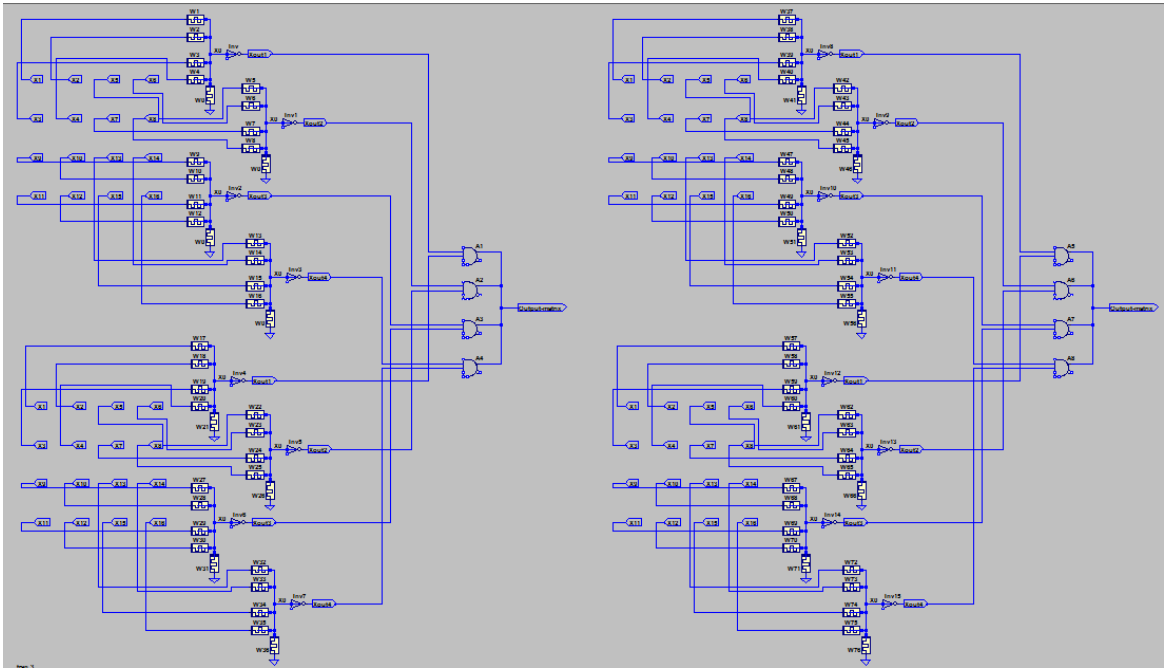


Figure 4. LTSPice schematic of 4x4 pixel image

IV. CONCLUSION

In conclusion, memristor features with its ability of much faster operation compared to other systems where they face high component delay at high sampling rates. Also algorithmic simplicity plays at its favor. Our team would also recommend including RGB identification along with black and white, to be able to track the change in color too. This would be useful to watch the transaction of traffic light or fuel combustion. Additionally, it would also be useful to have several template images as samples for tested images to be compared. This would be useful in case you want to neglect or exclude the detection of some movement. Example would be a working fan.

AUTHORS

Rizukov Yerlan grew up in Uralsk, Kazakhstan, and graduated Kazakh-Turkish high school with several international winner awards in mathematics. Currently studying in Nazarbayev University majoring on Electrical and Electronic engineering and actively participation in deepening his knowledge on this sphere. The most important of them are onshore field engineering internship at KazTransOil Company and OCEAN Software

Development project at Schlumberger Company. Besides his study, Yerlan is passionate working with Phoposhop and programming in HTML/CSS to create attractive, unusual web designs. His future plan is to find balance between his interest and engineering, and then keep mastering these skills.

Ruskaliyev Aibek current student of Nazarbayev university graduated Kazakh-Turkish high school. Loves to spend his time coding in Java and C++ languages and solving problems from Khan Academy.

REFERENCES

- [1] Maan, A.K.; Kumar, D.S.; Sugathan, S.; James, A.P., "Memristive Threshold Logic Circuit Design of Fast Moving Object Detection," Very Large Scale Integration (VLSI) Systems, IEEE Transactions on , vol.PP, no.99, pp.1,1
- [2] T. D. Dongale, "An Overview of Fourth Fundamental Circuit Element- 'The Memristor'", School of Nanoscience and Technology, Shivaji University, Kolhapur, M.S-India

Simulation of the Generic Memristive Circuit Model with Parasitic Components.

Saltanat Salpenova
Electrical and Electronic Engineering
Nazarbayev University
Astana, Kazakhstan
szsalpenova@gmail.com

MereyBalgabayev
Electrical and Electronic Engineering
Nazarbayev University
Astana, Kazakhstan
merey.balgabayev@gmail.com

Abstract—The main aim of this project is to verify the work of the baseline paper by conducting the simulation of the generic memristive circuit model with parasitic components. The simulation of the model was conducted and the results were compared with the experiments from the baseline paper.

Keywords—memristor; parasitic components; SPICE; thermistor.

I. INTRODUCTION

Nothing is ideal. Despite the successful discovery of memristors [2], their mathematical modelling [3], promising features and perspective areas of application [6-9], the studies about them are mostly theoretical and based on the ideal prototypes.

The paper, on which this work is based, introduces the model (Fig. 1), which performs and reproduces the behavior and characteristics of the real memristor. According to Sah et al. [1], this may be achieved by adding to the memristor model four elements (small inductance, capacitance, small DC voltage and current sources) representing the parasitic effects of the real memristor. The schematic circuit is given in Fig. 1.

This concept was then checked experimentally on the Negative-Temperature-Coefficient (NTC) thermistor. As a result of the experiment, the IV characteristics of the thermistor were obtained by simulation; however, the hysteresis loops have not satisfied the zero-crossing feature of the memristors.

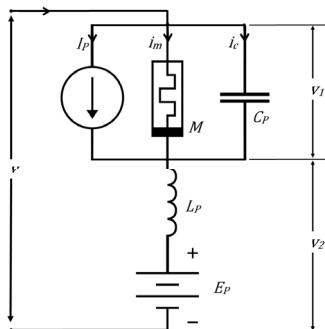


Fig. 1. Generic memristor model.

II. EXPERIMENTAL RESULTS

The simulation of the memristor model [3,4], with and without the parasitic components, was conducted and the results were compared with the baseline paper. The main parameters for the circuit elements for simulation are $E_p=1.5V$, $I_p=0.5mA$, $C_p=5nF$ and $L_p=2mH$.

However, some of these components' values from the paper were not applicable for the simulations conducted with the memristor model, because the results of the simulation were meaningless. Namely, the SPICE simulations, which correspond to the authors' experiments at 0.1Hz or 0.8Hz, were conducted at 1Hz. Other values were chosen by trial and error

In addition, it was observed, that minor changes in the parasitic current and inductance values have no significant effect on the hysteresis loops; whereas, parasitic voltage and capacitance values have some limits: $V_{max} \approx 0.03V$ and $C_{max} \approx 6mF$. In more detail, if the voltage exceeds approximately the value of 0.03V, the hysteresis loop starts to unreasonably band; on the other hand, continuous decreasing the voltage leads to the weakening of the parasitic effect. The same trend is characteristic for the capacitance value: after excess the value of 6mF, the hysteresis loop starts to fluctuate, whereas, too low value eliminates the parasitic effect.

The Fig. 2 demonstrates both the work of Sah et al. [1] on the NTC thermistors (left column) and the IV characteristics of the memristor model obtained from the conducted simulations. As it was mentioned, there were some changes in the components' values. In the right column are presented the results of the simulations obtained by both using the baseline paper's values and the described close to limits values.

The deviations of the achieved results from the expected are caused by using completely different models (thermistors and Verilog-A model of memristor). In contrast to thermistors, the results of the memristor model simulation satisfy the zero-crossing characteristics. However, despite the simulations with the parasitic voltage gave the results and tendencies slightly similar to the expected ones, the effect of the parasitic capacitance fell short of expectations.

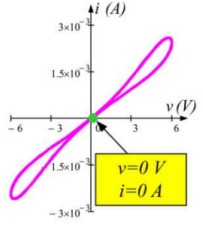
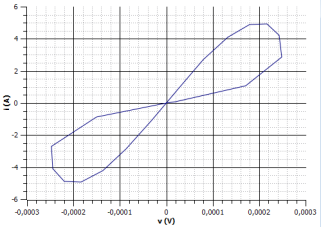
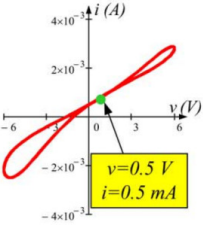
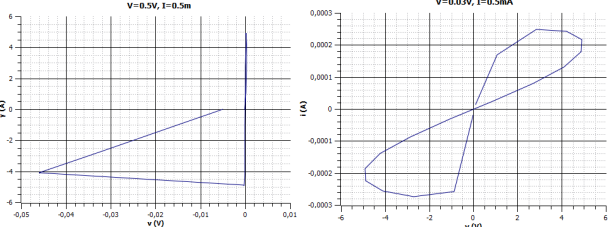
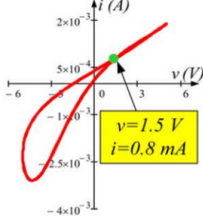
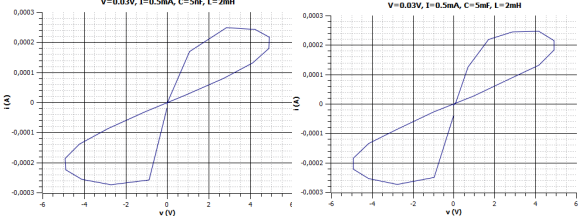
NTC thermistor	Memristor model	
Simulation results without parasitic circuit elements	Simulation results without parasitic circuit elements	
$f = 0.1Hz$	$f = 1Hz$	
		
Simulation results when $C_p=0F$, $L_p=0H$, $E_p=0.5V$, $I_p=0.5mA$	Simulation results when $C_p=0F$, $L_p=0H$, $E_p=0.5V$, $I_p=0.5mA$	Simulation results when $C_p=0F$, $L_p=0H$, $E_p=0.03V$, $I_p=0.5mA$
		
Simulation results when $C_p=5nF$, $L_p=2mH$, $E_p=1.5V$, $I_p=0.8mA$	Simulation results when $C_p=5nF$, $L_p=2mH$, $E_p=0.03V$, $I_p=0.5mA$	Simulation results when $C_p=5mF$, $L_p=2mH$, $E_p=0.03V$, $I_p=0.5mA$
$f = 0.08Hz$	$f = 1Hz$	
		

Fig. 2. The simulation results for a) NTC thermistors conducted by Sah et al. [1], b) memristor model.

III. CONCLUSION

This project has investigated the memristor model with parasitic components. As a result IV characteristic of the memristor model with different parasitic component values were examined. Although the research of Sah et al. [1] was not verified entirely, the parasitic effect was observed, but with different values.

In fact, the experimental part of the baseline work was conducted on the thermistors; however, considering the successful design of Hewlett-Packard laboratories [5] with the memristors, similar studies and calculations may be conducted on the real memristors and compared with the theoretical models with parasitic components.

REFERENCES

- [1] M.P. Sah, C. Yang, H. Kim, B. Muthuswamy, J.Jevtic and L. Chua, "A Generic Model of Memristors with Parasitic Components", IEEE Transactions on Circuits and Systems – I, Vol. 62, No. 3, pp.891-898, March 2015.
- [2] L.O. Chua, "Memristor – the Missing Circuit Element", IEEE Transactions on Circuit Theory, Vol. ct-18, No.5, pp.507-519, September 1971.
- [3] A. G. Radwan, M. Affan Zidan and K. N. Salama, "On the mathematical modeling of Memristors," 22nd International Conference on Microelectronics (ICM 2010), pp. 284-287, Egypt, December 2010.
- [4] A. G. Radwan, M. Affan Zidan and K. N. Salama, "On the mathematical modeling of Memristors," 22nd International Conference on Microelectronics (ICM 2010), pp. 284-287, Egypt, December 2010.
- [5] D.B. Strukov, G.S. Snider, D.R. Stewart and R.S. Williams, "The Missing Memristor Found", Nature, Vol. 453, pp. 80-81, May 2008.
- [6] Maan, A.K.; Kumar, D.S.; Sugathan, S.; James, A.P., "Memristive Threshold Logic Circuit Design of Fast Moving Object Detection," Very Large Scale Integration (VLSI) Systems, IEEE Transactions on , vol.PP, no.99, pp.1,1,doi: 10.1109/TVLSI.2014.2359801

- [7] James, A.P.; Kumar, D.S.; Ajayan, A., "Threshold Logic Computing: Memristive-CMOS Circuits for Fast Fourier Transform and Vedic Multiplication," Very Large Scale Integration (VLSI) Systems, IEEE Transactions on , vol.PP, no.99, pp.1,1,doi: 10.1109/TVLSI.2014.2371857
- [8] Ibrayev, T. , Fedorova, I. , Maan, A. and James, A. On Design of Memristive Amplifier Circuits. Circuits and Systems, 5, 2014, 265-273. doi: 10.4236/cs.2014.511028.
- [9] James, A.P.; Francis, L.R.V.J.; Kumar, D.S., "Resistive Threshold Logic," Very Large Scale Integration (VLSI) Systems, IEEE Transactions on , vol.22, no.1, pp.190,195, Jan. 2014,doi: 10.1109/TVLSI.2012.2232946



Saltanat Salpenova is a 3rd year student of Nazarbayev University, School of Engineering, Electrical and Electronics Engineering department. She was born in Arkalyk, Kazakhstan in 19th March, 1993. Then, after living in Karaganda city from 1995 to 1998, her family moved to Astana. She studied in three schools and graduated from "Nazarbayev Intellectual School" with the gold medal "AltynBelgi" in 2011. During the school years, she was engaged in national dances and participated in the national contest of the research projects in 2011. Currently, she learns German language.



Merrey Balgabayev is a 3rd year student of Nazarbayev University, School of Engineering, Electrical and Electronics Engineering department. He was born in Zhanakurgan, Kazakhstan in 30th December, 1993. He lived in Kentau until 1999, when his family moved to the capital city Astana. He studied in four schools and graduated from the high school "Nazarbayev Intellectual School" with honors in 2011. During the school years, he was engaged in ballroom dances and music school in dombra class. In high grades he participated in Math and Geography Olympiads on the city and regional stages, learned French language.

Simulation of Pinched Hysteresis Loops of Two Memristor SPICE Models

Akzharkyn Izbassarova and Daulet Kengesbek
 Department of Electrical and Electronics Engineering
 Nazarbayev University
 Astana, Kazakhstan
 aizbassarova@nu.edu.kz, dkengesbek@nu.edu.kz

Abstract—This paper compares two different SPICE models for memristor device by analyzing pinched hysteresis loops. A sinusoidal voltage source is applied in order to obtain i - v characteristics for both models. Then different set of simulations are done with distinct frequency and initial state values.

Keywords—memristor, pinched hysteresis loop, SPICE.

I. INTRODUCTION

The fourth passive element, named memristor, was firstly proposed 44 years ago by circuit theorist Leon Chua. The main feature of this two-terminal element is that it behaves like a nonlinear resistance and has nonvolatile memory. [1][7-10]. The first solid-state prototype of the memristor device was designed at Hewlett-Packard (HP) Laboratories in 2008. [2].

In this paper two memristor models, which were designed in order to observe application of memristor in microwave devices, are considered. [3] The scope of this paper is to compare these two models and identify whether they follow the same basic characteristics as a memristor in terms of pinched hysteresis loop.

II. MEMRISTOR SPICE MODELS

Memristor is a nonlinear device, which is characterized by three main properties. [4] [5]. The first feature is zero-crossing property. Despite the memory effect of memristor, there is no phase shifts and the output is always zero when the input is zero. The second important property of the memristor is that the i - v characteristics of the memristor has a form of pinched hysteresis loop when the bipolar periodic voltage or current is applied. In addition, one more property is a frequency response of the pinched hysteresis loop. The area of the hysteresis shrinks with the increase in frequency of the input signal and it tends to a straight line at significantly higher frequencies. The physical model of the memristor can be expressed with the following mathematical equations [6]:

$$v(t) = \left(R_{ON} \frac{\omega(t)}{D} + R_{OFF} \left(1 - \frac{\omega(t)}{D} \right) \right) i(t) \quad (1)$$

$$\frac{d\omega(t)}{dt} = \frac{\omega(t)(D-\omega(t))}{D^2} \cdot \mu_v \frac{R_{ON}}{D} i(t) \quad (2)$$

where D is the thickness of titanium dioxide device designed by HP laboratory, $\omega(t)$ is the width of doped TiO_{2-x} , μ_v is dopant mobility, $v(t)$ is the voltage across and $i(t)$ is the current through the memristor, R_{ON} and R_{OFF} are on-state and off-state resistances of the memristor, respectively. By replacing $\frac{\omega(t)}{D}$ with $x(t)$ and $\mu_v \frac{R_{ON}}{D^2}$ with k , (1) and (2) become

$$v(t) = R_{OFF}i(t) + (R_{ON} - R_{OFF}) \cdot x \cdot i(t) \quad (3)$$

$$\frac{dx(t)}{dt} = kx(t)(1-x(t)) \cdot i(t) \quad (4)$$

$x(t)$ is known as an internal state of the memristor and its range is located in the interval $[0,1]$.

A. Model A

Fig. 1. Represents the first proposed model that consists of a voltage-dependent voltage source (VSDS), a low pass filter (LPF), and buffer. [3]. Operational amplifier (Op-AMP) is used as an integrator to solve the differential equation (4). In general, Model A is characterized by the following equation:

$$v_{out}(t) = -\frac{1}{R_1 C_1} \int v_{in}(t) dt + V_0 \quad (5)$$

where V_0 is the initial applied voltage. For the simulation in SPICE the following parameters are used: $R_{ON} = 100 \Omega$, $R_{OFF} = 10 k \cdot \Omega$, $k = 1 \cdot 10^{12}$, $R_{LOAD} = 10^6 \Omega$. The SPICE code for this model is given in Appendix A.

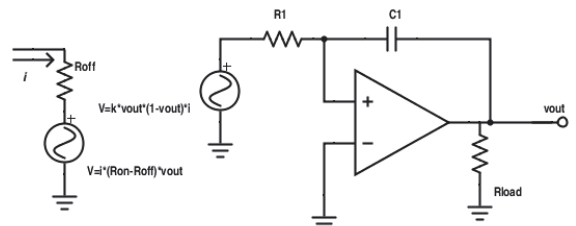


Fig. 1. Proposed memristor Model A

B. Model B

Model B, shown on Fig.2, is designed by using an integrator, consisting of the following components: a capacitor, a resistor, a current dependent source and a VDVS. [3]. The same values for parameters, as given in Model A, are used. The formula for output voltage is given as

$$v_{out}(t) = \frac{1}{RC} \int v_{in}(t) dt + V_0 \quad (6)$$

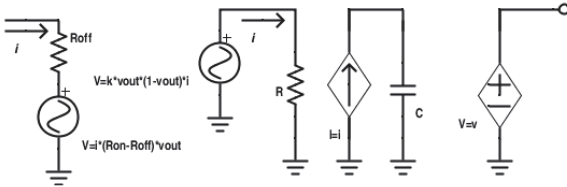


Fig. 2. Proposed memristor Model B

In order to identify whether the proposed models satisfy the three main properties of the memristor, they simulated in LTSpice. Taking the same initial state value

III. SIMULATION RESULTS

Models are simulated using LTSpice simulator. In order to compare two aforementioned models, simulations are done under the same conditions for frequency and initial state. Analyzing simulation results, the following observations can be emphasized:

A. Comparison of Model A and Model B

The graphs obtained show that two models are identical in terms of frequency response for initial state values between $x(0) = 0.2$ and $x(0) = 0.8$. This can be observed on Figs. 3-6. In case of initial state $(0) = 1$, $i-v$ characteristics of two models are different. Model A does not give any results and simulation shows error at frequencies higher than 10 MHz. However, Fig. 7. shows that at small frequency $f=100$ kHz the pinched hysteresis loop for Model A becomes a straight line but at higher frequencies, up to 20 MHz. There is also error at frequency value 100 MHz.

When $x(0) = 1$, the memristor is fully doped and acts as a resistor. The difference between two models when $x(0) = 1$ can be explained by the different threshold values for frequency under which they do not change the main characteristics of linear resistor.

$x(0)$, but changing the frequency of the input signal will give frequency response curve for both models. Then, $x(0)$ also can be changed in order to explore the relation between the initial state and $i-v$ characteristics of the two SPICE models for different frequency values of the applied sinusoidal signal.

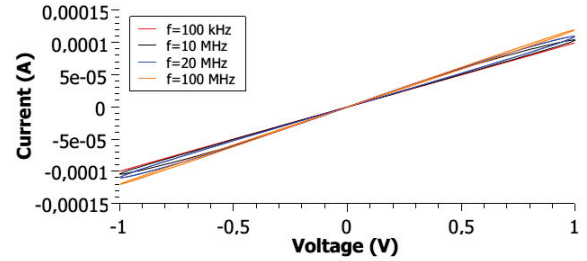


Fig. 4. Simulated transient $i-v$ characteristics of the Model B, where initial state $x=0.2$

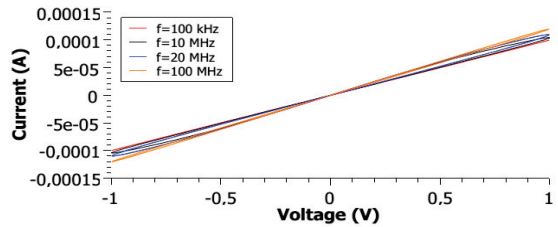


Fig. 3. Simulated transient $i-v$ characteristics of the Model A, where initial state $x=0.2$

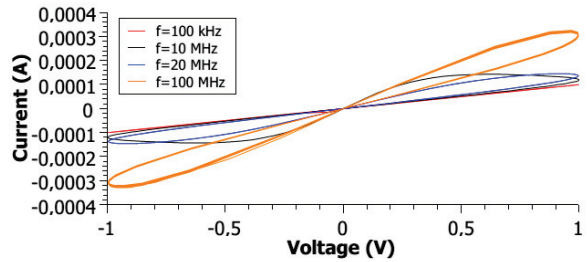


Fig. 5. Simulated transient $i-v$ characteristics of the Model A, where initial state $x=0.8$

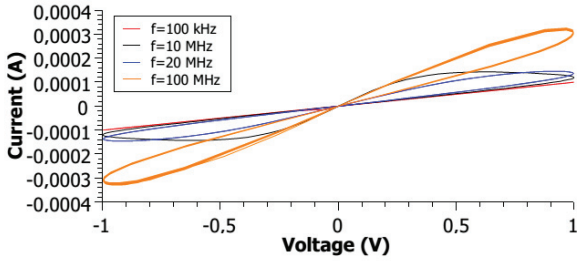


Fig. 6. Simulated transient $i-v$ characteristics of the Model B, where initial state $x=0.8$

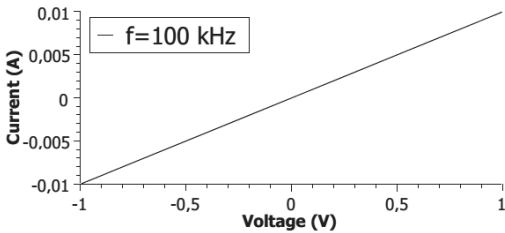


Fig. 7. Simulated transient $i-v$ characteristics of the Model A, where initial state $x=1$

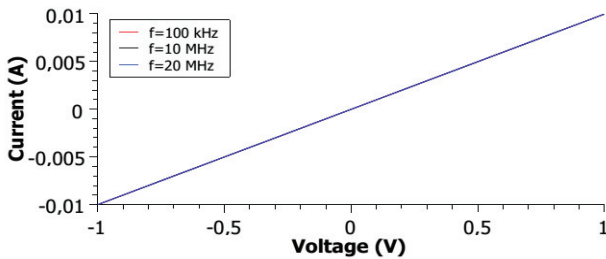


Fig. 8. Simulated transient $i-v$ characteristics of the Model B, where initial state $x=1$

B. Dependence of $i-v$ curve on initial state

For the same frequency values but for an arbitrary value of the initial state, $i-v$ curves of two memristor models obtain different shapes. As shown on Figs. 3-6, the area of pinched hysteresis loop expands when $x(0)$ is changed from 0.2 to 0.8. It can be explained that by increasing the width of doped

region we also increase the difference between the R_{OFF} and R_{ON} states.

C. Dependence of $i-v$ curve on frequency

When both memristor models are simulated by applying different frequencies of sinusoidal signal, pinched hysteresis loops shrink or expand depending on frequency. At very low frequency $f=100$ kHz there is no hysteresis because the resistance has enough time to settle to certain value for each of the instantaneous values of voltage fed.

In addition, the slope of hysteresis loop increases in direct proportion to the frequency. Hence, for high frequency $f=100$ MHz the conductivity of memristor is also relatively high. Moreover, the slight vibration during transient time can be observed in the figures for high frequencies.

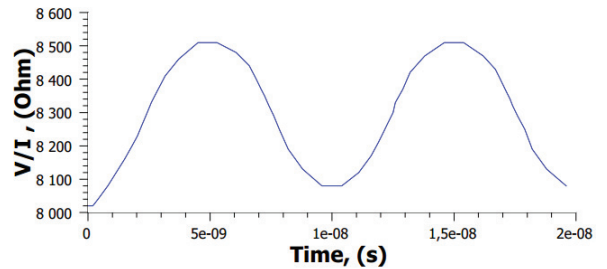


Fig. 9. High and Low level state

The conductive region of the memristor refers to R_{ON} (LOW) state. The resistive region, acting as an insulator, is known as R_{OFF} (HIGH) state. The hysteresis loops, obtained before, can be divided into two sections. The first part includes two straight lines, corresponding to R_{ON} and R_{OFF} states, whereas two bending parts refer to transition region between these two states. Fig. 9. Shows how fast it takes to switch between these two states when $x(0) = 0.2$ and $f = 100$ MHz.

IV. CONCLUSION

In this paper two SPICE models are simulated using LTSpice. Similarities and differences are identified and analyzed. Both models satisfy three main properties corresponding to the memristor. Further work can be conducted on identifying threshold frequency value for which the model of memristor behaves as a resistor.

APPENDIX A

SPICE CODE OF THE MEMRISTOR MODEL A

```

Roff 1 2 10000
V1 0 1 SINE(0 1 10Meg)
B1 2 0 V=I(B1)*(-9900)*(V(8))
B2 0 3 V=V(8)*(1-V(8))*1e12*I(B1)
    
```

```
Rin 4 0 1e12
E1 5 0 4 0 1e8
R2 5 6 1000
C2 6 0 1e-20
E2 7 0 6 0 1
R3 7 8 1u
R1 3 4 1
C1 8 4 1 IC= 0.5 V
Rload 8 0 1e6
.tran 0 800ns 0.01ns UIC
.end
```

APPENDIX B

SPICE CODE OF THE MEMRISTOR MODEL B

```
* C:\Users\Akina\OneDrive\Documents\Draft4.asc
Roff 1 2 10000
V1 0 1 SINE(0 1 100Meg)
B1 2 0 V=I(B1)*(-9900)*(V(6))
B2 0 4 V=V(6)*(1-V(6))*1e12*I(B1)
R1 4 0 1
B3 0 5 I=I(B2)
C1 0 5 1 IC=0.5 V
E1 6 0 0 5 1
.tran 0 800ns 0.01ns UIC
.end
```

REFERENCES

- [1] L.O. Chua, "Memristor-the missing circuit element" IEEE Trans. Circuit Theory, vol. 18, no. 5, pp. 507-519, 1971.
- [2] J. M. Tour and T. He, The fourth element, Nature 453, pp. 42-43, May 2008
- [3] K. D. Xu, Y. H. Zhang, L. Wang, M.Q. Yuan, Y.Fan and W. T. Joines, "Two Memristor SPICE Models and Their Applications in Microwave Devices" IEEE Trans. on Nanotechnology, vol. 13, no. 3, May 2014
- [4] L. O. Chua and S. M. Kang, "Memristive devices and systems," Proc. IEEE, vol. 64, no. 2, pp. 209-223, Feb. 1976.
- [5] L. O. Chua, "The fourth element," Proc. IEEE, vol. 100, no. 6, pp. 1920-1927, Jun. 2012
- [6] D. B. Strukov, G.S. Snider, D. R. Stewart, and S. R. Williams, "The missing memristor found," Nature, vol. 453, no. 7191, pp. 80-83, May 2008
- [7] Maan, A.K.; Kumar, D.S.; Sugathan, S.; James, A.P., "Memristive Threshold Logic Circuit Design of Fast Moving Object Detection," Very Large Scale Integration (VLSI) Systems, IEEE Transactions on , vol.PP, no.99, pp.1,1 doi: 10.1109/TVLSI.2014.2359801
- [8] James, A.P.; Kumar, D.S.; Ajayan, A., "Threshold Logic Computing: Memristive-CMOS Circuits for Fast Fourier Transform and Vedic Multiplication," Very Large Scale Integration (VLSI) Systems, IEEE

Transactions on , vol.PP, no.99, pp.1,1 doi: 10.1109/TVLSI.2014.2371857

- [9] Ibrayev, T. , Fedorova, I. , Maan, A. and James, A. On Design of Memristive Amplifier Circuits. Circuits and Systems, 5, 2014, 265-273. doi: 10.4236/cs.2014.511028.
- [10] James, A.P.; Francis, L.R.V.J.; Kumar, D.S., "Resistive Threshold Logic," Very Large Scale Integration (VLSI) Systems, IEEE Transactions on , vol.22, no.1, pp.190,195, Jan. 2014 doi: 10.1109/TVLSI.2012.2232946

DauletKengesbek was born in Taraz, Kazakhstan in 1993. He is 3rd year Electrical and Electronics student at Nazarbayev University, Astana, Kazakhstan. His interests include renewable energy sources and he has experience in working at solar panel plant.

Akzharkyn Izbassarova was born in Oral, Kazakhstan in 1994. She is 3rd year Electrical and Electronics Engineering student at Nazarbayev University, Astana, Kazakhstan. Akzharkyn interests are in signal processing and implementation of piezoelectric generators.

The development of object recognition application to automatically count the number of passengers entering the bus

Serikbolsyn Myrzakhmet
Department of Electrical and Electronic Engineering
Nazarbayev University
Astana, Kazakhstan
Serikbolsyn.myrzakhmet@nu.edu.kz

Abzal Adilzhan
Department of Electrical and Electronic Engineering
Nazarbayev University
Astana, Kazakhstan
Abzal.adilzhan@nu.edu.kz

Abstract – In Kazakhstan, bus operating companies traditionally hire bus conductors for manual fare collection from the passengers. However, the control of correspondence of the produced revenue with the issued tickets by the conductor is a critical problem. As a result of controller injustice the bus companies might receive less revenue, and respectively, pay less amount of governmental tax. Also, it might result in imprecise bus scheduling and route management. Therefore, the passenger flow count is a crucial concern for bus companies. This research paper presents the concept and algorithm of developed application for passenger flow count in the bus. This project aims to create an object recognition application which will automatically count the number of passengers entering the bus. We used C++ language and OpenCV library to create passengers recognition application which uses the video cameras. A method which will be applied to detect passengers for this application is the background subtraction. As a result, the application will be developed which will automatically count the passengers getting on a bus transit systems in the cities of Kazakhstan. Consequently, the issued tickets will be checked by the number of passengers in the bus during the bus working hours. Indeed, this project will expand the application areas of OpenCV library.

Keywords—*object recognition, OpenCV library, passenger count*

I. INTRODUCTION

Nowadays, buses are one of the most common types of public transportation within the cities of Kazakhstan. For instance, the bus services of Astana city are required to provide services for ten thousands of people every day since there are no any other public transportation services for residents. Moreover, this type of transportation is convenient and comparatively inexpensive. However, since bus companies hire bus conductors for manual fare collection from the passengers they are incapable to control conductors from embezzlement of company revenue. In fact, the bus companies can only check the passenger tickets during bus working hours by hiring extra employees which is economically inefficient. At the present time, many cases are identified where conductors do not provide ticket in

response for passenger fare payment. Certainly, such actions negatively impact on the budget of the company and, as a result of less collected revenue the bus companies receive incorrect statistics about number of passengers. It might lead to inaccurate bus timetable and route management which will possibly be problematic for local people. Therefore, an application could be technologically advanced to verify the number of passengers in the bus.

The project can be developed based on software applications. This technique is more effective in comparison with detecting sensors since computer applications can process more data and details [4]. According to Mukherjee et al. [3], the usage of video cameras is the most technologically advanced counting method, however, the installation and maintenance costs of this technology are comparatively high. Therefore, the motivation of this project is to develop an application for buses with existing vertical cameras and for buses with single operating entrance for economic efficiency.

The purpose of this project is to develop an application which will automatically count the passengers getting on a bus in the cities of Kazakhstan. The project can be employed in other application areas such as object tracking, congestion control and similar object counting projects. Our main contribution is the advancement of passenger count algorithm and logic.

II. METHODOLOGY

This project aimed to develop a method for counting the number of passengers entering the bus. In order to implement this project idea the application was developed by using C++ program and OpenCV library. The process of project implementation can be divided into several steps.

A. Video capture

Firstly, the video camera should be vertically installed at the entrance of the bus. Hence, a real-time captured video will be sent to the central processing unit where the application runs [4]. During the program development stages we examined the video files with objects shift.

B. Background Subtraction

After starting the video capture from the web camera and receiving data, a background subtraction is carried out by applying 'BackgroundSubtractorMOG2' function in OpenCV library. In this method the moving foreground, passengers, will be extracted from the static background [1]. The performance of background subtraction can be greatly improved by Mixture of Gaussians (MOG) because of its ability to adapt to a change of the background [5]. Thus, the extracted object foreground mask is stored in a separate window.

C. Reducing noise and separating objects

In order to reduce noise (small objects) and separate objects a morphological opening and a morphological closing techniques are applied. Indeed, these methods employ 'erode' and 'dilate' functions of OpenCV library. 'Erode' replaces the current pixel with the minimum pixel value found from pixels nearby, whereas, 'dilate' replaces the current pixel with the maximum pixel found from pixels nearby [2].

Likewise, 'GaussianBlur' function can be applied for the same purpose instead of previously mentioned techniques.

D. Removing shadows

At this stage we delete shadows of the objects by 'threshold' function (setting threshold value so that it removes gray tracks).

E. Defining object contours

Now, the moving objects are tracked by assigning boundary contours. With the aim of carrying out this step the function 'findContours' of OpenCV library was used which extracts object connected with a set of pixels in a binary image [2].

We designate a rectangle shapes around the displacing objects with the intention of motion observation. Moreover, 'if' condition was stated so that for the further analysis continuation the detected object's rectangle area or contour size must be larger than particular appointed value (to disregard smaller objects). Therefore, the rectangle shapes will merely be allocated to the objects with greater dimensions than the threshold by using 'rectangle' function.

F. Determining mass center

After drawing the rectangle shapes a mass center of the moving object is defined by calculating the contour moments, and we illustrate this point in the frame by using 'circle' function.

G. Counting detected objects

Finally, it is aimed to count the number of moving objects. For this purpose we allocate the region (red rectangle with the range of 10 pixels) on the frame, this will be the range of interest. It is considered that two or more objects might cross the region simultaneously, therefore, we allocated four parallel regions to count objects at the same time. The width of each region was adjusted with respect to

approximate dimensions of single person. Moreover, each region was virtually split into two parts in order to check in which direction the passenger moves since it is targeted to count only entering passengers. As soon as the centroid coordinates of the object cross the range of interest, 'if' condition checks whether the y coordinate value of the object centroid is bigger or smaller than the y coordinate of the region of interest's center. The logic behind this idea is that the centroid of any object appears several times in the region since the region range is quite large, and the first centroid entered the region will anyway cross one of the halves of range. If it is bigger, we consider it as entering object, and the counter is activated and the coordinates of the centroid are stored, otherwise, the object is not counted, but the coordinates of the centroid are also stored. Furthermore, at the end of each frame we define condition where the coordinates of the centroid will be checked in order to know if the object is inside the range so far or not, if so, the counter will not count the same object twice or more in the range.

Figure 1 represents the flowchart of the implementations.

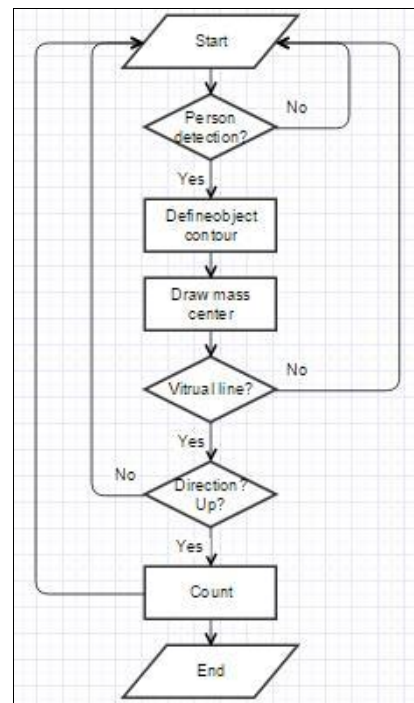


Figure 1. The flowchart of the algorithm.

III. RESULTS AND ANALYSIS OF DATA

This part of the paper provides obtained results of the project implementation and analysis of these data.

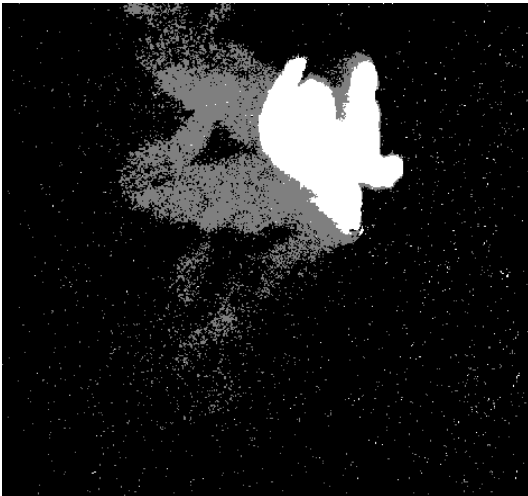


Figure 2. The screenshot of the foreground mask window.

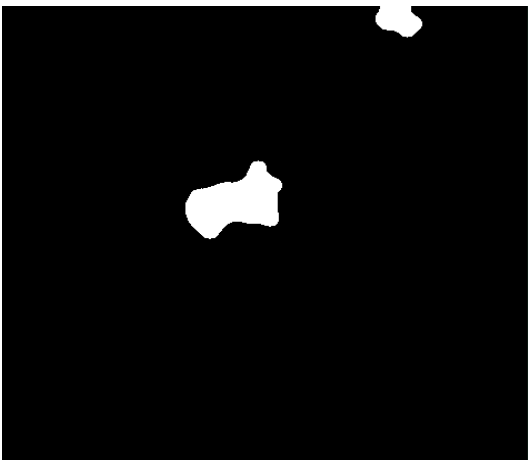


Figure 3. The screenshot of the foreground mask with removed shadow window.

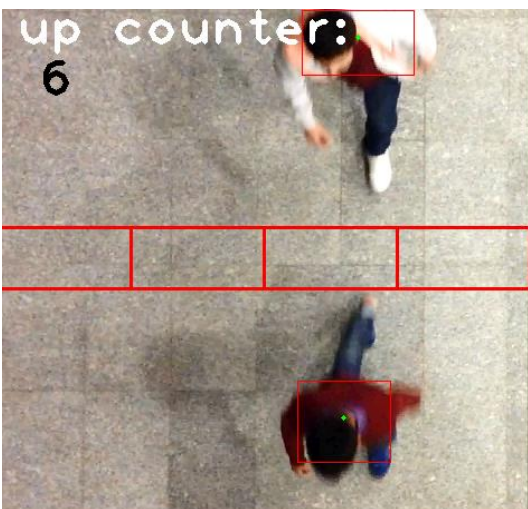


Figure 4. The screenshot of the original frame.

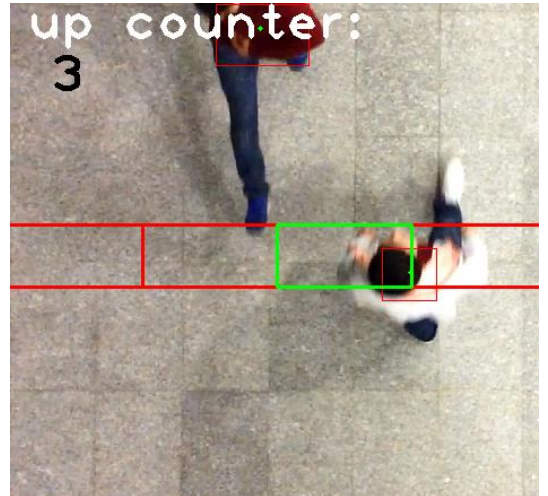


Figure 5. The screenshot of the original frame.

This project aimed to develop C++ code by using OpenCV library which counts the number of passengers entering the bus. Pursuant to methodology the application was developed and it was programmed to detect and count people when they pass through the virtual region. From the project results we came to the conclusion that the application fulfills our targets – it is able to capture video, implement background subtraction, reduce noise and separate objects, remove shadows from the foreground mask, define the object contours and mass center, and finally, it is able to count entering passengers.

A window represented in Figure 2 shows the video frame with the foreground mask of the object. This foreground mask was achieved through ‘BackgroundSubtractorMOG2’ function. As it can be seen from this image the frame contains noise, disturbances and shadows. Figure 3 illustrates the foreground mask with removed shadow, reduced noise and eliminated holes. This frame was used to calculate the object’s contour and center mass. Figure 4 shows the original frame with rectangle shapes around the moving objects for observation, green colored centroid, red colored regions of interest for counting, and displayed number of entered passengers. Figure 5 represents the case when the object centroid is inside the range of interest. According to this picture it can be referred that when the counter was activated, the region modified its color to green.

During the project development stages problems occurred when two passengers crossed the region simultaneously and program counted them as one person. The problem was solved by drawing 4 parallel virtual regions so that only one passenger can cross one of the virtual regions at a time. Also, the application counted both entering and leaving passengers, yet it was required to count only number of entered passengers. The problem was fixed by inspecting the object centroid coordinate in the virtual region so, we can define in which direction the object moves.

Nevertheless, a problem occurs when the intensity of the light significantly varies since the background subtraction technique is sensitive to light changes. This problem can be solved by detecting objects in a static condition and adjusting application to both daytime and nighttime bus light conditions [4].

Moreover, since the method of this project is based on object detection, in addition to people count this application computes objects with significant size. Yet, this issue was ignored due to the fact that large objects must also be provided with tickets.

IV. CONCLUSION

In conclusion, after implementing research methodology we could obtain simulation results. According to the results it might be said that the application can capture video, implement background subtraction, reduce noise and separate objects, remove shadows from the foreground mask, define the object contours and mass center, and it counts only entering passengers. The limitations of the project are the sensitivity of the method on light conditions, some possible errors when two passengers pass the region very close, and that it might be efficient only for busses with single operating door. For the future similar projects it is recommended to develop a count method which can differentiate and count people based on human head parameters.

REFERENCES

- [1] Bradski, Gary and Adrian Kaebler, *Learning OpenCV*. United States of America: O'Reilly Media, 2008.
- [2] Laganiere, Robert, *OpenCV2 Computer Vision Application Programming Cookbook*. Birmingham: Packt Publishing Ltd, 2011.
- [3] Mukherjee, Satarupa, Stephani Gil and Nilanjan Ray, "Unique people count from monocular videos", *The Visual Computer*, pp1-13, Sep.2014.
- [4] Putra, Samuel Mahatma, Renan Prasta Jenie, I Made Vidyasthana, Harry Yanto, and Agustinus Wijiaya, "Designing object detection prototype for people counter using computer vision," unpublished.
- [5] Wang, Hanzi, and David Suter, "A re-evaluation of mixture of Gaussian background modeling (video signal processing applications)." In *Acoustics, Speech, and Signal Processing, 2005. Proceedings.(ICASSP'05). IEEE International Conference on*, vol. 2, pp. ii-1017. IEEE, 2005.



Abzal Adilzhan

He was born in 19th of April in 1994. Graduated Nazarbayev University Foundation program specialized for Mathematics and Physics in 2013. Currently, he is a second year undergraduate student studying Electrical and Electronic Engineering at Nazarbayev University.

He is an active member of the Instutuion of Engineering and Technology (IET).



Serikbolsyn Myrzakhmet

He was born in 3rd of September in 1994. Graduated Nazarbayev University Foundation program specialized for Mathematics and Physics in 2013. Currently, he is a second year undergraduate student studying Electrical and Electronic Engineering at Nazarbayev University.

He is an active member of the Instutuion of Engineering and Technology (IET) and Institution of Mechanical Engineers.

Memristor Logic Applications: A brief summary

Sherin Sugathan
Member, IEEE.

Enview R&D Labs, India.
Email: sherin2701@gmail.com

Alex Pappachen James
Senior Member, IEEE.
Nazarbayev University.
Email: apj@ieee.org

Abstract—Memristors are conceived to be the fourth electronic component and circuits based on them are gaining attention in diverse application areas. The use of memristors is a major advancement towards creating efficient non-volatile memories. This overview provides the potential uses of our methods of using memristor in the implementation of threshold logic for solving different problems in image processing, logic gates and pattern matching.

Index Terms—Memristor, Threshold Logic, Neuromorphic Circuits.

I. BACKGROUND

In addition to the very known basic electronic components like resistors, capacitors and inductors, a fourth component named Memristor was developed in 1971 by Leon Chua [1]. The capability of remembering or storing data in terms of resistance values is the main characteristic feature of memristors. This feature contributes to the development of non-volatile memories [2].

II. APPLICATIONS OF MEMRISTORS IN COMPUTING AND PATTERN RECOGNITION

The ability of memristors to accommodate so many different states or configurations makes it a useful candidate in learning based systems. Here we take a brief survey of prospective application areas where memristors can play a useful role. This article emphasizes the suitability of memristors in few of the learning architectures which are based on a neuron-like processing unit proposed in [3].

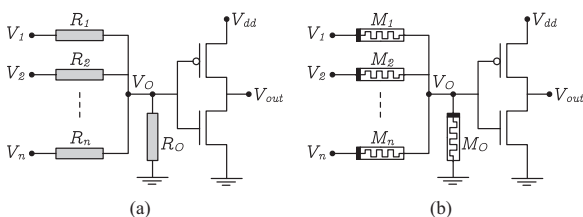


Fig. 1. The (a) cognitive cell proposed in [3] and its (b) memristor based counterpart.

In [3], a hardware based memory cell is proposed for solving cognitive tasks. The proposed memory cell based architecture proves to be capable of avoiding the crossover wirings required in a neural network and it achieves the same functionality as of a neural network. Unlike other hardware based learning systems, the cell proposed in [3] does not

require several iterations in order to learn a pattern but uses a bi-state weight model for quick learning. The learning potential of that architecture can be further improved if the bi-state model is extended to an n-state weight model using memristors. This may be achieved at the cost of additional driving/control circuits for the memristors.

A universal NOR gate using the cognitive cell is presented in [4]. In [5], the idea of cognitive cells were utilized for locating lesion probable regions in film mammography. Here, the cognitive cell parameters were adjusted according to the local and global input image statistic. In [6], [7], novel cognitive cell based architectures are used to find edges in digital/analog images. It was observed that the edge response obtained (Figure. 2(a)) by the use of cognitive cells was satisfactory. Exploiting the advantage of high processing speeds offered by cognitive cell based learning, the work in [8] proposed a method for real-time processing of medical data. The input considered were intraoperative MRI images (Figure. 2(c)) and they were processed to generate the heart activity graph (Figure. 2(d)).

Later in [9], the architecture proposed in [3] was studied for memristors. They studied memristor based architectures for implementing digital logic gates. Having the basic gates implemented using memristors, we can develop systems that perform higher level computing at great speeds. The work illustrated in [10] is an example proving that memristor based systems can be deployed for performing complex cognitive tasks like object detection and tracking shown in Figure.2(b).

The work in [11], proposes an implementation of Fast Fourier Transform and Vedic Multiplication using memristors. They highlighted the importance of memristors by reporting the lower chip area, THD and controllable leakage power.

III. CONCLUSION

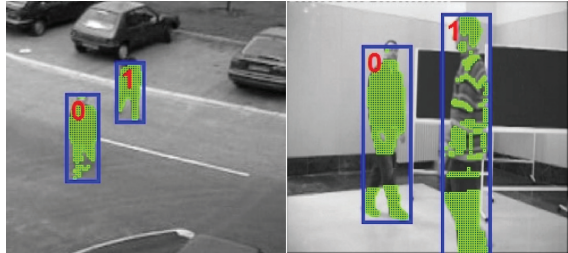
We covered a brief summary of memristors used in pattern recognition applications. The combination of cognitive cells with memristors seems to be a promising turn to achieve better speed and accuracy. In other words, the advantages of memristors like speed are fully utilized only in those learning systems that offer less training time.

REFERENCES

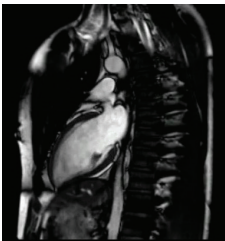
- [1] L. O. Chua, "Memristor-the missing circuit element," *Circuit Theory, IEEE Transactions on*, vol. 18, no. 5, pp. 507–519, 1971.
- [2] L. Chua, "Resistance switching memories are memristors," *Applied Physics A*, vol. 102, no. 4, pp. 765–783, 2011.



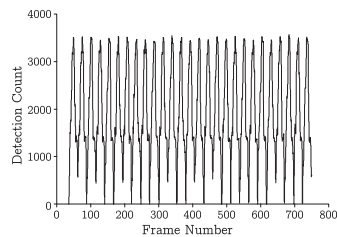
(a) Edge Detection [6]



(b) Object Detection and Tracking [10]



(c) iMRI data [8]



(d) Heart rate measured from iMRI [8]

Fig. 2. Example results obtained for cognitive cell based systems.

- [3] A. P. James and S. Dimitrijević, "Cognitive memory network," *Electronics Letters*, vol. 46, no. 10, pp. 677–678, 2010.
- [4] D. S. Kumar, L. Rose, and A. James, "Resistive mosfet brain-inspired threshold logic gates," *International Journal of Machine Intelligence and Sensory Signal Processing*, vol. 1, no. 2, pp. 192–198, 2014.
- [5] A. P. James and S. Sugathan, "Parallel realization of cognitive cells on film mammography," in *Trust, Security and Privacy in Computing and Communications (TrustCom), 2013 12th IEEE International Conference on*. IEEE, 2013, pp. 1873–1878.
- [6] S. Sugathan and A. P. James, "Directional edge detection using parallel cognitive logic cells," in *Advances in Computing, Communications and Informatics (ICACCI), 2013 International Conference on*. IEEE, 2013, pp. 694–697.
- [7] A. Pappachen James, A. Pachentavida, and S. Sugathan, "Edge detection using resistive threshold logic networks with cmos flash memories," *International Journal of Intelligent Computing and Cybernetics*, vol. 7, no. 1, pp. 79–94, 2014.
- [8] S. Sugathan and A. P. James, "Intraoperative cardiac mri processing using threshold logic cells," in *Advances in Computing, Communications and Informatics (ICACCI), 2014 International Conference on*. IEEE, 2014, pp. 451–455.
- [9] A. James, L. Francis, and D. Kumar, "Resistive threshold logic," *Very Large Scale Integration (VLSI) Systems, IEEE Transactions on*, vol. 22, no. 1, pp. 190–195, Jan 2014.
- [10] A. Maan, D. Kumar, S. Sugathan, and A. James, "Memristive threshold logic circuit design of fast moving object detection," *Very Large Scale Integration (VLSI) Systems, IEEE Transactions on*, vol. PP, no. 99, pp. 1–1, 2014.
- [11] A. James, D. Kumar, and A. Ajayan, "Threshold logic computing: Memristive-cmos circuits for fast fourier transform and vedic multiplica-

tion," *Very Large Scale Integration (VLSI) Systems, IEEE Transactions on*, vol. PP, no. 99, pp. 1–1, 2015.

The model of TiO₂ metal-oxide-metal memristor based on device's physical parameters

Rassul Bairamkulov, student, BEng
Nazarbayev University
Astana, Kazakhstan

Abstract— memristor (short for memory resistor) is the fundamental electronic device theoretically proposed by Chua in [1] and physically designed in HP labs [2]. The invention of physical memristor caused the significant interest among researchers. Many attempts for creation of precise device model were made [3, 4]. The new approach for memristor modeling was proposed basing on the device's dimensions and material properties. The findings reveal interesting relations such as the nonlinear relationship between the device area and the width of pinched hysteresis loop and positive relationship between resistivity of the device and the are inside the pinched-hysteresis loop.

Keywords—memristor; SPICE modeling;

Introduction

The memristor devices have the large potential for future implementation in integrated circuits. As the modern CMOS technology approaches to the technical limit of density, a newly invented memristor that can be scaled up to 4 nm is very promising [5]. Many papers have proposed the usage of memristor is sensors, oscillators, neural systems, etc. Thus, the study of properties of this new device is very important for the future technology development. However, the literature review did not reveal any research on the memristor model considering the device physical parameters such as dimensions and material properties. This paper is intended to create the such model and to investigate the relationship between the device behavior and its physical parameters.

I. IDEAL MEMRISTOR MODEL EQUATIONS

The main parameter of the device is memristance that relates the parameters of magnetic flux induced by current through device and charge that have passed through device (1).

$$M = \frac{d\phi}{dq} \quad (1)$$

The unit of memristance is the same as for the resistance as memristance relates the time derivatives of the voltage and current.

The physical realization of the device is shown on figure 1 below [6]. Two terminals of memristor are separated by the specific material (e.g. titanium dioxide) whose passive electrical properties can be changed. There are two regions in the memristor: the doped region that has low resistance R_{ON} and the undoped region that has large resistance R_{OFF} . By applying the voltage, to the device terminal, the width w of the doped region can be increased or reduced, that changes the device resistance value. Mathematically:

$$M = R_{ON} \frac{w}{D} + R_{OFF} \left(1 - \frac{w}{D}\right)$$

$$M(x) = R_{ON}x + R_{OFF}(1 - x) \quad (2)$$

where D is the total length of the device. The term w/D is often replaced by x ($0 \leq x \leq 1$) and the difference between R_{OFF} and R_{ON} is replaced by ΔR that transforms equation 2 into:

$$M = R_{ON}x + R_{OFF}(1 - x) = R_{OFF} - x(R_{OFF} - R_{ON})$$

$$M = R_{OFF} - x\Delta R \quad (3)$$

where ΔR represents the difference between resistances in OFF and ON states.

According to [3], the rate of change of the doped region width to the total length ratio is given as:

$$\frac{dx}{dt} = ki_M(t)f(x) \quad (3)$$

$$k = \frac{\mu_v R_{ON}}{D^2}$$

where i_M is current through memristor, μ_v is the dopant mobility (treated as constant at the value of approximately $10^{-14}m^2s^{-1}V^{-1}$) and $f(x)$ is window function that models the nonlinear dopant drift. From (3) it can be suggested that the physical meaning of the window function is the relationship between the rate of change of the doped region width and the doped region width itself.

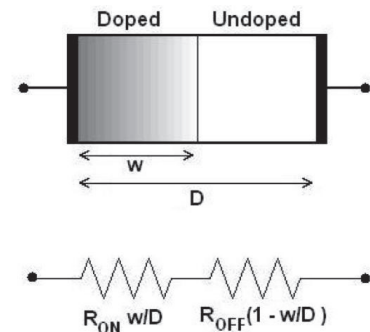


Fig. 1. Memristor coupled-variable resistor model

The existing models of window function include Strukov [2], Joklegar [7], Biolek [3] and Prodromakis [8] window function models and are presented below:

$$\text{Strukov: } f(x) = x - x^2$$

$$\text{Joklegar: } f(x) = 1 - (2x - 1)^{2p}$$

$$\text{Biolek: } f(x) = 1 - (x - \text{sgn}(-i(t)))^{2p}$$

$$\text{Prodromakis: } f(x) = 1 - ((x - 0.5)^2 + 0.75)^p$$

All the presented models are defined between $x = 0$ and $x = 1$. All of them, except Biolek's model, hold maximum value at $x = 0.5$ and the zero value at the boundaries ($x = 0$ and $x = 1$). The plots of the above equations are presented on figure 2. Biolek's model has nonsymmetrical shape because the model takes direction of current into consideration.

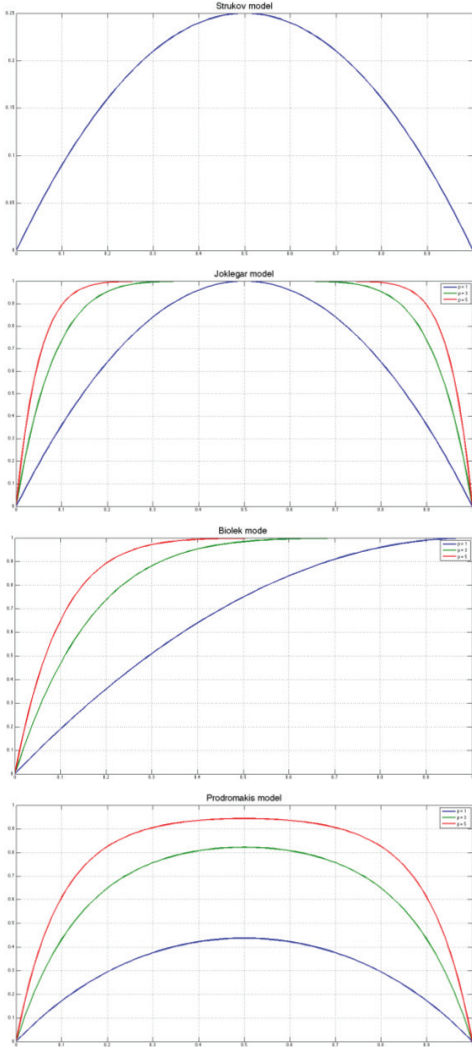


Fig.2. Comparison of the proposed window functions

Strukov's model provides the general understanding of the nonlinear dopant flow. However, due to the absence of control parameter, the model precision is reduced.

It can be seen from figure 2 that the larger value of the exponential term p causes the overall increase in the window

function value. In addition, the larger value of p corresponds to the faster rise of window function to its maximum value. Thus, with the increase in p , the memristor switching time from R_{ON} to R_{OFF} decreases. This trend increases the highest frequency of the voltage source at which the memristor's IV characteristic can remain a pinched-hysteresis loop.

The significant disadvantage of Joklegar and Biolek models is the requirement for p to be the natural number. Prodromakis model eliminates this disadvantage by allowing p to be any real positive number and, thus, allowing greater extent of flexibility. For the sake of robustness and flexibility, the Prodromakis window function model will be used for the analysis further in this paper.

II. PHYSICAL MODEL OF METAL-OXIDE-METAL MEMRISTOR

The memristor model taking parasitic effects into consideration was proposed in [9]. The model consists of the capacitor and current source in parallel with the ideal memristor, inductor and battery are connected in series with the above circuit. However, it was pointed in [9] that the parasitic current source and parasitic voltage sources can be neglected in real memristive devices. Therefore, these devices were excluded from the model and the reduced model is presented on fig. 3.

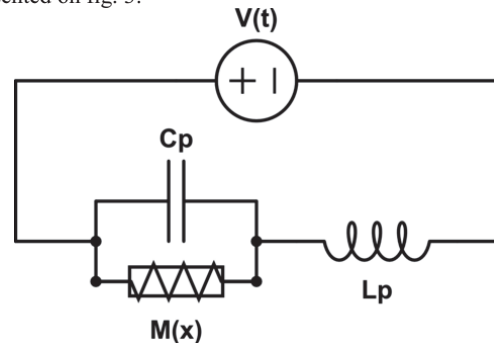


Fig.3. Memristor model with parasitic parameters

Two equations of the device are found using KVL:

$$V(t) = i_M(t)M(x) + L_p \frac{di}{dt} \quad (4)$$

$$M(x)i_M(t) = \frac{1}{C_p} \int_0^t i_c(t) dt \quad (5)$$

where i is current through the inductor, i_c is current through capacitor. Differentiating both sides of Eq.5 we get:

$$M(x) \frac{di_M}{dt} + i_M \frac{dM(x)}{dx} \frac{dx}{dt} = \frac{1}{C_p} (i - i_M) \quad (6)$$

Here we note that memristance is function of time, so, its differentiation was performed using chain rule. It should be noted that the x -derivative of memristance function is constant for the currently used model:

$$\frac{dM(x)}{dx} = R_{ON} - R_{OFF} = \text{const}$$

indicating the reduction of memristance with the increase of x . Rearranging Eq.4 and 6 and combining with Eq.3 we get:

$$\frac{di}{dt} = \frac{1}{L_p} (V(t) - i_M(t)M(x)) \quad (7)$$

$$\frac{di_M}{dt} = \frac{i(t) - i_M(t)}{C_p M(x)} - k i_M^2(t) f(x) \frac{dM(x)}{dx} \quad (8)$$

Equations 3, 7 and 8 together comprise the system of three ODEs with three unknowns.

For further analysis, the physical structure of memristor was considered. Metal-oxide-metal memristor consists of two metal plates separated by dielectric. The equivalent parasitic capacitance, thus, is given by:

$$C_p = \frac{\epsilon_0 \epsilon_r A}{D} \quad (9)$$

Where, ϵ_0 is permittivity of free space, ϵ_r is relative permittivity of undoped region and A is the cross-sectional area of the device. In modern integrated circuits, the conducting devices usually have high width-to-length ratios, therefore, the capacitance of the device may be significant enough to affect circuit behavior.

Using, similar approach, the memristance of the device can be calculated from physical parameters as well. Expanding Eq.2 using physical parameters, the following equation for memristance is obtained:

$$M(x) = R_{ON}x + R_{OFF}(1-x) = \frac{\rho_{ON}D}{A}x + \frac{\rho_{OFF}D}{A}(1-x)$$

$$M(x) = \frac{D}{A}(\rho_{OFF} + x(\rho_{ON} - \rho_{OFF})) \quad (10)$$

The equation of inductance is largely dependent on the shape of the device. The shape of the device is assumed to be square with width a as the most probable device shape in crossbar array. The inductance of conducting bar with rectangular cross-section was approximated in [10] as:

$$L_p = \frac{2D\mu_r}{10^7} \left(\ln\left(\frac{2D}{r}\right) - 1 + \frac{r}{D} \right)$$

where μ_r is relative permeability of material and r is the geometric mean distance of the bar cross-section that is equal to $0.447a$ for square.

It should be noted that the model does not include the external effects such as mutual coupling and inter-device capacitance. In case of highly dense placement of elements on the integrated circuit, these effects should also be taken into account.

III. EFFECTS OF THE DEVICE PARAMETERS

The above model of the memristor was simulated using LTSPICE. The netlist codes are provided in the Appendix 1 and the R1 memristor model provided by [3] with the Prodromakis window function was used for analysis. Initially, the device's physical parameters were set as: $a = 223\mu\text{m}$, $\rho_{OFF} = 1M\Omega \cdot m$, $\rho_{ON} = 5k\Omega \cdot m$, $\epsilon_r = 226$, $V_m = 1.5V$, $f = 2\text{Hz}$, $v(t) = V_m \sin(2\pi ft)$, $\mu_r = 1$.

The results obtained during the simulation are shown on fig.4.

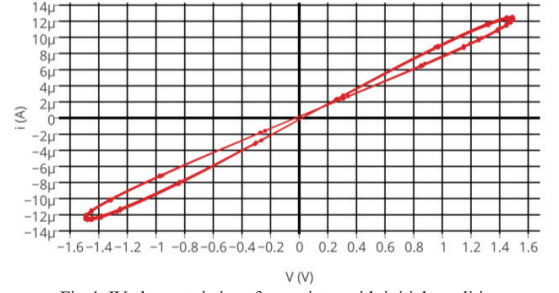


Fig.4. IV characteristics of memristor with initial conditions

It can be seen from figure, that the pinch of intersection of IV curve with itself (pinch point) has been distorted from the zero point. The loop intersection is located in the first quadrant at point $(0.195V, 1.70\mu A)$. The reason for the shifted position of the hysteresis loop is the effect of capacitance discussed widely in [9]. As the parasitic capacitance increases, the pinch point shifts from zero point to the first quadrant. At extremely high capacitance, the IV-curve can become ellipse-shaped, i.e. lose the pinch point.

The effect of parasitic inductance is opposite to the effect of parasitic capacitance. The parasitic inductance causes pinch point to move towards the third quadrant. Therefore, the movement of the pinch point toward the first quadrant is due to the capacitive effect, whereas motion toward the third quadrant is due to the inductive effect.

A. Effects of the area change

In order to investigate the effect of memristor's area change the simulations were conducted with changing the values of a . The figure 5 shows the IV-characteristics of memristor with $a = 1.784\text{mm}$.

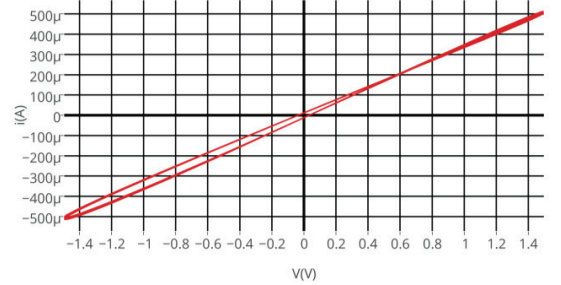


Fig.5. IV characteristics of memristor with $a = 1.784\text{mm}$

It can be seen, that the current through the memristor increased, R_{on} and R_{off} decreased, C_p and L_p increased, and the pinch point has been shifted further from the zero point to point $(0.61V, 210.75A)$.

Next, the value of a was reduced below the initial value to $a = 158\mu\text{m}$. The results are shown on fig.6.

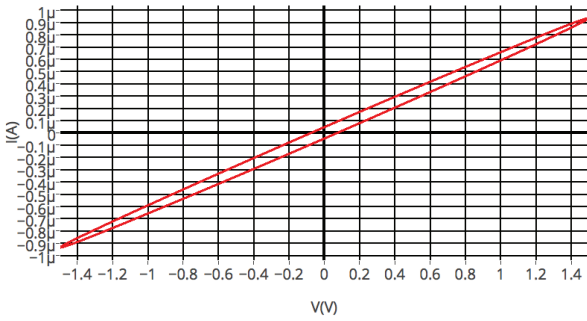


Fig.6. IV characteristics of memristor with $a = 158\mu\text{m}$

Observations indicate that the pinch point has firstly been shifted out of the zero point and then disappeared due to parasitic effects. From the analysis of three figures, it can be concluded that the pinch point deviation from zero point has nonlinear relationship with device area. There is a value of area for which the pinch point deviation is minimum. When the device size is increased, the parasitic effects become more considerable. The interesting finding is that because of the reduction with area, parasitic capacitance reduces, whereas its impact on the device behavior may increase. This effect may put limitations on the device size.

B. Effects of the length change

Similar approach as in part A was used to investigate the effect of the device length on the memristor IV characteristics. The initial conditions were set to all parameters. The simulation was conducted twice with length of device adjusted to $D = 50\text{nm}$ and $D = 5\text{nm}$. The results of simulations are shown on fig. 7 and fig.8

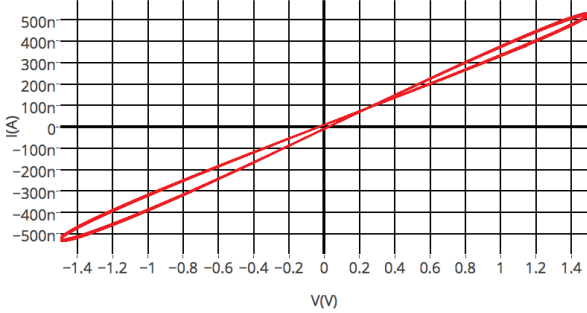


Fig.7. IV characteristics of memristor with $D = 500\text{nm}$

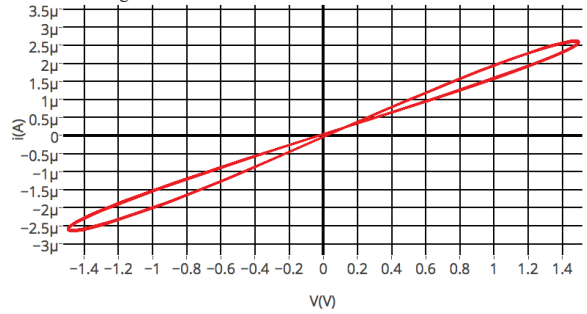


Fig.8. IV characteristics of memristor with $D = 50\text{nm}$

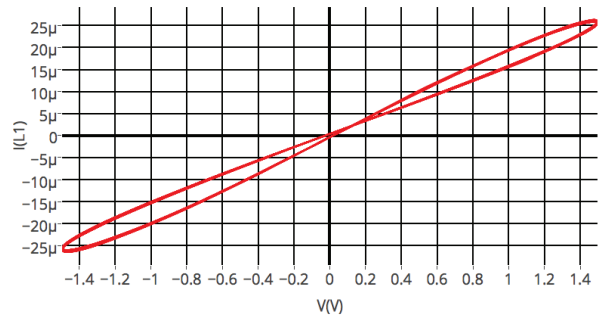


Fig.9. IV characteristics of memristor with $D = 5\text{nm}$

The simulation results demonstrate that generally, the length of the device has weak positive relationship with the device's pinch point voltage. The pinch voltage increased 1.34V at $D = 5\text{nm}$ to 0.27V at $D = 500\text{nm}$. As expected, the current demonstrated negative relationship with the device length due to increase in R_{ON} and R_{OFF} . Inductance did not vary considerably throughout the simulations, whereas, the capacitance reduced with the device length.

C. Effects of the resistivity changes

The electrical resistivity of the titanium dioxide may vary largely due to external and internal reasons. The increase in temperature can reduce resistivity of the device [11]. The presence of Magnéli phases of titanium oxide may also affect the electrical properties of the memristor [12]. The device parameters were set to initial conditions, with changes in the resistivity of OFF and ON states.

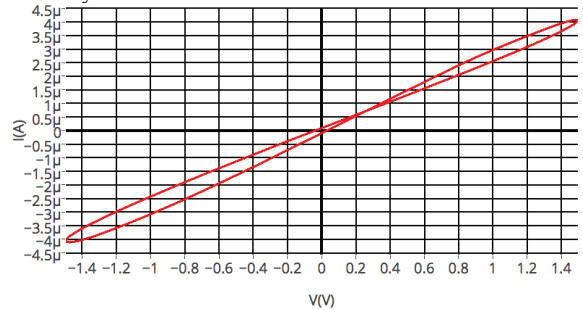


Fig.10. IV characteristics of memristor with $\rho_{OFF} = 2\text{M}\Omega\text{m}$ and $\rho_{ON} = 5\text{k}\Omega\text{m}$

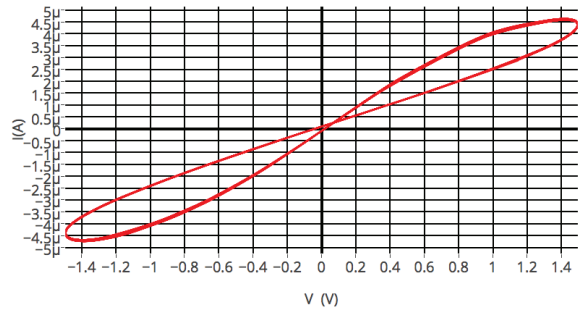


Fig.11. IV characteristics of memristor with $\rho_{OFF} = 2\text{M}\Omega\text{m}$ and $\rho_{ON} = 10\text{k}\Omega\text{m}$

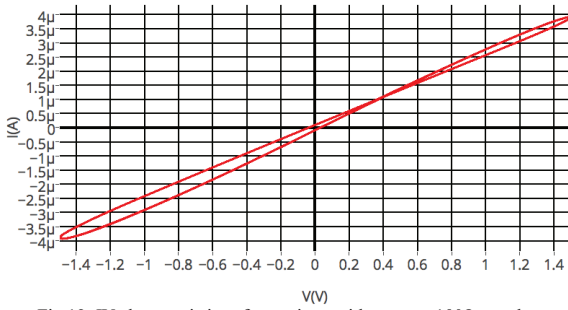


Fig.12. IV characteristics of memristor with $\rho_{OFF} = 1M\Omega$ and $\rho_{ON} = 10k\Omega$

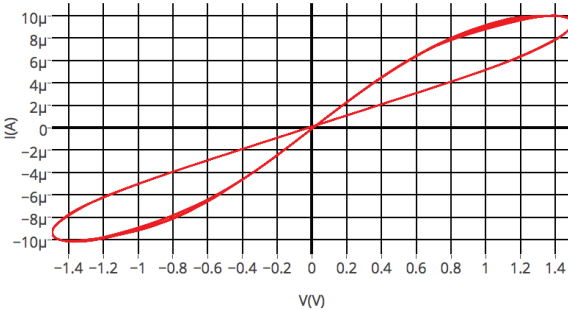


Fig.13. IV characteristics of memristor with $\rho_{OFF} = 0.5M\Omega$ and $\rho_{ON} = 10k\Omega$

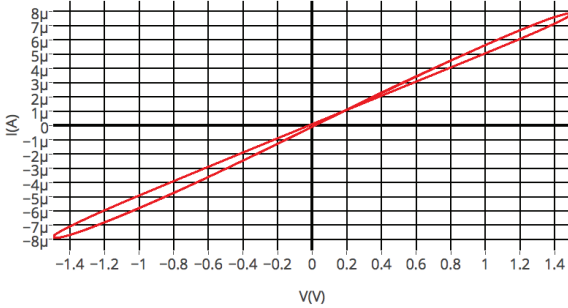


Fig.14. IV characteristics of memristor with $\rho_{OFF} = 0.5M\Omega$ and $\rho_{ON} = 5k\Omega$

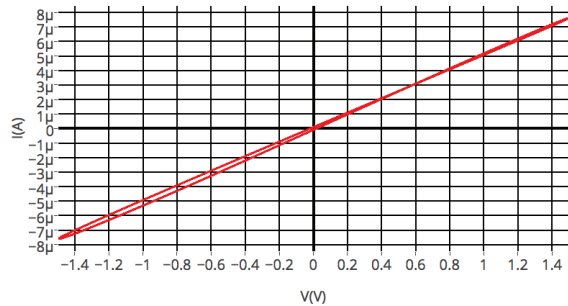


Fig.15. IV characteristics of memristor with $\rho_{OFF} = 0.5M\Omega$ and $\rho_{ON} = 2.5k\Omega$

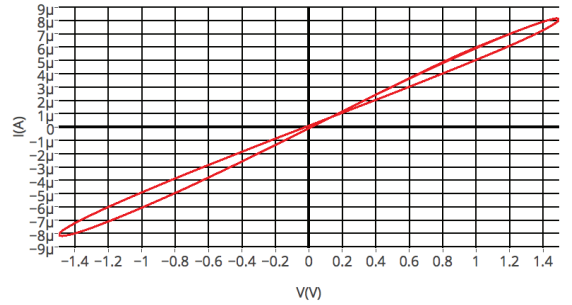


Fig.16. IV characteristics of memristor with $\rho_{OFF} = 1M\Omega$ and $\rho_{ON} = 2.5k\Omega$

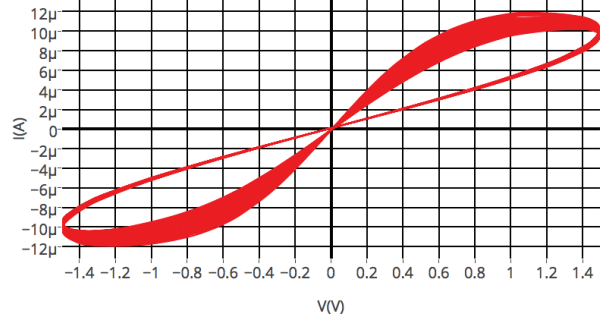


Fig.17. IV characteristics of memristor with $\rho_{OFF} = 2M\Omega$ and $\rho_{ON} = 2.5k\Omega$

Several observations can be noted from the above plots. Firstly, the value of ρ_{ON} affects the area inside the pinched-hysteresis loop. Reader may notice that the value of the ρ_{ON} on the fig.11,12,13 is constant, whereas, the ρ_{OFF} reduces. As the ρ_{OFF} takes lower values, the pinched loop width reduces to minimum and then increases. The area close to minimum for $\rho_{ON} = 2.5k\Omega$ is shown on the fig. 15. As the ρ_{OFF} increases, the area of the loop increases as well.

Secondly, the increase of ρ_{OFF} increases the area inside the hysteresis loop. The gradual widening of the loop can be seen at fig. 15, 16 and 17.

Thirdly, the pinch point moves closer to 0 with the reduction of ρ_{ON} that can be seen at fig. 12 and 16. While ρ_{OFF} stays constant, the pinch point moves closer to zero as the ρ_{ON} reduces.

IV. CONCLUSION AND FURTHER WORK

The paper proposes the new perspective of analysis of the memristor, where, the physical parameters of the device are studied, rather than electrical elements. The effects of the physical dimensions and material properties on the IV-characteristics were demonstrated. The analysis included the effect of parasitic capacitance and inductance.

Several findings can be noted from the above discussion. Firstly, the analysis showed that the pinch point distance from zero point nonlinearly depends on the device area. There is an optimal area of the device for which the effects of parasitics are minimized. If the area increases or decreases from this value, the parasitic effects may become dominant in the circuit. Secondly, despite the increase of the capacitance, the

effect of capacitance on the circuit reduce with the device cross-sectional area. Thirdly, the device length weakly affected the pinch point, whereas, the current values were affected the most. The current through the device generally reduced with the device length. Finally, the variation of memristor resistivity causes the set of interesting effects, such as widening of hysteresis loop with the increase in ρ_{ON} and ρ_{OFF} and motion of pinch point further from zero point with the increase in ρ_{ON} .

The accurate model considering first-order parasitic effects was presented. The scope of the model is limited to the metal-oxide-metal memristor, and is intended to give the accurate results for the particular device dimensions.

As the further development of this model, the second-order effects may be considered in future models, such as temperature effects and the variable capacitance and inductance, that would give even more accurate results than the model presented in this paper.

V. ACKNOWLEDGEMENTS

The author would like to thank Dr. Alex James for the opportunity to participate in the ICP conference, Dr. Alexander Ruderman and Dr. Dongming Wei for for help in deep understanding of the circuit behavior

VI. APPENDIX

```
V1 N001 0 SINE(0 1.5 2 0 0 50)
XU1 N001 N002 memristor
C1 N001 N002 19.89259458n Rser=0.00001
L1 N002 0 425.100841760448µ
.tran .2s 50s 30s
.lib/Memristor.txt
.backanno
.end
```

VII. REFERENCES

- [1] L.O. Chua, "Memristor - The Missing Circuit Element," IEEE Transactions On Circuit Theory, vol. CT-18, no.5, pp. 507-519, September 1971.
- [2] D.B. Strukov, G.S. Snider, D.R. Stewart and S.R. Williams, "The missing memristor found", Nature 453, 80-83 May 2008
- [3] Z. Biolek , D. Biolek and V. Biolkova "SPICE model of memristor with nonlinear dopant drift", Radio Eng., vol. 18, no. 2, pp.210 -214 2009
- [4] S. Kvatinsky, E.G. Friedman, A. Kolodny and U.C.Weiser "TEAM: ThrEshold Adaptive Memristor Model", Circuits and Systems I: Regular Papers, IEEE Transactions vol. 60, no.1 pp. 211-221, January 2013
- [5] R. S. Williams, "How We Found the Missing Memristor," in *Memristors and Memristive Systems SE - 1*, R. Tetzlaff, Ed. Springer New York, 2014, pp. 3–16.
- [6] M. Mahvash and A. Parker, "A memristor SPICE model for designing memristor circuits," in MWSCAS, no. 2, 2010, pp. 989-992.
- [7] Y. N. Joglekar and S. J. Wolf, "The elusive memristor: Properties of basic electrical circuits," *Eur. J. Phys.*, vol. 30, no. 4, pp. 661–675, Jul. 2009.
- [8] T. Prodromakis et al. "A Versatile Memristor Model With Nonlinear Dopant Kinetics," IEEE Trans. on Electron Devices, vol. 58, no. 9, 2011.
- [9] M.P. Sah et al. "A Generic Model of Memristors With Parasitic Components." IEEE Trans. on Circuits and Systems, vol. I.
- [10] E.B. Rosa. "The self and mutual inductances of linear conductors." Bulletin of the Bureau of Standards, vol.4, no.2, Washington, September 1907.
- [11] D. Regonini, V. Adamaki, C.R. Bowen, S.R. Pennock, J. Taylor, A.C.E. Dent. "AC electrical properties of TiO2 and Magnéli phases, Ti_nO_{2n-1} ." Solid State Ionics, vol. 229, pp. 38–44., December 2012
- [12] J. R. Smith and F. C. Walsh, "Reviews in applied electrochemistry. Number 50 - Electrodes based on Magnéli phase titanium oxides: the properties and applications of Ebonex (R) materials," *J. Appl. Electrochem.*, vol. 28, no. 50, pp. 1021–1033, 1998.

VIII. ABOUT AUTHOR



Rassul Bairamkulov is currently junior student pursuing his BEng in Electrical and Electronic Engineering at Nazarbayev University, Astana, Kazakhstan. His research include: low-power integrated circuits, power converters, visible light communications.

The real-time heart rate monitoring using fingertip and its application in health care

Nurbolat Aimakov

Department of Electrical and Electronics Engineering,
Nazarbayev University,
Astana, Kazakhstan
nurbolat.aimakov@nu.edu.kz

Diana Sadykova

Department of Electrical and Electronics Engineering,
Nazarbayev University,
Astana, Kazakhstan
diana.sadykova@nu.edu.kz

Following sedentary lifestyle leads to undesirable health problems of different kinds starting from rachiocampsis (i.e. curvature of backbone) and ending with such serious diseases as obesity or spinal hernia. This is a widespread issue because in the XXI century most types of the jobs are office oriented and the employees spend most of the time in static, sitting position. Our contribution to solve this problem consists of an innovative idea to modify ordinary vending machines by installing a system, which will offer products with decreased prices in substitution to performing physical exercises, and verify this by monitoring the change in the heart rate. This modification is an optimal solution to the health problems, as performing physical exercises is considered to be the easiest way to prevent diseases and probably it will increase productivity of the employees.

Keywords — health; vending machine; OpenCV; heart rate; threshold; noise reduction; sedentary lifestyle;

I. INTRODUCTION

With technology development most of the professions became computer oriented. Consequently, people spend approximately 7-8 hours per day sitting in front of the computer without changing their position. In most, this leads to different health issues starting from rachiocampsis (i.e. curvature of backbone) and ending with such serious disease as obesity or spinal hernia [1]. One of the possible preventing measures is to perform periodically physical exercises.

This article describes a new system designed to be installed in ordinary vending machines, which will provide an opportunity to get a discount for goods instead of workout exercises.

Here you can see our contribution list:

- We choose heart rate as a control tool for the application. Particularly, it will examine the values of heartbeat before and after exercises were performed to check the feasibility of the change.
- The system detects pulse through a fingertip, as this method requires no additional tools except a video camera. Its innovative feature of the unique methodology is described in Section II.

- Real-time video capture is modified by applying several image processing techniques of OpenCV library such as color conversion, threshold and noise reduction.
- We constructed a five stage algorithm based on “if-else” operation statements to monitor fluctuations of video brightness due to inflow and outflow of blood in a finger and to display the value of the heart rate as the output.

II. METHODOLOGY

A. Video acquisition

Firstly, the program initiates real time video acquiring through an available camera, which was HP laptop webcam in our case. During the process a finger has to be in touch with the camera, but the contact should not be too strong in order to allow blood circulation. Due to the fact that fingers are not completely opaque, some portion of light will pass through, namely red spectrum of light will be detected by the camera. On the output, we will have a red image with fluctuating brightness. The theory behind it is when blood flows into a finger, its light transmittance decreases and vice versa. Sample image can be seen on the fig. 1.

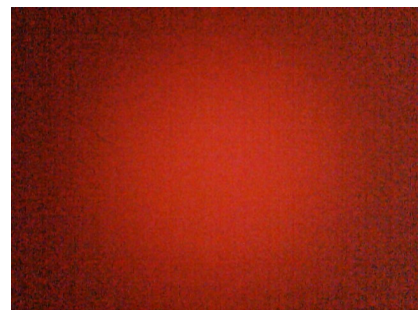


Figure 1. The light transmittance with blood outflow

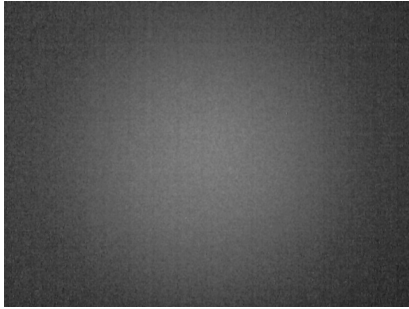


Figure 2. Sample frame converted to black and white colors

B. Black-white conversion

The frames are converted to black-white version for convenience in the further steps in terms of selecting definite colors. The output of the step is seen on the fig.2.

The intensity of the pixels in the image is ranging from 0 to 255, where 0 means completely black pixel and 255 corresponds to completely white pixel. Graphical representation is shown on the fig. 3.

C. Band-pass filtering

Now we need to apply band pass filtering to the video in order to cut off the relative dark sides and clearly observe the occurring changes. The level of threshold depends upon the illumination level of the environment. During the program examination illumination level was reasonable and the value to 100 out of 255 was selected based on the experimental data. Therefore, if a pixel has the intensity value below 100 it will be changed to 0 and, reciprocally, if the value is greater than 100 it will be set to the maximum of 255 (see fig. 4).

D. Noise reduction

Our calculation steps are related to obtaining the amount of white pixels every frame and counting the up and down peaks in the sequence of numbers. Considering the fact, this arrangement of pixels in frames is not efficient to use because of noise effect at the borderlines.

109	109	109	107	108	109	111	116
109	108	108	107	107	107	107	111
103	103	105	104	104	104	103	103
101	102	104	103	104	102	98	98
101	103	104	104	104	102	98	97
107	107	104	103	104	103	102	102

Figure 3. The intensity of the black-white pixels ranging from 0 to 255

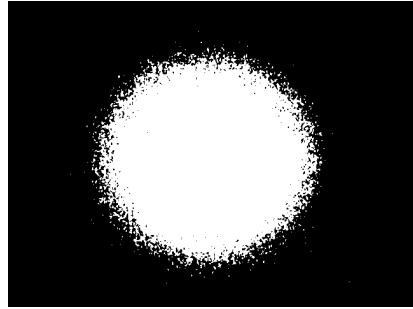


Figure 4. Sample frame with implemented band-pass filtering

Therefore, noise reduction technique has to be implemented before the actual heart rate calculation step. This is done by collecting groups of similar pixels into blocks and rejecting the one that are not included. Finally, the final frames we are working with appear to be as it is shown on the fig. 5.

E. Algorithm implementation

At the part image processing process turns to heart rate calculation process. The key point of this method is in measuring the amount of white pixels in every frame and process the sequence of numbers such that the program adds one every time when the sequence reaches local maximum or local minimum. The effect is achieved by implementing 4 variables and 5 “if-else” statements. Using special function related to time counting the process lasts 20 seconds. Resulting number of heartbeat is multiplied by 3, in order to display the heart rate value in terms of beats per minute. Additionally mathematical operator ‘ceil’ was used in order to round up answer due to the fact that inside the calculation process the heart beat counter is divided by 2 and the output is designed to consist of whole numbers only. After the first trial “exercises” which the user desires to do will executed and the value will be calculated again. The system provides discount if the difference between the final and initial heart beat values is greater than or equal to 15. The number is chosen based on the experimental data.

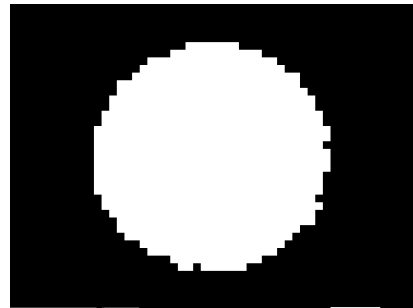


Figure 5. Sample frame with implemented noise reduction technique

Finally, in order to use the software installed in a vending machine, its hardware has to be adapted for the software specifications and an additional hardware component, in terms of low-end camera, has to be supplemented.

III. RESULTS AND ANALYSIS OF DATA

We organized a survey consisting in total of 10 people to examine the application. The test was conducted in the room with good artificial illumination. All volunteers were students roughly within the same age, ranging from 19-22 years. In our trials we used HP ENVY 15 Notebook PC (2.40GHz, Intel® Core™ i7-4700MQ CPU) running Windows 8.1 and Ceemple software version 1.0.3. The camera which was used to capture video was HP Truevision HD, installed in the laptop. The results obtained from the computer were compared to manual estimation of the heart rate.

During the measurement all volunteers were sitting in the same position. They sat right in front of the computer, putting a thumb of a right hand on the camera. Manual computations were done by the one person, who placed two fingers on the inside of the wrist and gently pressed the vein, until the heartbeat could be perceived and then estimated.

Results of conducted test are presented in Table 1, where 'A' and 'M' are attempts made by our application and by the manual estimation correspondingly. All volunteers completed three successful trials using both methods with duration of each trial equal to 20 seconds. The absolute errors vary from 1.22 bmp to 3.67 bmp, with average error equal to 2.13 bmp. Therefore, the application can be considered to be accurate enough to detect pulse change.

TABLE I. The Heart rate measurement using application and manual methods

No	Using our application (bpm)			Using manual calculations (bpm)			Absolute Error
	A1	A2	A3	M1	M2	M3	
1	71	72	72	74	74	73	2,00
2	78	84	81	83	79	82	3,67
3	63	65	62	66	64	64	2,00
4	54	51	53	52	50	51	1,67
5	66	64	68	65	64	65	1,33
6	74	77	75	73	73	74	2,00
7	68	71	69	69	68	70	1,67
8	65	69	68	67	65	66	2,67
9	71	67	72	70	68	69	1,67
10	73	78	71	74	75	75	2,67
Average							2,13
Error :							bmp

IV. SUMMARY. CONCLUSIONS AND RECOMMENDATIONS

One of the important aspects of our project is the limitations that we faced during the software design process. First of all, due to the fact that the accuracy of the results based on the detected white circle-shaped area strictly depends on the illumination of the environment. The problem can be solved by mounting a specific light source so that the output will not be dependent on the light intensity of the environment. Secondly, sampling frequency of the used camera should be much greater than average heart rate in order to prevent missing out a pulse. Thirdly, people with heart diseases (e.g. with too high or low heartbeat) will not be allowed to use our application.

The application can be further modified by applying more advanced image processing, e.g. fill the circle type shapes up to complete circles in order to achieve steady changes of the amount of white pixels.

REFERENCES

- [1] Owen, Neville and Adrian Bauman, "The Descriptive Epidemiology of a Sedentary Lifestyle in Adult Australians," *Int. J. Epidemiol.* (1992) 21 (2): 305-310, accessed March 31, 2015, doi:10.1093/ije/21.2.305

The representation of memristor model in MATLAB[®] and Simulink[®] environment

Sanzhar Askaruly
 Department of
 Electrical Engineering
 Nazarbayev University
 Astana, Kazakhstan 010018
 Email: s.askaruly@gmail.com

Baktiyar Rakhmetov
 Department of
 Electrical Engineering
 Nazarbayev University
 Astana, Kazakhstan 010018
 Email: brakhmetov@nu.edu.kz

Abstract—The work describes the various methods of memristor modeling and simulation in the MATLAB[®] and Simulink[®] environment. Previously published papers about memristors and their features are used as the foundation of the work. There are three various methods used in the MATLAB and Simulink for the differential and other equations formulation. The first equation uses the standard system core offer for the Ordinary Differential Equations solutions (ODE) in the m-file form. The second solution is the model construction in Simulink environment. The third method includes a physical modeling using the built-in Simscape[™] system. The results are the basic memristor characteristics and appropriate time courses. The characteristics of all models and their computer simulations are described in the paper.

I. INTRODUCTION

Initially, there were 3 basic passive elements - resistors, inductors and capacitors in the modern analogue electronics, see Fig. 1. Based on the square symmetry, another element

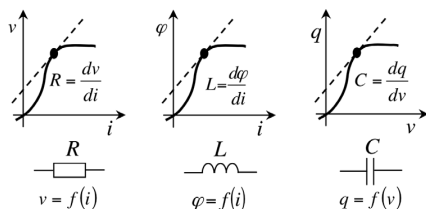


Fig. 1: The passive element parameters definition.

called memristor (memory resistor) was presented in 1971, according to [1]. Leon Chua summarizes the four elementary passive elements, follow Fig. 2.

It contains of a direct connection between flux and a charge. In other words, memristors show that resistance is dependent on a passing charge. As a results, it can be seen that memristors do not need any energy to keep data in terms of recording and reading. Therefore, the fourth passive element is able to hold information about the net amount of charge gone through. The resistance of memristor can be varied constantly with current within certain limits.

The first real memristor was built by Hewlett-Packard (HP) scientist in 2008 [2]. Its nano-part was made of titanium oxide with size of 10 to 30 nanometers hold between two platinum electrodes. The titan layer does not have oxygen atoms that make it to behave as a semiconductor. The other part acts as

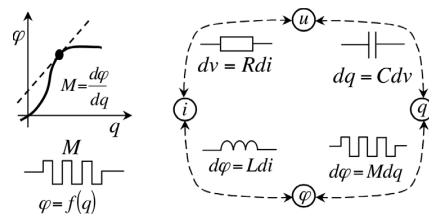


Fig. 2: The memristor and a passive elements quaternion.

an insulator. The main functioning principle of memristor is that semiconductor layers width changes when current passes.

The main purpose of the paper is to evaluate the memristor through modeling it in MATLAB and Simulink.

II. MATHEMATICAL MEMRISTOR MODEL

The mathematical memristor model, which was taken from [3], explains the substance of the models.

The basic geometrical image of a manufactured memristor is represented in Fig.3. Thickness of the whole component is marked with D , the thickness of the doped layer with w . Its value is though dependent on the passing current (memory effect with regard to the total charge). In Fig.3, D is the thickness of memristor; W - the width region, which is a function of current flowing through (memory effect).

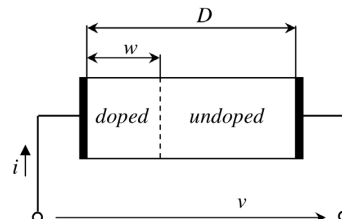


Fig. 3: Basic geometrical image of the memristor according to HP laboratories.

The exciting voltage is derived from Ohm's Law:

$$v(t) = R_{mem}(x)i(t) \quad (1)$$

R_{mem} - total resistance of doped and undoped region; $x = w/D \in (0,1)$. Moreover, dynamic state equation of the current

dependence to x state is to be defined:

$$\frac{dx}{dt} = kf(x)i(t), k = \frac{\mu_v R_{ON}}{D^2} \quad (2)$$

where $\mu_v = 10^{-14} m^2 s^{-1} V^{-1}$ is a dopant mobility. The limiting values for the resistance of memristor $w = 0$ and $w = D$, which are represented as R_{ON} and R_{OFF} . Total resistance can be rewritten as

$$R_{mem}(x) = R_{ON}x + R_{OFF}(1-x) \quad (3)$$

The function $f(x)$ in the equation (2) models nonlinearities of the charge carrier transport and called window function. One proposed version [3] of this term is:

$$f(x) = 1 - (2x - 1)^{2p} \quad (4)$$

The relations illustrate (1) to (4) show the mathematical model of memristor that was discovered up to today. Theoretical background provided up to this point is enough to move further.

III. MEMRISTOR MODELING IN MATLAB

In this part, the practical part of memristor modeling in MATLAB is demonstrated. First, memristor behaviour is reproduced in the m-file form. This file has two functions with standard definition and corresponding ODE solution. In the Fig.4. source code of the memristor model is provided. Within the frame of the Memristor a MATLAB function is a key line is the chosen ODE solver which is the actual ODE numerical integration method. The solver of type *ode23t* shows that modified stiff/Trapezoidal method is used.

The initial value memristor resistance is given by R_{init} . MATLAB ODE solver *ode23t* uses the function *ODEMemriA* as its parameters for output. The variables marked with [t,x] are returned back. Hence the x state outputs time course, as it can be noticed from equation (2). The vector of current flowing through a memristor can be found from the same equation. The harmonic course of the V voltage with the 1V amplitude and 1Hz frequency. Therefore the model can be considered to be full, when the voltage and course vectors are defined. Moreover, charge versus flux graph is obtained, since it also describes memristor explicitly.

From the theory, it is known that in order to obtain charge and flux calculation, indefinite integration is required. To struggle this, the IIR type digital filter are often used to perform these operations. The filter command is next multiplied by sampling period to get the proper scale. The digital filter is originally defined with the following relation:

$$H(z) = \frac{z}{z-1} \quad (5)$$

where z is the Z-transform operator. Accurately obtained Fig. 5 and Fig. 6 demonstrate the simulation results for the given input harmonic voltage. The MATLAB source text can be modified by dividing them into two or several m-file parts for working with more extensive systems.

```
% Model of memristor in MATLAB environment
%-----
function Memristor_Matlab
    Ron=100; Roff=16e3;
    Rinit=11e3; DR=Roff-Ron;
    tmin=0; tmax=3; % time interval
    N=500; % number of steps is N+1
    OsaT=tmin:(tmax-tmin)/N:tmax; % time axis
    x0=(Roff-Rinit)/DR; % initial condition
    [t,x]=ode23t(@ODE_Memri_A,OsaT,x0); % calling ODE
    V=1*sin(2*pi*1*t); % input voltage
    I=V./(Roff-x*DR); % current
    %--- drawing the results ---

    %--- integration of U and I ---
    Flux=(t(2)-t(1))*filter(1,[1 -1],V);
    Charge=(t(2)-t(1))*filter(1,[1 -1],I);

    %--- ODE definition ---
    function dx=ODE_Memri_A(t,x)
        D=10e-9; Ron=100;
        Roff=16e3; DR=Roff-Ron;
        uv=1e-14; % dopant mobility
        k=uv*Ron/D^2; p=10;
        %--- ODE definition ---
        V=1*sin(2*pi*1*t); % input voltage
        Fx=(1-(2*x-1)^(2*p));
        dx=k*(V/(Roff-x*DR))*Fx;
```

Fig. 4: Memristor model in MATLAB

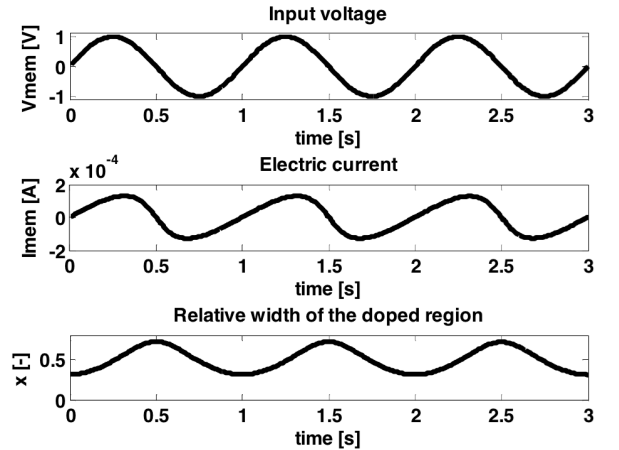


Fig. 5: Memristor key time courses simulation

A. Input-output model in Simulink

Simulink environment is a better option when the memristor is to be modelled as an element of complex systems. Basically, the environment offers modeling the form of input-output relationship. However, since the memristor is not possible to be represented as two-terminal element, there is another way to model it though. It is shown as device with the input of voltage and the output of current. Fig. 7. illustrated demonstrates a functional memristor model. The appropriate blocks are responsible for mathematical operations that were

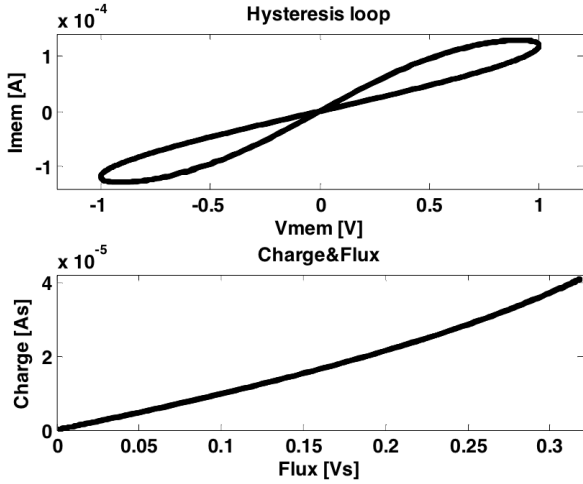


Fig. 6: Elementary memristor characteristics simulation.

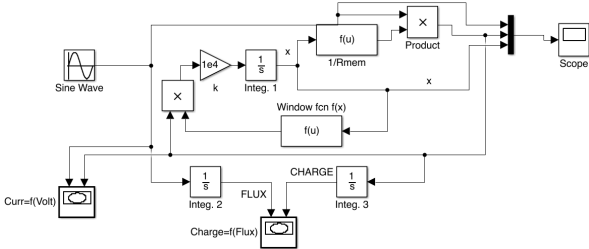


Fig. 7: Memristor model in Simulink system

given before in the equations from (2) to (4).

$$x(t) = \int_t k f(x) i(t) \quad (6)$$

$$i(t) = \frac{v(t)}{R_{OFF} - x \Delta R}, \Delta R = R_{OFF} - R_{ON} \quad (7)$$

The equations (6) and (7) are strictly followed by the arrangement of the blocks developed in Simulink. The initial condition of the integrator is defined as:

$$x_0 = \frac{R_{OFF} - R_{INIT}}{\Delta R} = \frac{16.10^3 - 11.10^3}{16.10^3 - 100} = 0.3145[-]. \quad (8)$$

The other constant values are the same as in the previous model. The simulation results remain as in the previous model. Other settings were remained by default.

The basic advantage of this modeling method is comparable speed, simplicity and descriptiveness. More attention is paid to blocks separation and simulation parameters configuration. The existing harmonic voltage source uses the same values as in the previous model.

Configuration of Simulink environment takes place in the ODE solution parameters, which it to be set for *ode45* (Dormand-Prince) type of ODE solver, which uses Runge-Kuth method explicitly. Maximum step was set to 0.015 value.

B. Physical memristor model

Simulink environment also contains Simscape block library, intended for multidomain modeling of physical systems. It also gives opportunity to simulate systems of different engineering fields. Before approaching, the principle scheme is to be developed [3], which is presented in Fig. 8.

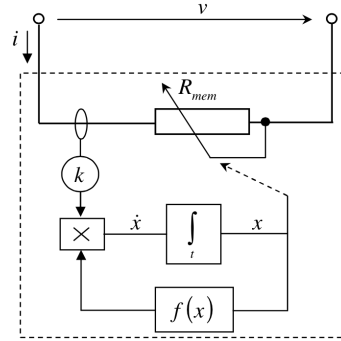


Fig. 8: Principle memristor scheme in Simscape

From the Electrical Elements library of the Simscape system, the three terminal Variable Resistor component was used. The two are the input and output of the resistor, and the third terminal is the regulatory input regulating resistance, which is dependent on the random variable principle (signal). This component basically includes the construction of the memristor model according to Fig. 8.

Fig. 9 demonstrates the full physical memristor model. Some blocks serve for the mathematical model implementation, whereas a few other blocks are applied to convert between Simscape and Simulink environments as well as obtaining outputs on the oscilloscope. Apart from the blocks of drawing on the right, the physical model is exactly implementation of scheme of Fig. 8. At the right side, the Current Sensor and Voltage Sensor blocks are needed to test the current and the voltage values. Moreover, PSS converters are used to interchange Simulink-Simscape library blocks so that the model can behave as entire system.

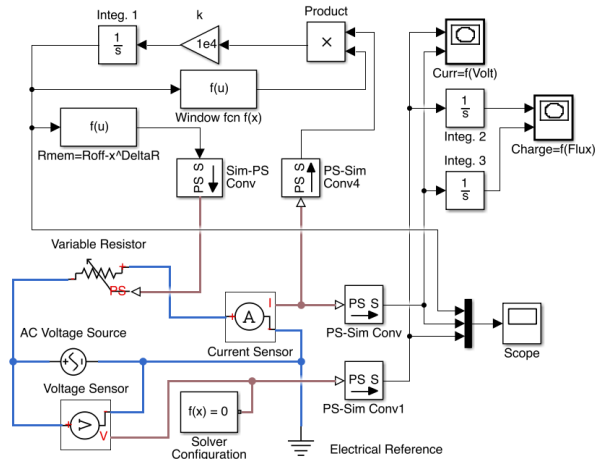


Fig. 9: Physical memristor model in Simulink & Simscape

Model in the Fig. 9 is a representation of combined use of Simulink&Simscape. Therefore, the given system would probably be more efficient in terms of functionality. Similar to the model that was presented in Simulink, the integration is provided with $1/s$ integrator blocks. The Simscape AC Voltage Source block is a representation of harmonically variable voltage source accordingly.

IV. CONCLUSION

This work was based on the previous papers on memristor modeling. It sets goal to try various methods of modeling memristor in MATLAB and Simulink. As a result, a few models were obtained. First, m-file of source code solution to ODE was shown. Next, Simulink block diagram in terms of input-output model was built. It was then further developed with the help of Simscape block library, by adding variable resistor, necessary current and voltage sensors. To conclude, in the perspective the work that is planned is results checking by comparing obtained outputs with future SPICE model simulations.

ACKNOWLEDGMENT

The authors would like to thank Dr. Alex P. James, for the motivation and further review in the development of this publication.

MATLAB, Simulink and Simscape are registered trademark of The MathWorks, Inc.

REFERENCES

- [1] Chua, L.O. Memristor - the missing circuit element, *IEEE Trans. Circuit Theory*, 1971, vol. CT-18, no. 5, p. 507-519
- [2] Strukov, D., Snider, G., Steward, D., Williams, R. The missing memristor found. *Nature*, 2008, vol. 453, 1 May 2008, p. 80-83.
- [3] Biolek, Z., Biolek, D., Biolkova, V. SPICE Model of Memristor with Nonlinear Dopant Drift. *Radioengineering*, 2009, vol. 18, no. 2, p. 210-214. ISSN 1210-2512.

Traffic light recognition system for people with color blindness

Timur Ibrayev
School of Engineering
Nazarbayev University
Astana, Kazakhstan
timur.ibrayev@nu.edu.kz

Radkhan Sarmukhanov
School of Engineering
Nazarbayev University
Astana, Kazakhstan
radkhan.sarmukhanov@nu.edu.kz

Abstract—This paper suggests the solution of traffic light color recognition problem for people with color vision deficiency. Solution will include the developed Windows OS compatible application that is further adapted to android platform. The application was initially developed by the C++ programming language with the Open Computer Vision (OpenCV) library. During the development of program the combination of Image Thresholding and Hough Circles object detection methods was used to detect the traffic light itself. After that the color of the traffic light was identified and written notification defining the color name was displayed on the screen. The algorithm is then used to write an application prototype for android based devices. It is expected that this program will assist people with color blindness in traffic light color detection.

Keywords—color blindness, traffic light recognition, object recognition, shape recognition, color recognition, OpenCV, C++, Android

I. INTRODUCTION

Approximately 500 million people are affected by color vision deficiency nowadays. Unique property of this disease is that it cannot be cured, thus people with color blindness become vulnerable at some situations. Experts imply that red-green color deficiency is the most widespread defect type. Hence, traffic light color identification can probably be considered the most encountered problem for color blind people. Spread of this disease among pedestrians and drivers is likely to increase the number of car accidents. Thus, the necessity for development of the application that will assist color blind people with traffic light color recognition cannot be underestimated.

Today image and video processing are mainly performed with the usage of OpenCV library. The application that we propose in this paper is based on two different functions: one of which is used for color thresholding and other is for shape detection. The main idea is by combining two functions implement algorithm for detecting traffic lights on camera or video stream. Consequently, program will recognize the color of the displayed signal by applying different color filters.

Finally, the program is planned to notify the user with the corresponding sound signal. This application was firstly designed for computers operating on Windows OS. Since

web-camera is expected to be the main input source, laptop's location in the car is required. However the algorithm was further used with Android programming language to create prototype of mobile application. This option potentially will be more convenient for drivers and pedestrians.

II. PROCEDURE

This section will explain the step-by-step procedure of the application realization. Firstly, the restrictions applied to the sample video data will be described.

Secondly the procedure of how object detection was realized in the program is described by explaining two different methods used to detect objects based on either color or shape. After explaining these and defining the drawbacks of using two methods separately, the core of the proposed algorithm will be presented by describing how these two methods complement each other in order to form traffic light recognition program.

After explanation of how the program will find traffic lights on video stream, the color identification technique used in the program will be explained.

A. Sample Data

The very first step in the design process was to obtain appropriate video samples. This version of the program was only considering the case when traffic lights were clearly visible and close to the recording device. This was done in order to see if the proposed logic works as required when there is a minimum amount of disturbing objects on the video. However, in turn, this means that program still should have the future improvements to deal with the cases when there is more objects introducing noise. The images of the frames with red, red and yellow, and green traffic light signals being on are displayed in Fig. 1.

B. Image Thresholding Method

This is a method that is basically used for object detection that is based on its color properties. The BGR colored image is converted into HSV color space image. Then HSV image is thresholded by manually adjusting the HSV values using *inRange* function and track bars, so that the required color is represented as white and the rest of the image is represented



Fig. 1. The sample of Traffic Light used in the program design with red (a), red and yellow (b), and green (c) light signals being displayed

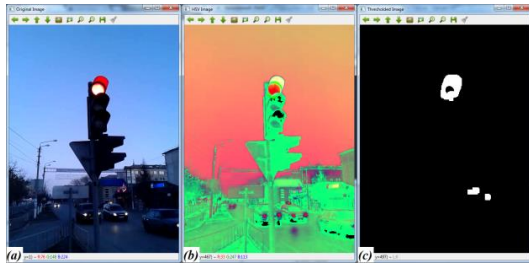


Fig. 2. The example of red traffic light contour detection using conversion of original image frame (a) into HSV color space image (b) and then applying threshold (c)

as black color. Consequently, *findContours* function together with *moments* method applied to find and store the white colored contours from thresholded image. The example of such image conversions for thresholding red color is illustrated in Fig. 2.

As it can be seen the red colored object is easily extracted by thresholding HSV values. However, the drawback is that function *findContours* finds any white colored contour that was found in thresholded image. The morphological operations (such as erosion and dilation) are able to eliminate noise effects, but still there may be objects of not only the same color, but also of the bigger size than targeted traffic light. Consequently, the function may not only be unable to recognize the traffic light signal but also by making an error recognize another object instead of it. Moreover, it does not make a difference between the shapes of the contour found. Hence, the design of the proposed program adds another function to detect the shapes of the objects in the video stream.

C. Finding Hough Circles Method

HoughCircles function is introduced into the program to find the objects of the circled shape. In order to use this function, the original frame image from the video is initially converted to grayscale image and then blurred. The conversion is done because the function works on only 8-bit images. Blurring is then applied to reduce the noise and avoid the false circle detection. Example of applying this function to detect the circled shape of red colored signal is illustrated in Fig. 3.

As it can be seen the *Hough Circles* function has detected only one circle, which is the shape of traffic signal. However,



Fig. 3. The example of red traffic light circle shape detection using conversion of the original image (a) into grayscale image (b), and blurring it and displaying the circle shapes found (c) by the Hough Circles method

the drawback of using this method alone for object detection is that if there are multiple objects with circled shape, the function will find all of them. For the specific problem that the following application is aimed at finding circle shapes without much emphasize on its color is not enough.

D. Combination of two methods to achieve better object detection

The main advantage of the proposed application is the implementation of two functions together.

Firstly, the program searches for circle shapes using Hough Circles and, as it can be seen from Fig. 3, defines the boundary coordinates of them. Then, the coordinates are used to compare with every contour that has been found by thresholding the image to required color. It can be said that the main role of these coordinates is to filter out unnecessary contours, and to only display targeted traffic light signals. After potentially traffic light signal was detected, it is tracked and displayed by the program. Fig. 4 illustrates an example of how this object detection works for red signal.

However, this only detects the position of the required object on the image frame and serves as a training stage for determining HSV values for each of the required colors, but does not define it explicitly. For the program to automatically identify which color was thresholded another function was introduced.

E. Color Detection Technique

The color detection part of this program is working on the fact that the sets of HSV values for each of the three colors are determined in training stage. Each of these sets is then used to create color filters for three colors of traffic signal.

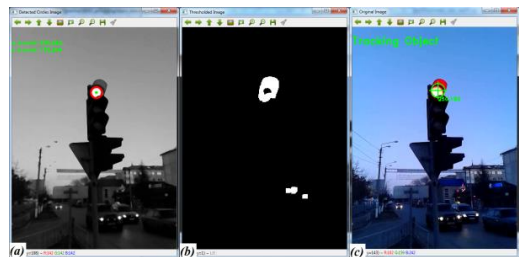


Fig. 4. Example of object tracking by comparing the boundaries found by HoughCircles function (a) with coordinates of contours found by thresholding (b) and displaying the tracked object on original image (c)

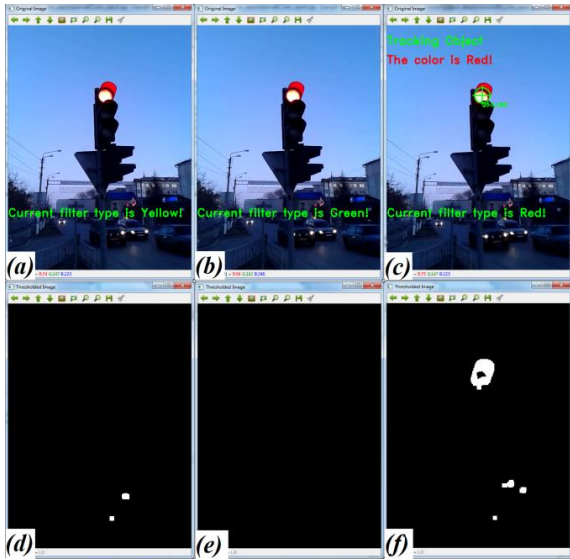


Fig. 5. The color detection implemented by the sequential application of yellow color filter (a), green color filter (b), and red color filter (c) to original image, each of filter being thresholded by HSV values for yellow color (d), green color (e), and red color (f)

These are then sequentially used in a loop form to create a function that automatically changes the threshold values. In case the object is found, the function stops changing the filter and displays the corresponding color value. When the object is lost because of traffic signal change, the application recalls the function and make color filter change to the next one. For example, one turn of the color recognition is illustrated in Fig. 5.

The algorithm that was utilized to construct the application for Windows can be graphically represented by the flowchart shown in Fig. 6.

III. RESULTS OF APPLICATION FOR WINDOWS OS

The Fig. 7 illustrates the cases of successful identification of red, yellow, and green signals by the program on its own, without any user manipulations on HSV threshold values.

Despite the program works appropriately for the determined range of HSV values, there are still occasions when the program misinterpret displayed signal. The common case is when traffic light displays both red and yellow signals. This can be seen from Fig. 8.

Moreover, it should be remarked that such scenario of signal identification is very simplified for initial design purposes, but will not work if there are more objects on the video that can cause errors in identification processes.

IV. ANDROID IMPLEMENTATION

After the program for Windows, despite of being not fully finished, worked well for traffic light used as a main sample, we tried to write an application having the same purpose and algorithm for Android platform devices. Precisely, the main interest was on constructing an application for mobile phones,

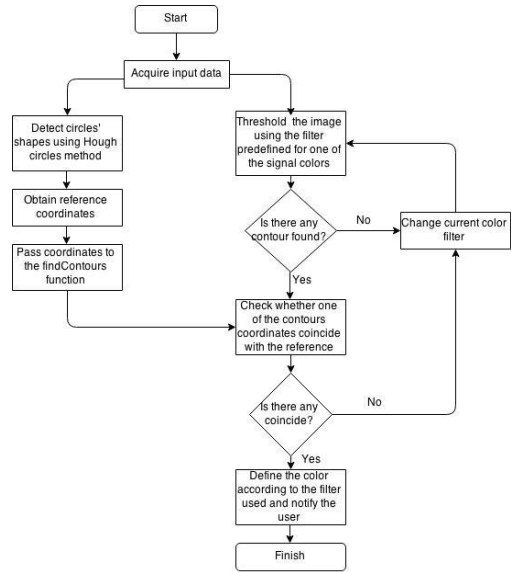


Fig. 6. Flowchart of the proposed algorithm for traffic light recognition application

because there is now increasing number of android mobile phone users as well as the rapid developments on increasing their operation capabilities.

The application at its final version is planned to be capable of identifying the traffic lights from the camera preview of the mobile phone, recognizing the color of signal being displayed, and finally providing sound notifications to the user.

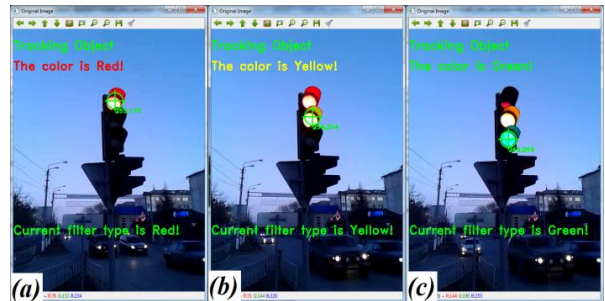


Fig.7. Examples of successful traffic light recognition with red color (a), yellow color (b), and green color (c) signals being displayed and identified



Fig.8. Example of misinterpreting traffic light signal when both red and yellow color signals displayed

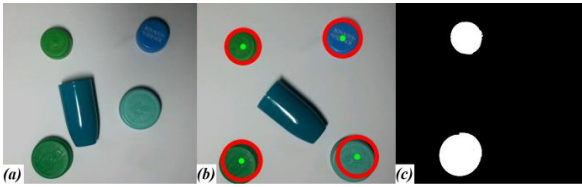


Fig. 9. Android application realization process of testing example samples in RGB color scale (a) for Hough Circles detection (b) and for thresholding green colored objects (c) using Android OS mobile device.

Due to time limitations for accomplishment of this project and low level of required skills in programming on Java programming language, for the first stage we put the main goal to create a working application that will separately implement functions to find circle shaped objects and to threshold video frames. The samples illustrated in Fig. 9 indicate successful accomplishment of this step.

The second part of the program development was to make program compare between these two functions, and to represent an object that satisfies both the circled shape and color of the traffic signal. In order to do this, the prototype version of application was tested on Galaxy S3 mobile phone utilizing Android version 4.3.1. The results of this stage accomplishment are represented in Fig. 10.

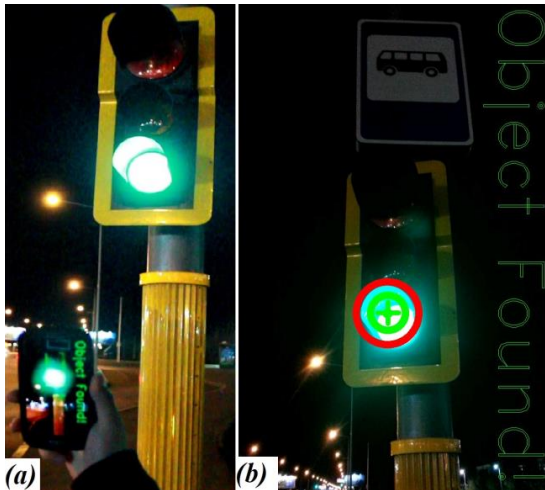


Fig. 10. Photo of Galaxy S3 mobile phone running preliminary version of the application (a) and the screenshot of the device (b) showing the coincidence of circle detection result (red circle) and of green color recognition result (green crosshair) and corresponding message

The further parts of android application realization will include the implementation of automatic color filter changing, and sound notifications for users.

V. CONCLUSION

This paper has proposed an application design for traffic light recognition for Windows based systems and its prototype for Android based devices. The significance of the following design is that the program was not only utilizing the threshold based object detection principles but also incorporated the

shape detection functions. This gave the possibility to eliminate any objects that may present on video frame and have the same color as these of traffic lights. Moreover, this ensures that the coordinates of the detected traffic light become also known.

However, the proposed design still has significant number of imperfections. So, the program was not tested for the case when there is the number of disturbing moving objects. In addition, the color recognition function based on filtering function is not appropriate for various light intensities. Hence, the program may fail to recognize color appropriately during different time of the day.

Hence, future improvements may include encountering time of the day, which may, in turn, be used to determine appropriate HSV values according to light and traffic intensity conditions.

VI. ACKNOWLEDGEMENT

Authors would like to express their gratitude to anonymous reviewers for spending their time to give useful comments which contributed to improving the quality of the paper and for raising motivation to accomplish the initial version of the program for android platform.

Special thanks to these people who kindly helped by providing their android devices/cameras for testing and data collection.

VII. REFERENCES

- [1] Abdallah, Mahmoud, and Eiland, Daniel. Traffic signal detection and tracking. Spring 2011.
- [2] Baggio, Daniel Lélis. *Mastering OpenCV with practical computer vision projects*. Packt Publishing Ltd, 2012.
- [3] Bin Mohd Mokji, Mussa, and Zaim Bin Hamzah, Ahmad. Traffic light signal detection using Windows phone. March 27, 2015.
- [4] Bradski, Gary, and Adrian Kaehler. *Learning OpenCV: Computer vision with the OpenCV library*. "O'Reilly Media, Inc.", 2008.
- [5] Docs.opencv.org. Finding contours in your image. Last modified February 25, 2015. http://docs.opencv.org/doc/tutorials/imgproc/shapedescriptors/find_contours/find_contours.html
- [6] Docs.opencv.org. Hough circle transform. Last modified February 25, 2015. http://docs.opencv.org/doc/tutorials/imgproc/imgtrans/hough_circle/hough_circle.html
- [7] Docs.opencv.org. Operations on arrays. Last modified February 25, 2015. http://docs.opencv.org/modules/core/doc/operations_on_arrays.html
- [8] Laganière, Robert. *OpenCV 2 Computer Vision Application Programming Cookbook: Over 50 recipes to master this library of programming functions for real-time computer vision*. Packt Publishing Ltd, 2011.
- [9] Lorsakul, Auranuch, and Jackrit Suthakorn. "Traffic sign recognition using neural network on opencv: Toward intelligent vehicle/driver assistance system." In *4th International Conference on Ubiquitous Robots and Ambient Intelligence*, pp. 22-24. 2007.
- [10] Chung, Yun-Chung, Jung-Ming Wang, and Sei-Wang Chen. "A vision-based traffic light detection system at intersections." *Journal of Taiwan Normal University: Mathematics, Science and Technology* 47, no. 1 (2002):67-68

Translational Biomechanics in Glaucoma

Match W. L. Ko

Abstract—Glaucoma is the second leading cause of blindness in the world. Intraocular pressure (IOP) is a primary indicator of glaucoma. The IOP measured in tonometry is generally compared to a threshold IOP level (21 mmHg) as a reference for clinicians to determine if the subject is at risk. Precision measurement of the IOP depends on accurate measurement of corneal geometries and corneal biomechanical properties. Both the measured IOP and threshold IOP, however, ignore the individual variations of the ocular tissue biomechanical properties in human eyes. The inclusion of individual ocular biomechanical properties is needed to improve the accuracy of measured IOP and clinical relevance of threshold IOP. This review will focus on the fundamental theories and practices of ocular biomechanics in glaucoma.

Index Terms—Corneal biomechanics; elastic Young's modulus; tangent modulus; cornea; ocular

I. INTRODUCTION

The eyes are one of the most important sensory organs and are specialized for the conversion of light into electrochemical signals so that our brain can interpret. The cornea is the principle refractive element in the eye and accounts for ~45 diopters of the total ~60 diopters of ocular power [1, 2]. The dual responsibilities of cornea are the maintenance of optical transmission of light and ocular mechanical stability, which are the foundation of many refractive procedures. The cornea not only protects the inner contents of the eye and maintains the ocular shape, but also refracts the light that passes into the eye. The cornea is located at the front part of the eye and functions like a window that controls and focuses light entering the eye. It is the only source from which the world is observed and recognized. However, disease (e.g. glaucoma [3, 4] and keratoconus [5, 6]), surgery (e.g. LASIK [7]) and injury [8] can alter the shape, thickness and biomechanical properties of the cornea, leading to serious changes in visual performance of the eye [5, 9-12]. For this reason, understanding the biomechanical response of the cornea to agents such as disease, surgery and injury is of great clinical importance.

In this review, the biomechanical responses of ocular tissues when subjected to pressure will be reviewed from the ocular structural perspective as well as from the ocular tissue perspective as a component in the ocular structure. The current and emerging methods to measure the ocular biomechanical properties will also be highlighted and discussed.

II. THEORY OVERVIEW

Material elasticity is a measure of how a material deforms in response to an external stress. It can be determined by

Match W. L. Ko is with the Department of Mechanical Engineering, Nazarbayev University, 53 KabanbayBatyr Ave., Astana, 010000, Kazakhstan (phone: +7-7172-709190; e-mail: matchkoust@gmail.com).

measuring the gradient of a representative portion from the constitutive stress-strain curve and a higher modulus of elasticity indicates a stiffer material [13]. The classical Young's modulus is a material property that describes the rate of change of a linear elastic material (Figure 1a). The rate of change is independent of the load on a linear elastic stress-strain curve. Literature regarding *ex vivo* study has shown that the cornea exhibits non-linear (hyperelastic) stress-strain behavior (Figure 1b) such that the corneal modulus of elasticity is not a constant but increases with increasing stress [13-16]. For nonlinear elastic material, its stress-strain curve is nonlinear and it is inappropriate to use the Young's modulus as a property descriptor of the nonlinear elastic behavior over different stresses (pressures). Tangent modulus, a measure of the instantaneous rate of change at a specific stress on the nonlinear stress-strain curve, should be used instead [17]. In addition, the cornea is known to be a viscoelastic material instead of an elastic material. Viscoelastic material is a material that exhibit both viscous and elastic characteristics under deformation and the mechanical behavior of a viscoelastic material is strain rate dependent (Figure 1c). The nonlinear viscoelastic behavior of the corneal tissue to stress requires a nonlinear structural model that can capture the stiffening induced by the stress at high strains. The above factors contribute to the wide range of variation of corneal elastic modulus reported in the literature, from 0.159 MPa [18] to 57 MPa [5], with many other studies reporting values somewhere in between [14, 16, 19-25].

The corneal stroma is composed of multiple sheets of parallel collagen fibrils, which accounts for about 90 percent of the corneal thickness. The collagen chemical composition and structure of corneal stroma are the basis for determining the corneal biomechanical properties [26-31] due to the high tensile stiffness of collagen fibrils and spatially varying distribution of lamellae in the stroma. In keratoconic corneal stroma, the collagen fibrils and interfibrillary substance loss and slippage lead to the corneal biomechanical instability and subsequently cause the alteration of corneal tomography [6, 32]. The mechanical strength of the cornea is reduced in keratoconus and the keratoconic corneas are more extensible than the normal corneas [5]. The decrease in mechanical resistance to load plays a significant role in the corneal protrusion in keratoconus.

Intraocular pressure (IOP) is the fluid pressure inside the eye. The eye is a closed system and is filled with aqueous humor and vitreous humor. The aqueous humor maintains the shape of the eyeball and nourishes the cornea and lens, and then leaves the eye through the trabecular meshwork, which is the drainage system of the eye. The delicate balance of aqueous production and absorption determines the IOP within the eye. The biomechanical behavior of the eyes has been investigated using micro-volume injection experiments [3]. The eyes are distensible at low pressure and large volumes can be

introduced into the eye with little increases in IOP. Large increases in IOP may result from small changes in volume at high IOP as the eyes are less compliant and less distensible at high IOP. The greater the elasticity of the cornea (less stiff, lower elastic modulus), the more protected the eye is from IOP surges. The greater elasticity may provide a larger buffer to sustain the fluctuation and evaluation of the IOP *in vivo*[3]. Central corneal thickness, one of the corneal geometrical factors, has been shown to play a role in the interpretation of IOP and has also been suggested as a glaucoma risk factor. Even though the cornea is far away from the primary site of glaucoma, lamina cribrosa (LC) of the sclera, the corneal biomechanics still contributed to the ocular biomechanics as a whole to protect the eye from the IOP surges.

Optic neuropathy in glaucoma causes visual field loss and blindness [33, 34]. The optic nerve damage in the lamina cribrosa (LC) of the sclera, the primary site of glaucoma, is correlated with the intraocular pressure (IOP) [35-38]. The linkage between IOP and glaucoma has been investigated using computational models [39-43]. The relation between the ocular stiffness and shear stresses in the LC was quantitatively studied[4, 44]. A 3-dimensional human eyeball model () was built in a computer-aided design (CAD) software (Solidworks 2007, DassaultSystemes Solidworks Corp.), and imported to a finite element analysis (FEA) software (ANSYS Simulation 11.0, SP1, ANSYS, Inc.) for computational simulation.

Glaucomatous vision loss starts at the periphery and progresses toward the center [45, 46]. Since the damaged nerves are shown to be sheared [35, 47], shear stresses from the computational model should be higher at the periphery and lower at the center of the LC. The local maximum shear stresses in the LC from our baseline model at 25mmHg are shown inFigure 3. The results showed that the local maximum shear stresses were highest at the peripheral anterior surface and lowest in the central anterior surface.The major simulation finding showed that nerve damage increased with tissue stiffening. The damage as a function of age is plotted inFigure 4. The plot showed the people with IOP less than 25mmHg have less than 30% damage, and normal age-stiffening in the elderly resulted only in minor vision loss.On the other hand, the plot also showed that people with inherently higher ocular tissue stiffness suffered more damage depending on IOP. This means that the elderly with age-stiffened ocular tissues are more susceptible to IOP-induced nerve damage compared to younger people[44].

Current screeningdiagnosis of glaucoma is performed by checking the IOP to estimate the glaucoma developmentpotential. Normally, clinicians use the IOP value of 21 mmHg to classify the glaucoma risk level of a patient into three levels. No risk for patient with IOP below 21 mmHg, intermediate risk for patient with IOP around 21 mmHg and high risk or patient with IOP above 21 mmHg.To identify the people at higher risk for glaucoma, methods for characterizing the *in vivo* ocular tissue stiffness should be developed. Individual adjustment on the threshold IOP (21 mmHg) based on information regarding ocular tissue biomechanical properties and age(Figure 5) may improve the accuracy of glaucoma risk assessment. This finding implies that, the clinical general screening guidance for the risk assessment of glaucoma based on the IOP is not enough. The parameter of corneal, scleral and LC elasticity should include

also in the diagnosis stage. Corneal elasticity can be clinically assessed by various commercially available medical devices (see part III - measurement method for details), while the clinical measurement of scleral and LC elasticity are currently obfuscated due to the lack of instruments. The corneal elasticity may be used as an independent parameter or to form a combined parameter with IOPfor the risk assessment of glaucoma development and progression.

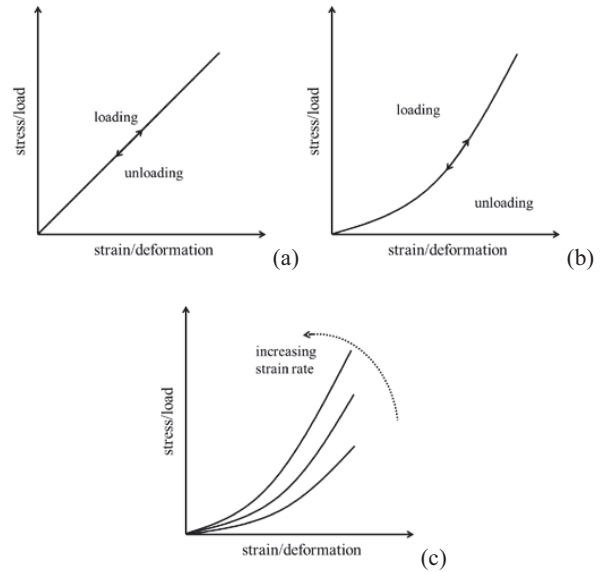


Figure 1 Schematic stress-strain behavior of (a) elastic, (b) nonlinear elastic (hyperelastic) and (c) viscoelastic material.

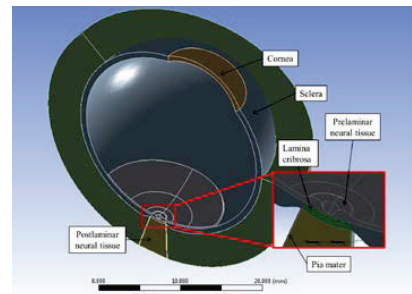


Figure 2 Three-dimensional FEM eyeball model used in this study. Adapted from [4, 44].

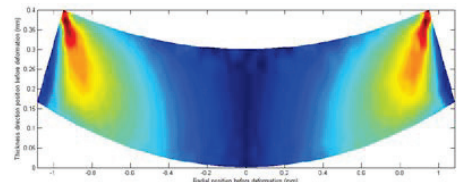


Figure 3 Effect of elevated IOP on shear stresses in the LC: Shear stress distribution in the diametrical cross-section of the LC. Adapted from [4, 44].

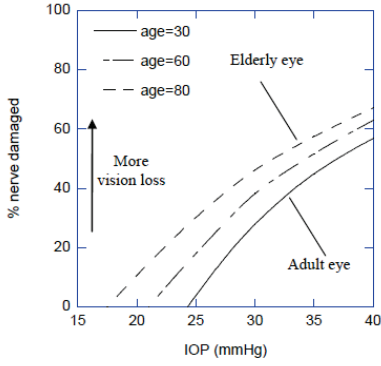


Figure 4 Effect of aging on nerve damage in normal eyes. Adapted from [44].

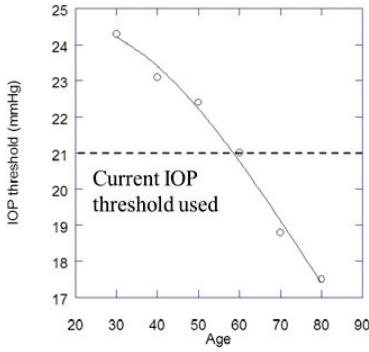


Figure 5 Effect of aging on threshold IOP.

III. MEASUREMENT METHODS

Current testing methods of the corneal biomechanical properties are basically separated into two groups, namely *ex vivo* destructive testing and *in vivo* nondestructive testing.

A. *Ex vivo* destructive testing

Ex vivo testing involves isolating the cornea *ex vivo* from the globe and testing the cornea under a controlled stress and stress/strain rate in a controlled humidity and temperature environment. The major advantage of *ex vivo* testing methods is that different loading patterns can be applied to specimen at a controllable manner. Strip extensometry test (Figure 6a) and inflation test (Figure 6b) are the most common testing methodologies used for the characterization of corneal biomechanical properties.

Strip extensometry [16, 21, 24, 29, 48-52] testing procedure is simple. A strip of corneal tissue with a constant width is dissected from the cornea and attached to grips of a strain rate-controlled uniaxial tensile machine. The specimen is subjected to uniaxial tensile loading while monitoring its behavior as a function of strip deformation. The corneal elastic modulus can then be determined from the load-deformation curve using the below equation[53],

$$E = \frac{\text{true stress}}{\text{true strain}} = \frac{T(1 + \xi/L)/A}{\ln(1 + \xi/L)}, \quad (1)$$

where E is the elastic modulus, T is the axial load, ξ is the specimen elongation, L is the initial length of the strip specimen, A is the initial cross-sectional area = $w \times t$, w is the width of the specimen and t is the thickness of the specimen. However, this tensile procedure involves several inherent deficiencies which reduce the accuracy of the results and reliability of this measuring methodology. The deficiencies come from the initially curved corneal structure and non-uniform corneal thickness. The corneal specimen is originated from the spherical corneal surface. The original length of specimen along the anterior surface is longer than that along the posterior surface. This straightening of the specimen from its curved form introduces residual stresses on the specimen. Residual tensile stresses are generated on the posterior side of the specimen and residual compressive stresses are generated on the anterior side of the specimen. The residual stresses on the specimen eventually lead to reduce tensile stress on the anterior side and increase the tensile stress on the posterior side, and lead to uneven stress distribution along the thickness direction of the specimen and affect the mechanical behavior under tensile loading. Moreover, the corneal thickness is not uniform, but is thinnest at the center, increase away from the center and thickest at the boundary. The assumption in the strip extensometry of constant uniform thickness leads to errors in constitutive stress-strain behavior derivation. The above deficiencies contribute to the perception that the strip extensometry test is a less reliable testing methodology to determine the corneal biomechanical properties [17].

Pressure inflation test [14, 15, 18, 52, 54-59] subjects the cornea to stimulation of the physiological condition of IOP surges. An intact cornea and a narrow ring of the connected surrounding scleral tissue are extracted from the eye to serve as specimen. The specimen is mounted onto a test rig that enables watertight edge fixity through clamping of the surrounding scleral tissue. The specimen is then subjected to gradual increase of the internal pressure (IOP) while monitoring the corneal apex deformation. The relationship between pressure and apex displacement data is recorded, and the corneal elastic modulus can be determined from the data curve based on a shell mathematical analysis [57].

$$E = \frac{IOP \cdot R_m^2}{2\delta t} (1 - \nu) \left[1 - e^{-\beta\eta} \cos(\beta\eta) \right], \quad (2)$$

where E is the elastic modulus, R_m is the radius of corneal median surface, t is the average thickness, ν is the Poisson's ratio, β is half the central angle of curvature = $\sin^{-1}(R_i/R_{ant})$, R_i is the radius of corneo-scleral intersection, R_{ant} is the radius of the corneal anterior surface and $\beta = \sqrt{R_m/t} \cdot \sqrt[4]{3(1-\nu^2)}$. The cornea in inflation test keeps intact and its original shape, and subjects to uniform intraocular pressure. Therefore, the inflation test is better than strip extensometry in term of eliminating the drawback of cutting the cornea into pieces and straightening the curved specimen for measurement. However, the mathematical analysis assumptions in inflation test would be its major source of error. The assumptions, including the spherical corneal topography and material homogeneity, introduce error to the analysis, and make the analysis less

reliable. In addition, the clamping of the corneal specimen onto test rig introduces another source of error. The boundary clamping condition of inflation test in the mathematic model may different from the natural bonding condition of the corneo-scleral interconnection and would introduce extra deformation.

Both strip extensimetry and inflation test are easy and convenience to use for characterization of corneal biomechanical properties with controlled stress and stress rate in a controlled humidity and temperature environment, however, the major and intrinsic problem of the two tests is that, they are both destructive to the eye and are not suitable for use in *in vivo* human testing. In addition, the experimental results on the isolated cornea are also hard to control due to the significant effects of corneal hydration [5, 52].

B. *In vivo* nondestructive testing

There has been an increasing emphasis on the development of methods for *in vivo* nondestructive testing of corneal biomechanical properties. Several potential *in vivo* measurements are subsequently developed, including the mechanical corneal indentation device[60, 61], surface wave elastometry [62-64], Ocular Response Analyzer (ORA) [65] and Corneal Visualization with Scheimpflug Technology (Corvis ST) [66].

The classical way to determinate the hardness of an object is to use a finger to touch the object, to feel the resistance of the object and estimate its hardness and elasticity. The indentation technique is a technique that uses the same idea but in a more precise and sophisticated way. Mechanical corneal indentation method is adapted from the classical indentation (Figure 7a). It uses a cylindrical flat-end indenter to indent the cornea while monitoring the corneal resistive load during the indentation at a specific indentation rate. The corneal resistive load during indentation is recorded simultaneously as a function of displacement (Figure 7b) and the corneal tangent modulus can be determined from the data curve using the below equation [61],

$$E|_{IOP} = \frac{a(R-t/2)\sqrt{1-\nu^2}}{t^2} \left. \frac{dF}{d\delta} \right|_{IOP}, \quad (3)$$

where $E|_{IOP}$ is the tangent modulus under IOP, F is the corneal indentation load, δ is the corneal displacement, R is the corneal radius of curvature, t is the central corneal thickness, ν is the Poisson's ratio and $dF/d\delta|_{IOP}$ is the corneal indentation stiffness which can be extracted from the load-deformation curve. The corneal tangent modulus is found to be rate-dependent (viscoelastic behavior) and IOP-dependent (hyperelastic behavior). A rate-independent corneal tangent modulus can be determined with an indentation rate beyond the threshold indentation rate in order to eliminate the viscous behavior. A linear proportional relationship is found between the corneal tangent modulus and the corneal in-plane tensile stress (\hat{A}) calculated by using Laplace' Law ($\hat{A}=R \cdot IOP/2t$). This implies that the corneal tangent modulus is not only a representation of corneal material property, but may also be used as an indicator of the corneal stress level. The mechanical corneal indentation method is a fast and convenient testing method. The most important point for its common use is that, it is non-destructive and does not damage the object indented. The device is tested in porcine eyes *ex vivo* and rabbit eyes *in vivo* and clinical trial on human eyes is currently undergoing.

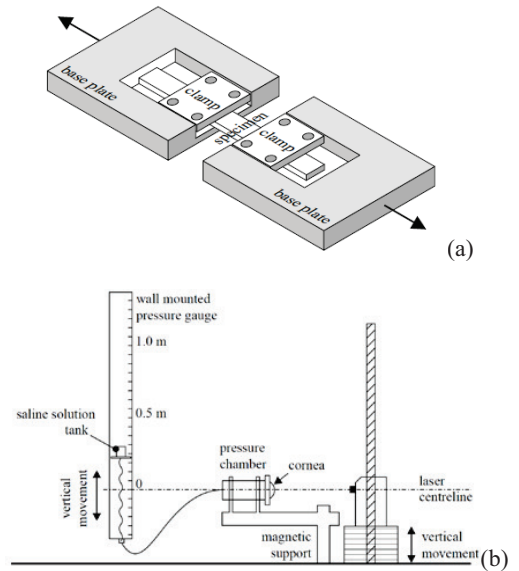


Figure 6 Schematic setup of (a) strip extensimetry and (b) inflation test. Adapted from [52]

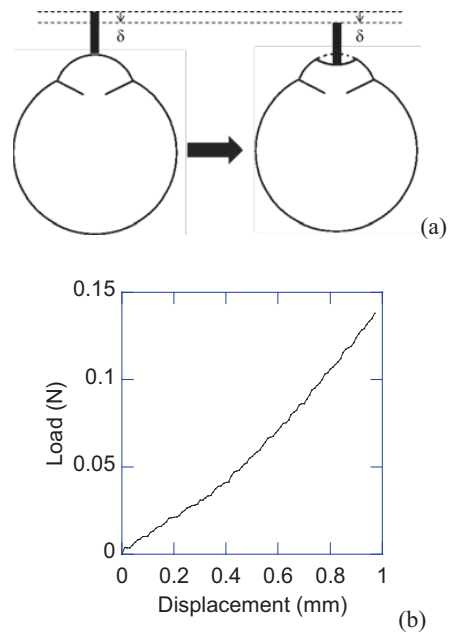


Figure 7 Schematic setup of (a) mechanical corneal indentation and (b) typical corneal indentation load versus corneal displacement curve.

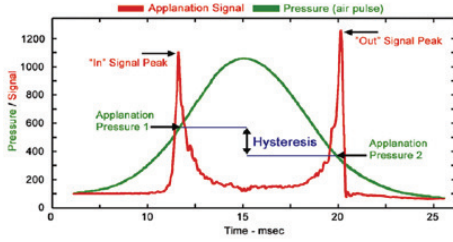


Figure 8 Applanation and pressure plots as determined by the ORA (Ocular Response Analyzer, Reichert, Depew, New York). Adapted from [65].

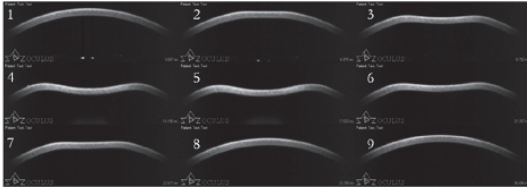


Figure 9 The deformation process observed by Corvis ST. Adapted from [66].

Surface wave elastometry is used for the assessment of corneal biomechanical properties [62-64]. The linear elastic approximated relationship between shear wave propagation speed and Young's modulus has been used to determine corneal mechanical properties *in vivo* [62],

$$E = 3\rho c_s^2 \quad (4)$$

where ρ is the volumetric mass density of the corneal plate and c_s is shear wave propagation speed. This technique has been tested in *ex vivo* tissue specimen; however, clinical applications have not been proved. Moreover, this method adopts the linear elastic model for the approximation of nonlinear viscoelastic corneal biomechanical properties and the indirect measurement of the corneal response to external load, this may lead to inaccurate determination of corneal mechanical properties. Eye immersion is also required for ultrasound technique which adds inconvenience of clinical implementation.

Ocular Response Analyzer (ORA, Reichert, Depew, New York) [65] is the first instrument that allows the evaluation of corneal biomechanical properties *in vivo*. It uses an air-puff to deform the cornea at high speed. Through the monitoring of the corneal deformation under the high speed air-puff, the difference in air pressure between inward and outward directions at the point of corneal flattening is reported as corneal hysteresis (CH) as shown in Figure 8 [65]. The device does not report the classical mechanics term of corneal elastic properties, but instead, it reports the value of corneal hysteresis. The CH may be produced with different combinations of elastic modulus and the viscous damping parameters [10]. Recent research has shown that a lower-than-average CH is observed in subjects who have been identified as "Normal Tension Glaucoma" (NTG) patients and CH is also associated with glaucomatous visual field progression. Currently, individuals who have NTG may be missed during routine IOP screening. If the CH proves to be a reliable indicator of this condition, the CH can be used as a new

assessment indicator for glaucoma screening and is definitely a significant advance in glaucoma research [11, 67-72]. Although corneal hysteresis is not the common classical mechanics term to describe corneal material properties, the early results suggest that the corneal biomechanical properties hold a considerable promise as IOP independent predictive variables for risk assessment of glaucoma development and progression [72].

Corneal Visualization Scheimpflug Technology (Corvis ST; Oculus, Wetzlar, Germany) [66, 73] is a clinical device based on a noncontact air puff tonometer combined with an ultrahigh speed Scheimpflug camera for the measurement of the corneal biomechanical properties since 2011. Corvis ST captures the corneal dynamic deformation under a standardized air puff excitation with the aid of the Scheimpflug camera at a rate of 4330 image frames per second (Figure 9). With the image analysis, several corneal biomechanical related parameters can be extracted, including, maximum corneal deformation amplitude, time of the highest concavity, lengths and times of the flattened cornea in the first and second applanation, and the corneal velocities during the first and second applanation moment. The corneal deformation amplitude during the air-puff indentation holds promise to yield relevant parameters related to corneal biomechanical properties, but none of the current parameters from Corvis ST can be deemed directly as corneal biomechanical properties [74]. Clinical results show that the deformation amplitude is highly sensitive in differentiating keratoconus from normal corneas [75]. The device is still under development and many new parameters are being introduced and investigated to the outputs [73, 76]. The corneal dynamic deformation video recorded by the Corvis ST provides useful information for the study of corneal biomechanics. Further research is needed to develop forward clinical applications based on these new corneal biomechanical parameters.

IV. CONCLUSIONS

Ocular biomechanics is a rapidly growing area of research and clinical interest. Ocular biomechanical properties play a central role in the pathology of glaucoma. Disease, surgery and injury can lead to serious changes in the visual performance of the eye, with the ever increasing improvement of measurement methods, a better understanding of the ocular biomechanics and biomechanical properties to the influence of disease, surgery and injury can be achieved.

The ability to measure a patient's ocular biomechanical properties *in vivo* may provide a clinical tool to assist clinicians to preform disease diagnosis and decision making regarding screening of eye disease and treatment methods. It is anticipated that, with the individual ocular biomechanical properties, it will help the clinicians to arrest those patients in high risk of glaucoma development and progression.

REFERENCES

- [1] B. Cassin, S. Solomon, and M. L. Rubin, *Dictionary of eye terminology*: Wiley Online Library, 1990.
- [2] E. B. Goldstein, *Sensation and perception*: Wadsworth Pub Co, 2009.
- [3] C. Johnson, S. Mian, S. Moroi, D. Epstein, J. Izatt, and N. Afshari, "Role of corneal elasticity in damping of intraocular pressure,"

- Investigative ophthalmology & visual science*, vol. 48, pp. 2540-2544, 2007.
- [4] M. W. L. Ko, "Effect of corneal, scleral and lamina cribrosa elasticity, and intraocular pressure on optic nerve damages," *JSM Ophthalmology*, vol. 3, p. 1024, 2015.
- [5] T. T. Andreassen, A. Hjorth Simonsen, and H. Oxlund, "Biomechanical properties of keratoconus and normal corneas," *Experimental eye research*, vol. 31, pp. 435-441, 1980.
- [6] K. M. Meek, S. J. Tuft, Y. Huang, P. S. Gill, S. Hayes, R. H. Newton, *et al.*, "Changes in collagen orientation and distribution in keratoconus corneas," *Investigative ophthalmology & visual science*, vol. 46, pp. 1948-1956, 2005.
- [7] D. Ortiz, D. Piñero, M. H. Shabayek, F. Amalich-Montiel, and J. L. Alió, "Corneal biomechanical properties in normal, post-laser in situ keratomileusis, and keratoconic eyes," *Journal of Cataract & Refractive Surgery*, vol. 33, pp. 1371-1375, 2007.
- [8] W. J. Dupps and S. E. Wilson, "Biomechanics and wound healing in the cornea," *Experimental eye research*, vol. 83, pp. 709-720, 2006.
- [9] F. S. Brightbill and M. Sakhalkar, "Corneal Disorders: Clinical Diagnosis and Management," *Archives of ophthalmology*, vol. 118, p. 303, 2000.
- [10] D. H. Glass, C. J. Roberts, A. S. Litsky, and P. A. Weber, "A viscoelastic biomechanical model of the cornea describing the effect of viscosity and elasticity on hysteresis," *Investigative ophthalmology & visual science*, vol. 49, pp. 3919-3926, 2008.
- [11] N. G. Congdon, A. T. Broman, K. Bandeen-Roche, D. Grover, and H. A. Quigley, "Central corneal thickness and corneal hysteresis associated with glaucoma damage," *American journal of ophthalmology*, vol. 141, pp. 868-875, 2006.
- [12] J. C. Downs, J. K. F. Suh, K. A. Thomas, A. J. Bellezza, R. T. Hart, and C. F. Burgoyne, "Viscoelastic material properties of the peripapillary sclera in normal and early-glaucoma monkey eyes," *Investigative ophthalmology & visual science*, vol. 46, pp. 540-546, 2005.
- [13] Y. Fung, *Biomechanics: mechanical properties of living tissues*: Springer, 1993.
- [14] S. Woo, A. Kobayashi, W. Schlegel, and C. Lawrence, "Nonlinear material properties of intact cornea and sclera," *Experimental eye research*, vol. 14, pp. 29-39, 1972.
- [15] A. Elsheikh, D. Alhasso, and P. Rama, "Biomechanical properties of human and porcine corneas," *Experimental Eye Research*, vol. 86, pp. 783-790, 2008.
- [16] D. A. Hoeltzel, P. Altman, K. Buzard, and K. Choe, "Strip extensimetry for comparison of the mechanical response of bovine, rabbit, and human corneas," *Journal of biomechanical engineering*, vol. 114, pp. 202-215, 1992.
- [17] K. Buzard, "Introduction to biomechanics of the cornea," *Refractive & corneal surgery*, vol. 8, pp. 127-138, 1992.
- [18] A. Elsheikh, D. Wang, M. Brown, P. Rama, M. Campanelli, and D. Pye, "Assessment of corneal biomechanical properties and their variation with age," *Current eye research*, vol. 32, pp. 11-19, 2007.
- [19] I. S. Nash, P. R. Greene, and C. S. Foster, "Comparison of mechanical properties of keratoconus and normal corneas," *Experimental eye research*, vol. 35, pp. 413-424, 1982.
- [20] G. P. Djotyran, R. M. Kurtz, D. C. Fernández, and T. Juhasz, "An analytically solvable model for biomechanical response of the cornea to refractive surgery," *Journal of biomechanical engineering*, vol. 123, p. 440, 2001.
- [21] J. Ø. Hjortdal, "Regional elastic performance of the human cornea," *Journal of biomechanics*, vol. 29, pp. 931-942, 1996.
- [22] G. J. Orsengo and D. C. Pye, "Determination of the true intraocular pressure and modulus of elasticity of the human cornea in vivo," *Bulletin of mathematical biology*, vol. 61, pp. 551-572, 1999.
- [23] T. Seiler, M. Matallana, S. Sendler, and T. Bende, "Does Bowman's layer determine the biomechanical properties of the cornea?," *Refractive & corneal surgery*, vol. 8, p. 139, 1992.
- [24] G. Wollensak, E. Spoerl, and T. Seiler, "Stress-strain measurements of human and porcine corneas after riboflavin-ultraviolet-A-induced cross-linking," *Journal of Cataract & Refractive Surgery*, vol. 29, pp. 1780-1785, 2003.
- [25] Y. Zeng, J. Yang, K. Huang, Z. Lee, and X. Lee, "A comparison of biomechanical properties between human and porcine cornea," *Journal of biomechanics*, vol. 34, pp. 533-537, 2001.
- [26] A. Kobayashi, L. Staberg, and W. Schlegel, "Viscoelastic properties of human cornea," *Experimental Mechanics*, vol. 13, pp. 497-503, 1973.
- [27] C. Boote, S. Dennis, Y. Huang, A. Quantock, and K. Meek, "Lamellar orientation in human cornea in relation to mechanical properties," *Journal of structural biology*, vol. 149, pp. 1-6, 2005.
- [28] S. Hayes, C. Boote, J. Lewis, J. Sheppard, M. Abahussin, A. J. Quantock, *et al.*, "Comparative study of fibrillar collagen arrangement in the corneas of primates and other mammals," *The Anatomical Record: Advances in Integrative Anatomy and Evolutionary Biology*, vol. 290, pp. 1542-1550, 2007.
- [29] T. R. Friberg and J. W. Lace, "A comparison of the elastic properties of human choroid and sclera," *Experimental eye research*, vol. 47, pp. 429-436, 1988.
- [30] M. Winkler, D. Chai, S. Kriling, C. J. Nien, D. J. Brown, B. Jester, *et al.*, "Nonlinear optical macroscopic assessment of 3-D corneal collagen organization and axial biomechanics," *Investigative ophthalmology & visual science*, vol. 52, pp. 8818-8827, 2011.
- [31] D. W. DelMonte and T. Kim, "Anatomy and physiology of the cornea," *Journal of Cataract & Refractive Surgery*, vol. 37, pp. 588-598, 2011.
- [32] A. Gefen, R. Shalom, D. Elad, and Y. Mandel, "Biomechanical analysis of the keratoconic cornea," *Journal of the mechanical behavior of biomedical materials*, vol. 2, pp. 224-236, 2009.
- [33] R. N. Weinreb, S. Shakiba, P. A. Sample, S. Shahrokhni, S. Van Horn, V. S. Garden, *et al.*, "Association between quantitative nerve fiber layer measurement and visual field loss in glaucoma," *American journal of ophthalmology*, vol. 120, pp. 732-738, 1995.
- [34] J. Katz, D. Gilbert, H. A. Quigley, and A. Sommer, "Estimating progression of visual field loss in glaucoma," *Ophthalmology*, vol. 104, pp. 1017-1025, 1997.
- [35] D. B. Yan, F. M. Coloma, A. Metheetairut, G. E. Trope, J. G. Heathcote, and C. R. Ethier, "Deformation of the lamina cribrosa by elevated intraocular pressure," *British Journal of Ophthalmology*, vol. 78, pp. 643-648, 1994.
- [36] A. Azuara-Blanco, V. P. Costa, and R. P. Wilson, *Handbook of glaucoma*: Informa HealthCare, 2002.
- [37] D. R. Anderson and A. Hendrickson, "Effect of intraocular pressure on rapid axoplasmic transport in monkey optic nerve," *Investigative ophthalmology & visual science*, vol. 13, pp. 771-783, 1974.
- [38] H. A. Quigley and E. M. Addicks, "Regional differences in the structure of the lamina cribrosa and their relation to glaucomatous optic nerve damage," *Archives of ophthalmology*, vol. 99, p. 137, 1981.
- [39] I. A. Sigal, J. G. Flanagan, and C. R. Ethier, "Factors influencing optic nerve head biomechanics," *Investigative ophthalmology & visual science*, vol. 46, pp. 4189-4199, 2005.
- [40] I. A. Sigal, J. G. Flanagan, I. Tertinegg, and C. R. Ethier, "Finite element modeling of optic nerve head biomechanics," *Investigative ophthalmology & visual science*, vol. 45, pp. 4378-4387, 2004.
- [41] I. A. Sigal, J. G. Flanagan, I. Tertinegg, and C. R. Ethier, "Modeling individual-specific human optic nerve head biomechanics. Part I: IOP-induced deformations and influence of geometry," *Biomechanics and modeling in mechanobiology*, vol. 8, pp. 85-98, 2009.
- [42] I. A. Sigal, J. G. Flanagan, I. Tertinegg, and C. R. Ethier, "Modeling individual-specific human optic nerve head biomechanics. Part II: influence of material properties," *Biomechanics and modeling in mechanobiology*, vol. 8, pp. 99-109, 2009.
- [43] C. F. Burgoyne, J. C. Downs, A. J. Bellezza, J.-K. F. Suh, and R. T. Hart, "The optic nerve head as a biomechanical structure: a new paradigm for understanding the role of IOP-related stress and strain in the pathophysiology of glaucomatous optic nerve head damage," *Progress in retinal and eye research*, vol. 24, pp. 39-73, 2005.
- [44] L. K. K. Leung, M. W. L. Ko, and D. C. C. Lam, "Effect of Age-Stiffening Tissues and Intraocular Pressure on Optic Nerve Damages," *MCB: Molecular & Cellular Biomechanics*, vol. 9, pp. 157-174, 2012.
- [45] R. R. Allingham, M. B. Shields, K. F. Damji, S. Freedman, S. E. Moroi, and G. Shafranov, *Shields' textbook of glaucoma*: Lippincott Williams & Wilkins, 2005.

- [46] S. M. Drance, "The glaucomatous visual field," *British Medical Journal*, vol. 56, pp. 186-200, 1972.
- [47] M. E. Edwards, S. S. W. Steven, and T. A. Good, "Role of viscoelastic properties of differentiated SH-SY5Y human neuroblastoma cells in cyclic shear stress injury," *Biotechnology progress*, vol. 17, pp. 760-767, 2008.
- [48] B. Boyce, R. Jones, T. Nguyen, and J. Grazier, "Stress-controlled viscoelastic tensile response of bovine cornea," *Journal of biomechanics*, vol. 40, pp. 2367-2376, 2007.
- [49] M. R. Bryant and P. J. McDonnell, "Constitutive laws for biomechanical modeling of refractive surgery," *Journal of biomechanical engineering*, vol. 118, pp. 473-481, 1996.
- [50] B. Jue and D. M. Maurice, "The mechanical properties of the rabbit and human cornea," *Journal of biomechanics*, vol. 19, pp. 847-853, 1986.
- [51] T. J. Shin, R. P. Vito, L. W. Johnson, and B. E. McCarey, "The distribution of strain in the human cornea," *Journal of biomechanics*, vol. 30, pp. 497-503, 1997.
- [52] A. Elsheikh and K. Anderson, "Comparative study of corneal strip extensometry and inflation tests," *Journal of The Royal Society Interface*, vol. 2, pp. 177-185, 2005.
- [53] R. L. Norton, *Machine design: an integrated approach* vol. 3: Pearson Prentice Hall New Jersey, 2006.
- [54] B. L. Boyce, J. M. Grazier, R. E. Jones, and T. D. Nguyen, "Full-field deformation of bovine cornea under constrained inflation conditions," *Biomaterials*, vol. 29, pp. 3896-3904, 2008.
- [55] J. B. Randleman, D. G. Dawson, H. E. Grossniklaus, B. E. McCarey, and H. F. Edelhauser, "Depth-dependent cohesive tensile strength in human donor corneas: implications for refractive surgery," *Journal of refractive surgery (Thorofare, NJ: 1995)*, vol. 24, pp. S85-9, 2008.
- [56] M. K. Smolek, "Interlamellar cohesive strength in the vertical meridian of human eye bank corneas," *Investigative ophthalmology & visual science*, vol. 34, pp. 2962-2969, 1993.
- [57] K. Anderson, A. Elsheikh, and T. Newson, "Application of structural analysis to the mechanical behaviour of the cornea," *Journal of The Royal Society Interface*, vol. 1, pp. 3-15, 2004.
- [58] B. K. Pierscionek, M. Asejczyk-Widlicka, and R. A. Schachar, "The effect of changing intraocular pressure on the corneal and scleral curvatures in the fresh porcine eye," *British Medical Journal*, vol. 91, pp. 801-803, 2007.
- [59] J. A. Bisplinghoff, C. McNally, S. J. Manoogian, and S. M. Duma, "Dynamic material properties of the human sclera," *Journal of biomechanics*, vol. 42, pp. 1493-1497, 2009.
- [60] M. W. L. Ko, L. K. K. Leung, and D. C. C. Lam, "Comparative study of corneal tangent elastic modulus measurement using corneal indentation device," *Medical engineering & physics*, vol. 36, pp. 1115-1121, 2014.
- [61] M. W. L. Ko, L. K. K. Leung, D. C. C. Lam, and C. K. S. Leung, "Characterization of corneal tangent modulus in vivo," *Acta Ophthalmologica*, vol. 91, pp. e263-e269, 2013.
- [62] M. Tanter, D. Touboul, J. L. Gennisson, J. Bercoff, and M. Fink, "High-resolution quantitative imaging of cornea elasticity using supersonic shear imaging," *Medical Imaging, IEEE Transactions on*, vol. 28, pp. 1881-1893, 2009.
- [63] J. Liu, X. He, X. Pan, and C. J. Roberts, "Ultrasonic model and system for measurement of corneal biomechanical properties and validation on phantoms," *Journal of biomechanics*, vol. 40, pp. 1177-1182, 2007.
- [64] W. J. Dupps Jr, M. V. Netto, S. Herekar, and R. R. Krueger, "Surface wave elastometry of the cornea in porcine and human donor eyes," *Journal of refractive surgery (Thorofare, NJ: 1995)*, vol. 23, p. 66, 2007.
- [65] D. A. Luce, "Determining in vivo biomechanical properties of the cornea with an ocular response analyzer," *Journal of Cataract & Refractive Surgery*, vol. 31, pp. 156-162, 2005.
- [66] R. Ambrósio Jr, D. L. Caldas, I. C. Ramos, R. Santos, and M. Belin, "Corneal Biomechanical Assessment Using Dynamic Ultra High-Speed Scheimpflug Technology Non-contact Tonometry (UHS-ST NCT): Preliminary Results," in *American Society of Cataract and Refractive Surgery-American Society of Ophthalmic Administrators (ASCRS-ASOA) Symposium and Congress. San Diego, CA*, 2011.
- [67] A. P. Wells, D. F. Garway-Heath, A. Poostchi, T. Wong, K. C. Y. Chan, and N. Sachdev, "Corneal hysteresis but not corneal thickness correlates with optic nerve surface compliance in glaucoma patients," *Investigative ophthalmology & visual science*, vol. 49, pp. 3262-3268, 2008.
- [68] F. Bochmann, G. S. Ang, and A. Azuara-Blanco, "Lower corneal hysteresis in glaucoma patients with acquired pit of the optic nerve (APON)," *Graefe's Archive for Clinical and Experimental Ophthalmology*, vol. 246, pp. 735-738, 2008.
- [69] D. Touboul, C. Roberts, J. Kérautret, C. Garra, S. Maurice-Tison, E. Saubusse, et al., "Correlations between corneal hysteresis, intraocular pressure, and corneal central pachymetry," *Journal of Cataract & Refractive Surgery*, vol. 34, pp. 616-622, 2008.
- [70] A. T. Broman, N. G. Congdon, K. Bandeen-Roche, and H. A. Quigley, "Influence of corneal structure, corneal responsiveness, and other ocular parameters on tonometric measurement of intraocular pressure," *Journal of glaucoma*, vol. 16, pp. 581-588, 2007.
- [71] C. Kirwan, M. O'keefe, and B. Lanigan, "Corneal hysteresis and intraocular pressure measurement in children using the Reichert ocular response analyzer," *American journal of ophthalmology*, vol. 142, pp. 990-992, 2006.
- [72] M. Sullivan-Mee, "The role of ocular biomechanics in glaucoma management," *Rev. Optometry*, vol. 15, pp. 49-54, 2008.
- [73] L. Tian, M. W. L. Ko, L. K. Wang, J. Y. Zhang, T. J. Li, Y. F. Huang, et al., "Assessment of ocular biomechanics using dynamic ultra high-speed scheimpflug imaging in keratoconic and normal eyes," *Journal of refractive surgery (Thorofare, NJ: 1995)*, vol. 30, pp. 785-791, 2014.
- [74] W. Lau and D. Pye, "Changes in corneal biomechanics and applanation tonometry with induced corneal swelling," *Investigative ophthalmology & visual science*, vol. 52, pp. 3207-3214, 2011.
- [75] L. Tian, Y.-F. Huang, L.-Q. Wang, H. Bai, Q. Wang, J.-J. Jiang, et al., "Corneal Biomechanical Assessment Using Corneal Visualization Scheimpflug Technology in Keratoconic and Normal Eyes," *Journal of Ophthalmology*, vol. 2014, p. 8, 2014.
- [76] S. Kling and S. Marcos, "Contributing factors to corneal deformation in air puff measurements," *Investigative ophthalmology & visual science*, vol. 54, pp. 5078-5085, 2013.



Match Wai Lun Ko received his B.Eng. and Ph.D. degree in Mechanical Engineering from The Hong Kong University of Science and Technology, Hong Kong, in 2009 and 2013, respectively.

From 2013 to 2014, he was a post-doctoral fellow at the Interdisciplinary Division of Biomedical Engineering, The Hong Kong Polytechnic University, Hong Kong. In 2014, he joined Nazarbayev University, Astana, Kazakhstan, and is currently an Assistant Professor in the Department of Mechanical Engineering. His research interests include biomechanics and biomaterial mechanical properties characterization using experimental testing and computational simulation, design and fabrication of related medical device to assist the clinicians to perform disease diagnosis and decision making regarding screening of disease and treatment management.

Vehicle detecting, tracking and counting for traffic control systems

Kamilla Aliakhmet¹, Temirlan Zharkynbek²

School of Engineering
Nazarbayev University
Astana, Kazakhstan

¹ kamilla.aliakhmet@nu.edu.kz, ² temirlan.zharkynbek@nu.edu.kz

Abstract — Vision based traffic control systems has been widely investigated to solve the problem of traffic congestion. They are mainly based on the vehicle flow estimation, which represents the current state of the traffic in particular region, and promote more advantages over traditional intrusive methods. Detecting and tracking of vehicles are critical steps for the traffic surveillance. This project aims to develop an effective algorithm to perform vehicle detection, tracking and counting using OpenCV libraries and available video databases. First frames are used to extract the foreground objects, and the resulting binary images go through morphological transformations to eliminate noises. Blob detection and contouring processes are performed simultaneously. The conditional statement we apply ensures that the vehicle is tracked only if the detected blobs and contours match. Counting is performed by comparing the coordinates of contour center with established reference lines.

Keywords—background subtraction; blob detection; contouring; vehicle counting

I. INTRODUCTION

In recent years, the importance of traffic data collection has been broadly discussed worldwide because of increasing demand on effective traffic management systems. Existing techniques provide an opportunity to gather information about average traffic speed, volume of the traffic in specified time, vehicle presence and occupancy rate, etc [1]. Traffic data collection methods involve intrusive technologies consisting of on-road data recorders and sensors such as magnetic loops, pneumatic road tubes, and piezoelectric sensors, as well as non-intrusive technologies, which are aimed to obtain data from remote distance [1]. The latter includes usage vision-based systems focusing on detection and tracking of vehicles in order to observe traffic performance on the road. CCD or CMOS video cameras are usually mounted on the pole of traffic lights or separately, and the movement of vehicles on the road is recorded for further processing. Most studies highlight the advantages of such type of systems over traditional methods, as their low cost and broader coverage of traffic parameters (vehicle count and classification, speed/acceleration estimations, parking areas, etc.) promote higher flexibility in designing traffic control applications [1], [2].

Detecting and tracking objects that are moving has raised much of interest in research area over the past years.

Literature review has revealed several methods of vehicle detection, including HAAR classifier that is originally based on Haar-like features proposed for face detection. The procedure is performed by considering an object as successful combination of simple feature classifiers in a cascade manner [3]. The work by Oliveira and Santos implements cascades for car detection particularly, though the results demonstrated false detections owing to the fact that the method is mainly applicable for vehicles at fast rates [4]. Blob detection is another common technique to detect and track the vehicle as soon as it appears on the video frame. It mainly considers a group of pixels in an image that are connected by the shared property (e.g. grayscale), and aims to find such regions and mark them. However, as blob detection requires binary input, background subtraction is used to segment foreground objects from background image [5]. Similarly, object contour recognition is widely applied to present the contour fragments and to detect the objects from the obtained binary images. It is worth mentioning that the blob detection and contouring techniques are separately implemented in image processing to detect moving objects, though there might be few studies focusing on combining those two techniques.

In this paper, we aim to introduce a system for more precise detection, tracking and counting of moving vehicles. Specifically, we will focus on obtaining binary images with noises removed, and then applying them to both blob detection and contouring procedures. It was tentatively estimated that the accuracy of detection can be increased by implementing contouring method in parallel to the blob detection. Selection of control parameters is also an essential part in our proposed program, as it will affect the whole performance of the system. If the system will operate properly within the given conditions, it is planned to test the program in the dark environment.

II. SYSTEM REVIEW

Our proposed system operates by detecting vehicle entering and leaving the scene. The input material is taken from traffic existing video databases. Working algorithm is presented in Fig. 1. Firstly, background image is initialized considering items such as roads, buildings, and trees, and then foreground objects are segmented from the background by adapting possible changes on the screen (moving

vehicle). The resultant binary image is calibrated to remove any noises, and then white regions of pixels are grouped together to detect blobs. In the video simulation window, detected blobs can be seen as green circles. Simultaneously, the contouring of the vehicle is performed, and the bounding rectangle with its corresponding center is computed. They are presented as blue dots inside red rectangles. Next step involves matching the blobs with the contours of the vehicle. If they are both detected, the program will count the cases when such vehicles pass through established reference line.

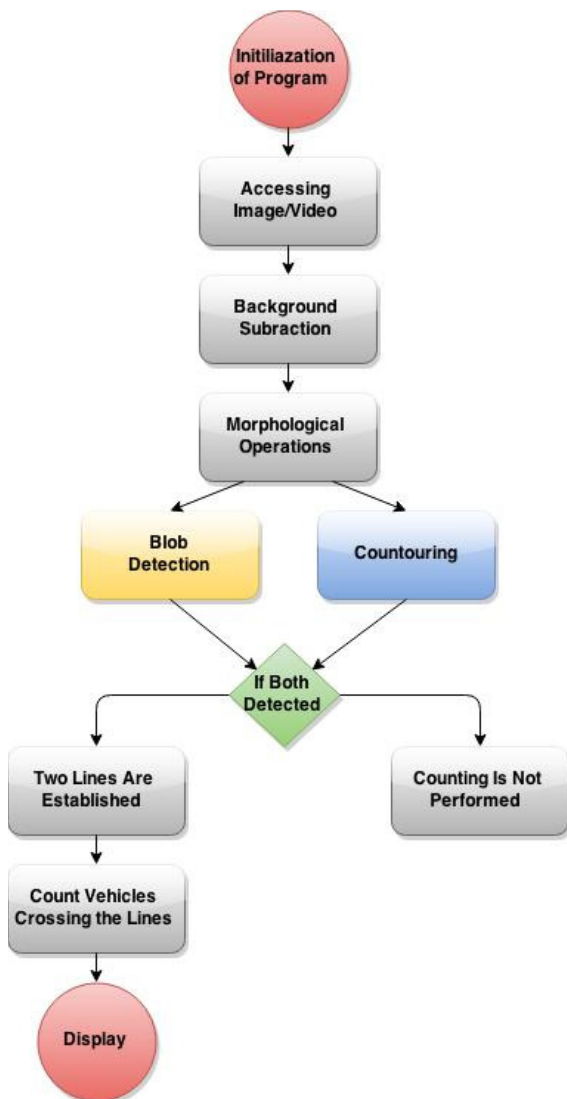


Figure 1. Working algorithm

A. Background Substraction

Background subtraction is a widely used technique to detect moving objects from stationary video cameras. It is based on differentiating current frame and background model (initially established with no moving objects), and constantly updating background model in response to changes in intensity of light and geometrical settings [6]. There are several approaches that have been discussed in existing literature, but our system considers Mixture of Gaussians. In the review of reports, it is concluded that this method has a higher level of accuracy as compared to other estimations [6]. Background segmentation *MOG2* algorithm based on Mixture of Gaussians as a part of built-in OpenCV libraries is implemented in our source code.

```
Ptr< BackgroundSubtractor> pMOG2
pMOG2=createBackgroundSubtractorMOG2()
```

The resulting binary images then undergo morphological transformations in order to eliminate noises.

B. Morphological operations

Morphological operations introduce a structuring element of specified shape that is scanned over the input image, resulting in the output image of the same size. For each pixel location, its corresponding neighbors are considered to compute maximum or minimum pixel values overlapped by the structuring element [7]. The basic morphological operations such as dilation and erosion, or combinations of them are widely used in OpenCV to remove noise, to separate individual elements and/or to combine distinct elements of the image [8]. Use of morphological transformations in our program can be explained by the following code.

```
Mat ellipse_el= getStructuringElement(MORPH_ELLIPSE,
Size(12,12), Point(3,3));
morphologyEx(fgMaskMOG2, binaryImg, MORPH_CLOSE, element);

dilate( binaryImg, destImg,
getStructuringElement(MORPH_ELLIPSE, Size(14,14)));

erode(binaryImg, destImg, getStructuringElement(MORPH_ELLIPSE,
Size(14, 14)));
```

The function *morphologyEx* applies closing operation to the binary image obtained from the background subtraction operation. Closing operation involves dilation first, resulting in a convolution of input image with the structuring element, and then followed by erosion that is equivalent to eliminating the boundaries of regions of foreground pixels. The main goal of using closing operation is to exclude isolated regions that are lower than their neighbors.

C. Blob Detection

After obtaining binary image with differentiated foreground objects, and removing any noises, it is possible to proceed to their detection. To do so, first technique that we applied is blob detection. The key idea is to connect the

regions, otherwise called “blobs”, in the image, where a group of connected pixels share the same properties. Such properties can be controlled depending on the shape and size of the detection object. Our program employs *SimpleBlobDetector* algorithm with the specified control parameters, as it was necessary to adjust them, so that the readings will be obtained based on the vehicles’ blobs. Specifically, the program is initiated to detect white regions (255 in a grayscale) in several binary images that were obtained by thresholding source image from a minimum threshold of **10** till the maximum of **200** with a default increment threshold value. We restrict the blob *area* till **800**, as this value revealed the most accurate detection during the experiments. The *shape* of the blobs is considered to be more elliptical, and this yields shape control parameters of **0.1**, **0.87** and **0.01**, where the values indicate that the blob is less close to a circle, more exposed to convexity as opposed to concavity and more elongated towards the ends. The blobs are detected from the input frame depending on the control parameters, and then stored in a vector form. They are drawn as green circles with the size of the circle corresponding to the size of the blobs. The pointer vector is later used in the counting step of the program.

D. Contouring

The next method we covered is contouring technique. Contours are represented by the list of points that constitute a curve in an image. In OpenCV, the location of every point on the curve can be found from the data in the previous entry [8]. The function *FindContours* () is used to compute the contours of binary images. When the function is called, it reveals the sequence of points of different types depending on the arguments passed into it. In our case, it is necessary to retrieve only the outermost contour of the foreground objects. Therefore, `RETR_EXTERNAL` mode is chosen from existing four options. Also, by selecting the method of contour approximation as `CHAIN_APPROX_NONE`, we ensure that all the points in the chain code are stored.

```
findContours(destImg, contours, RETR_EXTERNAL,
CHAIN_APPROX_NONE);
```

In order to characterize the detected contour further, we bounded them in a rectangle using *boundingRect()* function. It is worth mentioning that the area of bounding rectangle was also experimentally selected to be between **100** and **9500**. Its center is then found by computing contour moments. Two vectors are initiated, where one represents counters’ moments, and another is used to hold their coordinates. Bounding rectangle and its center are depicted in the pictures as red rectangles with blue dot inside.

E. Vehicle counting

As it was stated before, we apply both blob detection and contouring method to ensure more accurate detection of the vehicles. The main condition is that the program will track only those vehicles that are captured by block detection as well as by contouring. If it is satisfied, then counting is performed by establishing a reference line, and

comparing its coordinates with the center of contours at the moment when the vehicles cross it. For our source video, two reference lines are introduced; one is on the left, and another is on the right side of the road. When counting occurs, a color of the lines changes from red to yellow or vice versa. Final number of vehicles is then displayed at the display. The following code represents the condition for one of the reference lines; first four statements are applied for the sides of contour bounding rectangle, and the last is for the detected blobs.

```
if (((vpoint[i].y>=(3*height/5-5) &&
vpoint[i].y<=(3*height/5+5))&&((vpoint[i].x>=50) &&(width/2-
30)))&&(keypoints, true))
```

III. EXPERIMENTAL RESULTS

Testing process of source code was carried out using a laptop powered by an Intel Core i5 (2.67 GHZ) CPU and 4GB RAM. Raw video is taken from UK website picturing M6 motorway. Figures from 2 to 7 illustrate experimental results.



Fig.2 Original frame.

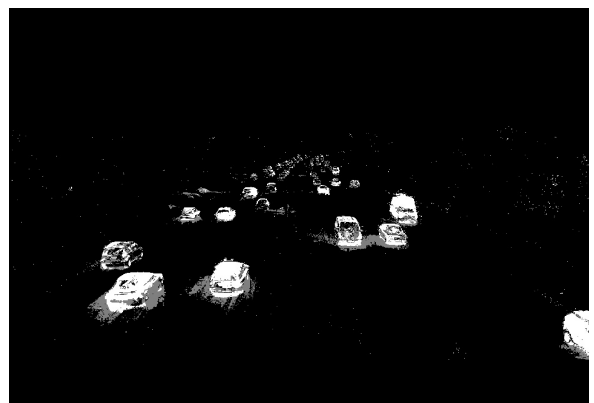


Fig.3 After background subtraction.



Fig.4 Noise rejection.



Fig.5 Counting vehicles crossing reference lines.

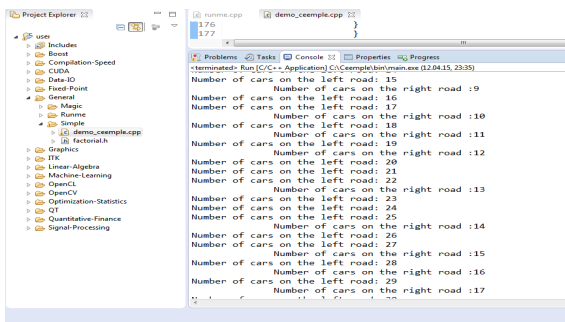


Fig.6 Displayed results.

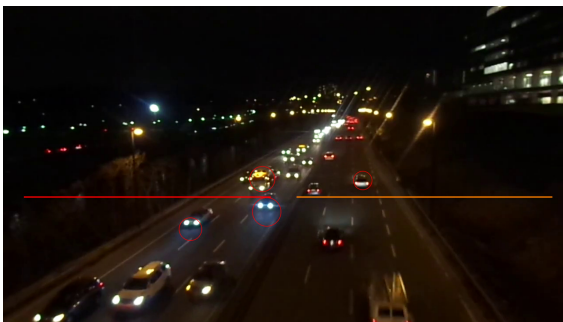


Fig.7 Detection in the dark environment.

The program was able to detect and count vehicles passing through the scene. It is noteworthy that the accuracy of testing has increased when the contour recognition was applied over the blob detection. Initially, the program recognized approximately 30 vehicles out of 100. However, combination of both methods enhanced the performance presenting 65 vehicles out of 100.

The testing in the dark environment revealed less accurate results. This happens owing to the fact that control parameters may vary from the day time settings.

IV. CONCLUSION

Potential growth of traffic congestion leads to a high demand of vehicle detection systems for an effective and low-cost traffic surveillance. This paper proposes vision based detection and tracking algorithm for the vehicles moving on the road.

The system is based on computer vision techniques including background subtraction, morphological transformations, and blob and contour detections. Vehicles are detected from video frames, tracked and then counted by the program, which is running on OpenCV.

Future aspects of concentration include:

- Adjust the program to perform detection in the dark environment;
- Establish timers to track vehicles only when required
- Combine other image detection techniques to increase the accuracy
- Implement algorithm into the existing traffic control system

REFERENCES

- [1] G. Leduc, "Road traffic data: collection methods and applications", JRC Technical Notes, Working Papers on Energy, Transport and, Climate Change, N.1, 2008.
- [2] R. Cucchiara, M. Piccardi, and P. Mello, "Image analysis and rule based reasoning for a traffic monitoring system", IEEE Trans. Intell. Transport. Syst., vol. 1, no. 2, pp. 119-130, June 2002.
- [3] P. Viola and M. Jones, "Rapid Object Detection using a Boosted Cascade of Simple Features", Conference on Computer Vision and Pattern Recognition CVPR, Hawaii, December 9-14, 2001.
- [4] M. Oliveira and V. Santos, "Automatic Detection of Cars in Real Roads using Haar-like Features", Portuguese Conference on Automatic Control, 2008.
- [5] A.S. Abdelhady, "Vehicle Classification For Automatic Traffic Density Estimation", unpublished.
- [6] M. Piccardi, "Background subtraction techniques: a review", Systems, Man and Cybernetics, IEEE International Conference, vol.4, pp.3099-3104, 2004.
- [7] K. Sreedhar and B. Panlal, "Enhancement of Images using Morphological Transformation", International Journal of Computer Science & Information Technology (IJCSIT), vol 4, no.1, pp.33-50, 2012
- [8] G.Bradschi and A.Kaehler, "Learning OpenCV", O'Reilly Media, Inc., Sebastopol, 2008.

WBC identification and counting

Detection and counting of white blood cells in blood test

Dauken Seitkali

2-year Electrical and Electronic Engineering Student
School of Engineering, Nazarbayev University
Astana, Kazakhstan

Madiyar Bazylkhanov

2-year Electrical and Electronic Engineering Student
School of Engineering, Nazarbayev University
Astana, Kazakhstan

Abstract— *In medical world the rapid and cost-effective blood cell count methods are required. However, the most used and traditional method of white blood cells counting is implemented in manual way under microscope by medical laboratory technician. The significance of the white blood cells (WBCs) also known as leukocytes, is that they play role in the diagnosis of different diseases. As a solution to this issue this project is aimed to provide the automatic computer application created with OpenCV software for white blood cell detection and counting. The application proposes two methods of WBCs identification and counting. Mainly using the image segmentation and contours detection functions were used to achieve desired results.*

Keywords— *White Blood Cells; computer application; medicine; blood analysis*

I. INTRODUCTION

Almost all diagnosis of diseases made by medical professionals can not be approved without blood analysis. In medical world the rapid and cost-effective blood cell count methods are required. The significance of the white blood cells (WBCs) also known as leukocytes, is that they play role in the diagnosis of different diseases. WBCs counting is important part of blood analysis and requires rapid implementation in order to make conclusion, since there various diseases such as leukemia which in case of long non-detection of it can progress in very rapid periods. However, the most used and traditional method of WBCs counting is implemented in manual way under microscope by medical laboratory technician. Hence, existed manual method is not effective from time and human factor error prospective, which is one of the most obvious and undesirable factor. It may results to inaccurate outcomes or significant mistakes; and all these cause an amount of stress to medical worker. One of the ways to solve this issue in contemporary world is creating of digital device, engineering system or computer program which will significantly facilitate the process of blood analysis. However, the existence of such hardware systems as the Automated Hematology Counter does not bring desirable results since its non-accessibility in developing countries and ordinary hospitals due to expensive price. As a solution to this issue this project is aimed to provide the automatic computer application for white blood cells detection and counting. Particularly, in this case the principles of programming software application will be used. This project will be implemented with OpenCV computer application, which creates different types of program usually intended to

recognizing object, using the digital cameras for various aims and etc. Specifically, the main principle and function of the software will be detection and counting of the white blood cells on microscopic images of the blood. Moreover, this application is aimed to be cost-effective, accessible and efficient as its alternative in recognizing and analyzing blood cells.

II. METHODOLOGY

Modern medicine involves various technical innovations which contribute to better investigations of the human body and its treatment. Generally, the price of such technical application and facilities are very expensive or available in developed countries where medicine is at very high-tech level. Unfortunately, considering post-Soviet countries such as Kazakhstan, the level of the medicine is still developing and there is a shortage of technical facilities which would make the job of the medical workers better and easier. And white blood cells analysis is one of such procedures which in category of manual implementation. Based on this fact we came up with the idea to develop a digital application for WBCs detection and counting, which will be available and easy controlled and possibly will make slight contribution to the medicine on the local level.

Firstly, there was decision to make brief investigation on blood analysis and blood cells and their features, specifications and many other things. As a result, we learned that white blood cells also known as leukocytes different from other blood cells by color factor. To be specific these cells usually exist in large amount in blood and have the shape and the size shown on the Figure 1.



Figure 1. White blood cells (here two blue colored cells)

Next, the manual way of defining the number of white blood cells will be briefly explained here. Standard Count of cell types is implemented with a Hemacytometer, which is also known as the Counting Chamber (CC) is shown on the Figure 2. The different blood cell types are used for count, which can be categorized into 2 areas: 1. Standard Count for Red Blood Cells (RBC), White Blood Cells (WBC) and Platelets (PLT); 2. Differential Count for WBC. Our preliminary project will provide standard count which means it will not distinguish different types WBCs.

The number of these cells provides information about condition of human's immune system. The larger the number of white blood cells the more serious problems in human's health needs to be determined. According to established rules blood cells are counted per unit volume (per liter); moreover, it is vital that the volume of blood, where the counting of cells is conducting corresponds to a known quantity. Usually, there are counting grids of the size 3mm x 3 mm, which create a special objective slides in CC. There are 2 such counting grids in the middle as it can be seen from the Figure 2.



Figure 2. Counting Chamber

The schematic representation of the counting grid is shown in the Figure 3. The counting grid consist of 9 big squares 1 x 1 mm each, which create central square with 25 medium sized squares, measuring 0.2 x 0.2 mm. Further, these squares divided into 16 small squares with size 0.05 x 0.05 mm. Due to these separations the RBC and PLT are established, as well as WBC and others.

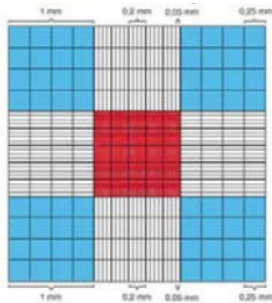


Figure 3. Schematic representation of the counting grid In the RBC and Platelet count, the erythrocyte grid in the middle is examined much closely.

This method is explained here with the aim to have brief understanding of manual way of counting cells.

Based on this knowledge experimental code for the application was created and tested various times. To

implement preliminary experiment we found various microscopic images of blood and used them as samples. During the procedures code was repaired and analyzed plenty of times debugging mistakes and inaccuracies. To provide more detailed information, firstly, the procedure was begun from creating the algorithm, where each step of computer application was thought. As the application starts, the microscopic images, used as samples in our case, are uploaded for further analysis and investigation. Next, main functions of the software begin to work, which is a creation of space for separate red, green and blue color channels and mask of the image. And, an application continues procedure by splitting the image to three RGB channels. Next, equalizing of each channel occur by increasing the intensity. The result of sample in view of green channel is used in threshold function to distinguish white blood cell areas making white color (255) and other regions black color (0). The next step is counting WBCs. In our project we proposed two methods of WBC counting.

The first one is simple we just calculate total number of white pixel which corresponds to leucocytes and divide it to the size of one cell.

The second one is more complex. Here, it finds contours and investigate each of them separately. Specifically, it takes each contour and checks if area of that contour greater than half of the one cell area, then divides that contour's area to the one cell's area and approximates the obtained value to the whole integer. The main advantage of this method is elimination of little unnecessary regions which can accumulate to the errors. Moreover, it helps recover lost areas caused by overlapping leukocytes.

Further, after various testing and analysis the preliminary C++ code of the program was created. The code of the application can be observed and considered in Appendix A.

III. RESULTS AND ANALYSIS OF DATA

Moving to the results we obtained the developed code created opportunity to test the samples of the microscopic images of WBCs. Two samples were examined to detect and count white blood cells. In the first image by manual counting we can see that there are 9 white blood cells (Figure 4). Moreover, Figure 5 shows that our program counted 9.5 white blood cells which almost equals to 9. However, that small error can accumulate to several blood cells if an image contains huge amount of blood cells. The main disadvantage of this method is overlapping leukocytes which may cause some area to be lost per intersection.

That is why we proposed second method of counting. Result of the second method is 9 which is 100% precise to the actual amount of WBCs (Figure 5) because in this case contours are identified and each contour investigated individually. The main idea of this method is elimination unnecessary little contours that accumulate to errors as in first method. Moreover, problem of overlapping leukocytes was solved by counting leukocytes and applying approximation to the whole integer number for each contour.

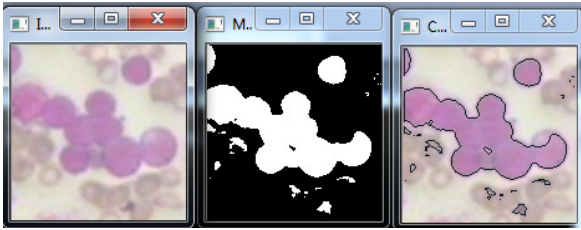


Figure 4. Input microscopic image of blood cells (a) and output image after making it binary (b) and contour drawings (c).

```

C:\Users\User\Documents\Visual Studio 2010\Projects\OPEN_CV_TEST\Debug\OPEN_CV_TEST.exe
Please choose the image. Press 1, 2 or 3: 1
Please, ENTER average size of one WBC (in square pixels): 576
-----METHOD 1-----
Total number of WBCs: 9.49132
-----METHOD 2-----
Total number of WBCs: 9
    
```

Figure 5. Output of the c++ code showing the amount of the WBCs.

Then next image with much more blood cells was analyzed by applying the same procedures (Figure 6, Figure 7, Figure 8). For this example by precise manual counting we obtained 202 WBCs. According to the results the program counted 209 WBCs and 201 WBCs by first and second methods respectively (Figure 9). From this point we can see that in first method the error accumulated to much more values than compared to previous example, as it was predicted. Result of the second method almost the same as actual amount of WBCs, with only one cell error. In manual counting an acceptable maximum limit of the error is 10%. From this point we can state that error of our program is in permissible region.

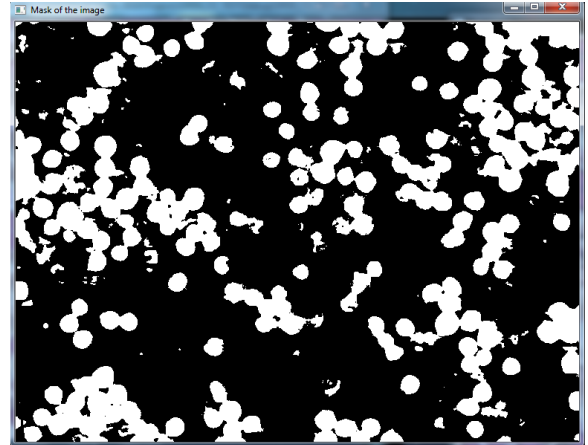


Figure 7. Output image after making input image binary.

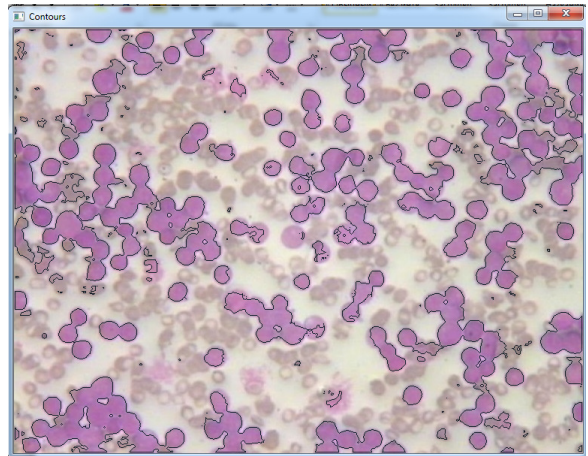


Figure 8 Drawing of the identified contours for second example.

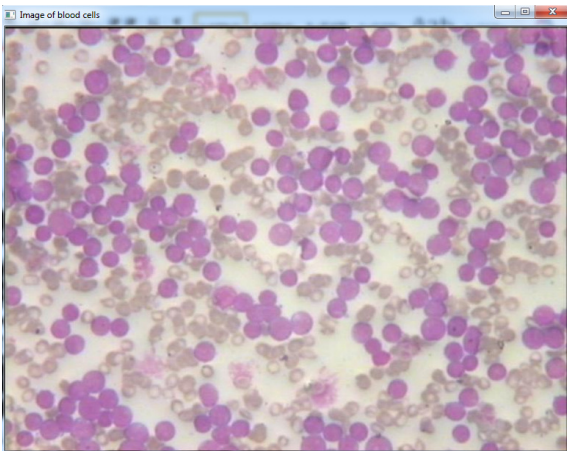


Figure 6. Second input microscopic image of blood cells.

```

C:\Users\User\Documents\Visual Studio 2010\Projects\OPEN_CV_TEST\Debug\OPEN_CV_TEST.exe
Please choose the image. Press 1, 2 or 3: 2
Please, ENTER average size of one WBC (in square pixels): 576
-----METHOD 1-----
Total number of WBCs: 209.038
-----METHOD 2-----
Total number of WBCs: 201
    
```

Figure 9. Output of the c++ code showing the amount of the WBCs for second image.

We investigated third image in order to be confident that our application can analyze different images (Figure 10). The actual precise number of leukocytes in this image is 313. Our application calculated by first method 430 and has huge error (Figure 12). From this point we can say that method 1 totally failed in this example. The second method counted 303 cells with only 3% error which is in permissible region.

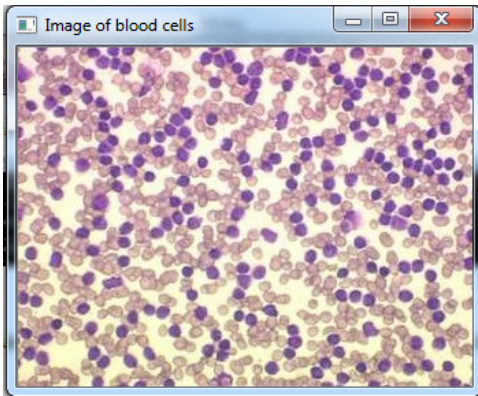


Figure 10. Third input microscopic image of blood cells.

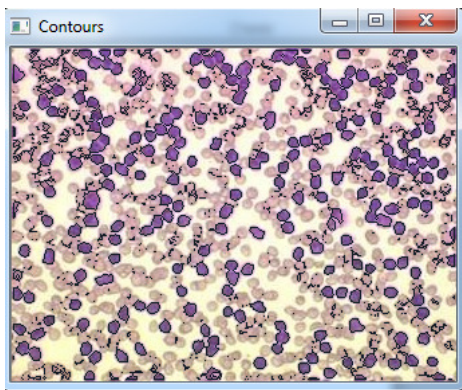


Figure 11. Drawing of the identified contours for third example.

```

C:\Users\User\Documents\Visual Studio 2010\Projects\OPEN_CV_TEST\Debug\OPEN_CV_TEST.exe
Please choose the image. Press 1, 2 or 3: 3
Please, ENTER average size of one WBC (in square pixels): 45
-----METHOD 1-----
Total number of WBCs: 430.289
-----METHOD 2-----
Total number of WBCs: 303

```

Figure 12. Output of the c++ code showing the amount of the WBCs for third image.

detection was made by image segmentation. We proposed two methods and implement them both in order to determine which one is more appropriate. Preliminary results of the project showed that our solutions met the basic concept. Analyzing the results, we came up with decision that second method is more reliable and precise. Specifically, contours identification and investigating them in second method helped us to eliminate errors accumulated in more simple first method. Moreover, the correctness of the experiment was verified by manual counting of the WBCs conducted by ourselves. Further studies and development of C++ code of the program could be done in order to do differential counting of WBCs distinguishing their types. Along with obtained results, we will continue improvement and development of the application by upgrading it. It is need to be mentioned, that although our experiment met expectations it still can not realize real time or immediate detection since we did not consider connection of digital microscope which will make microscopic images itself. Therefore, we will need to add this functions and procedures to the application. Moreover, we need to do more deep investigation of blood structure to make the application more useful and universal.

References

- [1] G.P.M Priyankara, O.W Seneviratne, R.K.O.H Silva, W.V.D Soysa, and C.R. De Silva, "An Extensible Computer Vision Application for Blood Cell Recognition and Analysis," Department of Computer Science and Engineering, University of Moratuwa, Sri Lanka, accessed Mar, 2015.
- [2] M. Maitra, R. K. Gupta and M. Mukherjee, "Detection and Counting of Red Blood Cells in Blood Cell Images using Hough Transform," International Journal of Computer Applications (0975 – 8887), vol.53, No:16, September 2012
- [3] L. Putzu and C.D. Ruberta. "White Blood Cells Identification and Counting from Microscopic Blood Image," World Academy of Science, Engineering and Technology International Journal of Medical, Health, Biomedical and Pharmaceutical Engineering vol.7, No:1, 2013

As it was demonstrated, the application implements its main purpose. Therefore, it needs to be finished out by improving the code and creating the interface and design of the application. Moreover, we need to consider connection of camera or digital microscope in order to have real time image of blood cells.

IV. SUMMARY, CONCLUSIONS AND RECOMMENDATIONS

To sum up, in our project we examined microscopic blood test images using OpenCV and C++ programming language to detect white blood cells and count their amount. Mainly cells

Madiyar Bazylkhanov

Date of birth: 26.09.1993

Place of birth: East Kazakhstan, Semipalatinsk

Graduated from Kazakh-Turkish High School in 2011

Studied 1 year at Almaty University of Power Energy and Telecommunication, Almaty, Kazakhstan
Faculty of Electroenergy

Currently 2-year electrical engineering student at Nazarbayev University, Astana, Kazakhstan

Dauken Seitkali

Date of birth: 08.01.1994

Place of birth: Kazakhstan, Almaty

Graduated from RSPMBS named O.Zhautykov in 2011

Studied 1 year at International Institute of Information Technologies, Almaty, Kazakhstan
Faculty of Information Technologies

Currently 2-year electrical engineering student at Nazarbayev University, Astana, Kazakhstan

Appendix A

Code of the computer application:

```
#include <iostream>
#include <stdio.h>
#include <opencv/cv.h>
#include <opencv/highgui.h>
#include <math.h>
/*****
Nazarabyev University, Astana city
Course title: Principles of Programming
Project title: Blood Test
Authors: Madiyar Bazylkhanov ID 201202190
        Dauken Seitkali ID 201203167
Last modified date: 01.04.2015
*****/
using namespace std;

int main(int argc, char * argv[])

{
    int choose_image;
    cout<<"Please choose the image. Press 1, 2 or 3: ";
    cin>>choose_image;

    IplImage* image;
    if (choose_image==1) image = cvLoadImage("D:\\ART\\i2Vmr.png");
    else if (choose_image==2) image = cvLoadImage("D:\\ART\\s58H1.jpg");
    else image = cvLoadImage("D:\\ART\\c11blood.jpeg"); //loading microscopic image file
    cvNamedWindow("Image of blood cells", CV_WINDOW_AUTOSIZE ); // creating input window
    cvNamedWindow("Mask of the image", CV_WINDOW_AUTOSIZE ); // creating output window

    cvShowImage("Image of blood cells", image ); //Show input image in input window

    //Creating space for separate r, g, b channels of the image and output masks of the image
    IplImage* r = cvCreateImage(cvGetSize(image), IPL_DEPTH_8U, 1); //r
    IplImage* g = cvCreateImage(cvGetSize(image), IPL_DEPTH_8U, 1); //g
    IplImage* b = cvCreateImage(cvGetSize(image), IPL_DEPTH_8U, 1); //b
    IplImage* mask = cvCreateImage(cvGetSize(image), IPL_DEPTH_8U, 1); //mask for white blood cells

    cvSplit(image, b, g, r, NULL); // Splitting into three channels in order to get separate RGB images

    // equalize r, g, b in order to increase intensity
    cvEqualizeHist( r, r ); //equalise r
    cvEqualizeHist( g, g ); //equalise g
    cvEqualizeHist( b, b ); //equalise b
    cvShowImage("Mask of the image", g);

    cvThreshold( g, mask, 72, 255, CV_THRESH_BINARY_INV); // making white blood cells grey
    // and other spaces black in new image named mask
    cvShowImage("Mask of the image", mask);

    double gray_size; // size of the white blood cell areas in pixels
    double cell_size; // cell size of the one white blood cell
    double cell_num_method1; // number of white blood cells for 1st METHOD

    cout<<"Please, ENTER average size of one WBC (in square pixels): ";
    cin>>cell_size; // entering premeasured size of one WBC

    cout<<endl<<"-----METHOD 1-----"<<endl;

    gray_size = cvCountNonZero(mask); // counting the size of the WBC areas
```

```

cell_num_method1 = gray_size/cell_size; // calculating final amount of the white blood cells
cout<<endl<<"Total number of WBCs: "<<cell_num_method1<<endl;

//-----METHOD-2---contour identification and drawing-----//

cout<<endl<<"-----METHOD 2-----"<<endl;
CvMemStorage* storage = cvCreateMemStorage();
CvSeq* first_contour = NULL;

// finding contours in image named "mask"
int Nc = cvFindContours(
    mask,
    storage,
    &first_contour,
    sizeof(CvContour),
    CV_RETR_LIST,
    CV_CHAIN_APPROX_SIMPLE
);
// drawing each found contour on the original image
for( CvSeq* c=first_contour; c!=NULL; c=c->h_next ) {
cvDrawContours(
    image,
    c,
    CV_RGB(20,30,40),
    CV_RGB(20,20,40),
    1,
    1,
    8
);
}
//-----finding APPROXIMATED number of WBCs in each individual contour-----
double cell_num_method2=0;
double contour_area=0;
for( CvSeq* c=first_contour; c!=NULL; c=c->h_next )
{
    contour_area=cvContourArea(c, CV_WHOLE_SEQ);
    if ( contour_area > cell_size/2) // ONLY considering contours with area greater than half area of one WBC
    {
        if (contour_area/cell_size - (int)(contour_area/cell_size) > 0.4)
            cell_num_method2 = cell_num_method2 + (int)(contour_area/cell_size) + 1;
        else
            cell_num_method2 = cell_num_method2 + (int)(contour_area/cell_size);
    }
    else continue;
}
//
cout<<"new: "<<cell_num_method2<<endl;
}

cout<<"Total number of WBCs: "<<cell_num_method2<<endl;
cvShowImage("Contours", image);
//Show output image in output window

cvWaitKey(0);
cvReleaseImage( &g);
cvDestroyWindow( "Mask of the image");

    return 0;
}

```


Author Index

- Adilzhan, Abzal 90
Aibek, Ryskaliyev 59
Aidaraliyev, Abuzhan 77
Aimakov, Nurbolat 101
Aliakhmet, Kamilla 86
Amantayeva, Zarina 83
Arman, Kapan 45
Askaruly, Sanzhar 71
- Bainazar, Yernar 38
Bairamkulov, Rassul 62
Balgabayev, Merey 42
Bazylkhanov, Madiyar 45
- Danyiar, Bekishev 38
- Ellis, Grant workshop1
- Ibrayev, Timur 104
Izbassarova, Akzharkyn 48
- James, Alex Pappachen workshop3
Junussov, Abduvakhit 68
- Kengesbek, Daulet 48
Ko, Match Wai Lun workshop4
Kulmukhanova, Alfiya 68
Kusmangaliyev, Janyzbek 79
Kypshakpayev, Yerden 54
- Leskhan, Dauren 77
- Massalimova, Aidana 83
Mukabak, Kuatbek 54
Myrzakhmet, Serikbolsyn 90
- Ornov, Nursultan 29
- Rakhmetov, Bakhtiyar 71
Rojas-Solórzano, Luis R. workshop2
- Sadykova, Diana 101
Salpenova, Saltanat 42
Saparov, Yerkebulan 52
Sapenova, Yerzhan 29
Sapiyev, Yerkhan 35
Sarmukhanov, Radkhan 104
Seitkali, Dauken 94
Sultangazin, Alimzhan 79
- Tazhkenov, Ruslan 38
Tlekov, Dauren 108
- Utekeyev, Azamat 35
- Yerlan, Rizukov 59
- Zhakupov, Aktanberdi 52
Zhapparov, Ratbek 112
Zharkynbek, Temirlan 86
Zhetessov, Aidar 108
Zhussip, Magaiya 112